

SHALLOW GROUNDWATER EFFECT ON LAND SURFACE TEMPERATURE
AND SURFACE ENERGY BALANCE:
DESCRIPTION, MODELING AND REMOTE SENSING APPLICATION

Fouad Alkhaier

Examining committee:

Prof. dr. E. van Beek	University of Twente
Prof. dr. V. Jetten	University of Twente
Prof. dr. ing. N. Sneeuw	Universität Stuttgart
Dr. G. N. Flerchinger	USDA/ARS
Dr.ir. J. H. M. Wosten	Wageningen UR/Alterra
Prof. dr. S. Uhlenbrook	UNESCO-IHE
Prof. dr. R. J. Schotting	Utrecht University

ITC dissertation number 198
ITC, P.O. Box 6, 7500 AA Enschede, The Netherlands

ISBN 978-90-6164-322-7

Cover designed by Fouad Alkhaier

Cover illustration: Water, Earth, Air, Fire and a Satellite: Groundwater and Surface Energy Balance from space.

Printed by ITC Printing Department

Copyright © 2011 by Fouad Alkhaier



UNIVERSITY OF TWENTE.

ITC

FACULTY OF GEO-INFORMATION SCIENCE AND EARTH OBSERVATION

SHALLOW GROUNDWATER EFFECT ON LAND SURFACE TEMPERATURE
AND SURFACE ENERGY BALANCE:
DESCRIPTION, MODELING AND REMOTE SENSING APPLICATION

DISSERTATION

to obtain
the degree of doctor at the University of Twente,
on the authority of the Rector Magnificus,
prof.dr. H. Brinksma,
on account of the decision of the graduation committee,
to be publicly defended
on Thursday 1 December 2011 at 12:45 hrs

by

Fouad Alkhaier

born on 24 January 1973

in Damascus, Syria

This thesis is approved by
Prof. dr. Zhongbo Su, promoter

Acknowledgements

I owe a dept of gratitude to the Ministry of Higher Education, Damascus, Syria and the Faculty for Geoinformation Sciences and Earth Observation (ITC), University of Twente, the Netherlands. The research described in this thesis could not have been realized without their munificent financial support.

Throughout my PhD research I had fruitful scientific cooperation with many people inside and outside ITC, and I would not have accomplished my research without their sincere help. Therefore I would like to appreciate all of those people.

My utmost appreciations go to my promoter Prof. Dr. Zhongbo Su for his precious guidance, fruitful discussions and invaluable contributions. I am deeply grateful for his incessant encouragement. He was always available to give his kind help in spite of his continuous and intense duties and responsibilities.

I would like to express my profound gratitude to Gerald N. Flerchinger from the U.S. Department of Agriculture - Agriculture Research Service, the developer of SHAW model which I used extensively within the course of my research. I am grateful for his constant support and helpful comments and suggestions.

I am deeply indebted to the staff of the General Organization of Land Reclamation, Ar-Raqqa, Syria. They were enormously generous in supporting my research and field campaigns in the study area, Syria. They were always there to provide technical labor and expertise, laboratory services, vehicles, machines and instruments. I specially thank the director of the investigations department, Geologist Tareef Al-Naeif. And my deepest thanks to Geologist Hassan Al-Eeisa who was of great help in conducting the field campaigns and providing his bright remarks and suggestions regarding enhancing the quality of the field measurements.

I am grateful to water resources department staff, those who were always providing their kind support. I specially express gratitude to Prof. Dr. Allard Meijerink, Dr. Suhyb Salama, Wim Timmermans, Robert Becht, Arno van Lieshout, Marcel van Helvoirt, Murat Ucer and finally to the two angels of the department Anke and Tina.

I would like to thank many ITC staff those who were of continuous help and encouragement during my PhD study. I specially thank Prof. Dr. Martin Hale, Gerard Reinink, Carla Gerritsen, Marion Pierik,

Bettine Geerdink, Gerrit Polman, Aiko Mulder, Loes Colenbrander and Roelof Schoppers. Special thanks to Saskia Groenendijk, Marjolein Woerlee and Annie van der Meer from IIH, for their kind support which made my stay in Enschede pleasant and comfort.

I would like to express my sincere appreciation to my friends and colleagues those who made my stay in ITC a pleasant period. I mention in particular Chaweepan Suangkiattikun, Nizar Taha, Zeng Yijian, Haris Akram Bhatti, Syarif Budhiman, Zahir Ali Yousafzai, Joris Timmermans, Enrico Balugani, Mustafa Gokmen, Alain Pascal Frances, Jahanzeb Malik, Lal Muthuwatta, Jeniffer Kinoti Mutiga and Kitsiri Weligepolage.

Finally, I do gratefully thank my parents in law for their kind support and encouragement. It is hardly possible to find appropriate words to express my gratefulness to my wife Ashwak and my daughter Leen for their incessant love and patience. I am deeply indebted to them both for sharing the difficult time I had throughout my research.

Table of Contents

Acknowledgements	i
Table of Contents	iii
List of figures	vi
List of tables	x
1 Introduction	1
1.1 Groundwater and temperature measurements	2
1.1.1 Geothermal behavior of groundwater systems	3
1.1.2 Surface water- groundwater interaction	4
1.1.3 Determining and constraining hydraulic parameters	6
1.1.4 Groundwater effect on surface soil temperature	7
1.2 Groundwater and remote sensing	11
1.2.1 Geologic mapping and lineaments tracing	11
1.2.2 Defining boundary conditions	11
1.2.3 Vegetation classification	12
1.2.4 Gravity measurements	12
1.2.5 Precipitation and evapotranspiration estimation	13
1.2.6 Groundwater effect on land surface temperature.....	13
1.3 Problem statement	15
1.4 Research objective.....	16
1.5 Outline of the thesis.....	16
2 Theoretical Background.....	19
2.1 Shallow groundwater systems	20
2.2 The energy balance at land surface and heat transfer within soil matrix	20
2.3 Shallow groundwater effect.....	22
2.3.1 The direct effect.....	22
2.3.2 The indirect effect	23
2.3.3 The combined effect	24
3 Materials and Methods	27
3.1 Study area and field measurements	28
3.1.1 Study area description	28
3.1.2 Field measurements	32
3.2 Numerical simulations	34
3.2.1 FlexPDE	34
3.2.2 SHAW.....	35
3.3 Remote sensing data manipulations	37
3.3.1 Satellite data	37
3.3.2 ILWIS.....	38
3.3.3 SEBS.....	38
4 Exploring Shallow Groundwater Effect on Surface Soil Temperature Using Field Measurements and a Simple Numerical Model.....	41
4.1 Introduction.....	42

4.2	Methods and materials	42
4.2.1	Field measurements	42
4.2.2	Numerical simulations.....	44
4.3	Results.....	45
4.3.1	Results from field measurements.....	45
4.3.2	Results from numerical simulations.....	50
4.4	Discussion and conclusions	52
5	The Thermodynamic Effect of Shallow Groundwater on Temperature and Energy Balance at Bare Land Surface.....	55
5.1	Introduction.....	56
5.2	Numerical experiments.....	57
5.2.1	Experiment 1	58
5.2.2	Experiment 2	60
5.3	Results.....	63
5.3.1	Experiment 1	63
5.3.2	Experiment 2	65
5.4	Discussion	73
5.5	Conclusions	76
6	The Combined Effect of Shallow Groundwater on Temperature and Energy Balance at Bare Land Surface	79
6.1	Introduction.....	80
6.2	Methodology	81
6.3	Simulation results and discussion.....	83
6.4	Conclusions and recommendations.....	92
7	Reconnoitering the Effect of Shallow Groundwater on Land Surface Temperature and Surface Energy Balance Using MODIS and SEBS	95
7.1	Introduction.....	96
7.2	Study area description and data collection.....	97
7.2.1	Field data	97
7.2.2	Remote sensing data	99
7.3	Surface energy balance and related maps calculations	99
7.4	Results and discussion.....	102
7.4.1	Water table depth and soil moisture maps	102
7.4.2	Soil temperature maps.....	105
7.4.3	Surface energy balance maps	106
7.4.4	The maps of evaporative fraction and actual daily evaporation	107
7.4.5	The soil moisture map estimated from SEBS' actual daily evaporation	108
7.5	Conclusions and recommendations.....	109
8	Conclusions and Recommendations.....	113
8.1	Conclusions	114
8.2	Suggestions for further work	118
	Appendix A: Some Useful Comments	119

A.1 Comments on Kollet and Maxwell (2008)	120
A.1.1 The spin-up process	120
A.1.2 The used integrated and distributed watershed modeling platform (PF.CLM)	122
A.1.3 Model validation against ground truth data	122
A.2 Comments on Maxwell and Kollet (2008)	123
Bibliography	125
Summary	141
Samenvatting	145
ITC Dissertation List.....	148

List of figures

Figure 1.1: Heating of water rising from depth to surface (After Kappelmeyer, 1957).....	8
Figure 1.2: Geologic cross section and horizontal thermal profiles at both wintertime and summertime. The shown profiles have been taken at spacing of 15 meters at a depth of 50 centimeters in east-central Illinios, USA (After Cartwright, 1968).....	9
Figure 1.3: Isotherms and flow lines for steady heat conduction through a soil (After Ingersoll et al., 1948, p.203 cited in Cartwright, 1968).	10
Figure 2.1: Schematic description of the two different effects of groundwater	23
Figure 2.2: Schematic description of shallow groundwater effect on land surface temperature and the different components of surface energy balance.	24
Figure 3.1: Study area location within Al-Balikh river basin in northern Syria.	28
Figure 3.2: Geological map of the study area by the ministry of industry department of geological and mineral research, 1963, the map is a part of a scanned 4 tableaus plats mosaic.	30
Figure 3.3: Scenes from the study area. Drilling a piezometer. The soil core of a borehole. A sample of a boreholes conducted by the General Organization for Land Reclamation, Ar-Raqqa, Syria.	31
Figure 3.4: Climate chart of the region.	32
Figure 3.5: Four cropping systems in the area (After Alkhaier, 2003).	32
Figure 3.6: Left: Soil moisture measurements device (Stevens' Portable Hydra Reader and Stevens' Hydra probe). Right: water table depth reading device.....	33
Figure 3.7: Two temperature loggers (HOBO Pendant) deployed in the soil at two different depths (approximately 5 and 10 cm).	34
Figure 3.8: A sample of FlexPDE graphical output of temperature at diverse depths within the soil profile.	35

Figure 3.9: Physical system described by the SHAW model. (T_a is temperature, u is wind speed, hr is relative humidity, St is solar radiation, i is precipitation, T is soil temperature, and θ/l is water content.) (After Flerchinger, 2000).....	36
Figure 4.1: Study area with observation locations (Google Earth image).	43
Figure 4.2: Min, max and average temperature vs. water table depth of the third day for temperature measurements at 5 and 10 cm depth.....	48
Figure 4.3: Min, max and average temperature vs. water table depth of the last day (wet soil) for temperature measurements at 5 and 10 cm depth.....	49
Figure 4.4: Soil moisture of the upper 5 cm vs. water table depth. .	50
Figure 4.5: Land surface temperature oscillations of the simulated year.	51
Figure 4.6: The difference between the simulated land surface temperatures of the two profiles (land surface temperature of the profile with groundwater perching at one meter, minus the land surface temperature of the dry profile). ..	51
Figure 5.1: a) Ground heat flux (Wm^{-2}) of the no-groundwater profile subtracted from those of profiles with water table depth of half meter (black), one meter (red) two meters (blue) and three meters (green). b) The same as (a) but for land surface temperature ($^{\circ}C$).	64
Figure 5.2: Land surface temperature ($^{\circ}C$) of the no-groundwater profile subtracted from those of profiles with groundwater at a) 0.5 m depth b) 1 m depth c) 2 m depth d) 3 m depth. Solid lines are first harmonics.	66
Figure 5.3: Ground heat flux (Wm^{-2}) of the no-groundwater profile subtracted from those of profiles with groundwater at a) 0.5 m depth b) 1 m depth c) 2 m depth d) 3 m depth. Solid lines are first harmonics.	67
Figure 5.4: Sensible heat flux of the no-groundwater profile subtracted from those of profiles with groundwater at a) 0.5 m depth b) 1 m depth c) 2 m depth d) 3 m depth. Solid lines are first harmonics.	68
Figure 5.5: Latent heat flux of the no-groundwater profile subtracted from those of profiles with groundwater at a) 0.5 m depth b) 1 m depth c) 2 m depth d) 3 m depth. Solid lines are first harmonics.	69

Figure 5.6: Outgoing longwave radiation (Wm^{-2}) of the no-groundwater profile subtracted from those of profiles with groundwater at a) 0.5 m depth b) 1 m depth c) 2 m depth d) 3 m depth. Solid lines are first harmonics.	70
Figure 5.7: Hourly values of temperature and energy fluxes of two profiles 1) with no-groundwater (red), 2) with groundwater at 50 cm depth (blue) and 3) the difference between them [(2)-(1)] (black), for two days: 23 Dec (left side) and 24 Jul (right side).	72
Figure 5.8: Schematic description of groundwater thermodynamic effect on land surface temperature and the different components of surface energy balance.	75
Figure 6.1: Monthly averaged data for minimum and maximum temperatures and precipitation for the simulation year. ...	82
Figure 6.2: Monthly averaged values of surface soil moisture, surface soil temperature and surface energy balance components for the simulated year.	84
Figure 6.3: Surface soil moisture, surface soil temperature and surface energy balance components for the two profiles in a winter day (January 3 of the simulated year).....	87
Figure 6.4: Surface soil moisture, surface soil temperature and surface energy balance components for the two profiles in a summer day (July 16 of the simulated year).....	89
Figure 6.5: Surface soil moisture, surface soil temperature and surface energy balance components for the two profiles in a wet summer day (June 19 of simulation year).	90
Figure 7.1: Study area location within Al-Balikh river basin in northern Syria (Google Earth image).	98
Figure 7.2: a) Digital Elevation Model (30 m pixel resolution), and b) NDVI map of the study area (250 m pixel resolution).	98
Figure 7.3: The interpolated raster maps for a) water table depth and b) soil moisture of the upper 5 cm. Locations of the point data collected in the field are also shown.....	103
Figure 7.4: Landsat 2, False Color Composite (Red = band 5; Green = band 6; Blue = band 4), August 08, 1975, 09:34 LT.	104
Figure 7.5: The cross-relationship between water table depth map and surface soil moisture map.	104

Figure 7.6: Land surface temperature maps (°C) of the study area on January 17, 2007. a) Daytime temperature, and b) nighttime temperature.....	105
Figure 7.7: Cross-relationships between water table depth and a) daytime land surface temperatures and b) nighttime land surface temperatures at January 17, 2007.....	105
Figure 7.8: The SEBS calculated maps of the instantaneous components of surface energy balance at 10:25 LT, January 17, 2007.....	106
Figure 7.9: The cross-relationships between water table depth and the variant instantaneous components of surface energy balance at 10:25 LT, January 17, 2007.	107
Figure 7.10: The cross-relationships between water table depth and a) the evaporative fraction and b) the actual daily evaporation.....	108
Figure 7.11: Soil moisture of the upper 5 cm measured in field by Stevens' Hydra probe against soil moisture estimated from evaporative fraction using equation (7.9).	109

List of tables

Table 4.1: The weather data for the experiment period and for some days before: Minimum and maximum air temperature ($^{\circ}\text{C}$), average relative humidity (%), average air pressure (mb), rain (mm) and average wind speed (ms^{-1}).	43
Table 4.2: Correlation coefficients between the min, max and average daily temperatures at the two depths (5 and 10 cm) and average water table depths.	46
Table 4.3: P-values for the Correlation coefficients of Table 4.2.	46
Table 4.4: Soil thermal properties used in the simulations.	50
Table 6.1: Texture composition and physical properties of soil in the two profiles.	83
Table 6.2: The yearly averaged values of surface soil moisture, surface soil temperature and the surface energy balance components for the simulated year.	86

1 Introduction

Groundwater is an extremely important resource in most parts of the world; it is often the primary source for domestic, industrial and agriculture water supply. Of all the water on earth, groundwater accounts for less than one percent, but still it is more than all of the planet's freshwater lakes, rivers and streams combined. Groundwater modeling is recognized nowadays as the best tool to support management of groundwater resources. Traditional hydrological measurements provide usually point data (e. water head), however groundwater models require spatially distributed input data. Some of these data can be satisfied by remote sensing.

1.1 Groundwater and temperature measurements

Leonardo da Vinci (1452-1519) has always referred to the body-Earth analogy: *"The flesh is the soil, the bones are the rocks that support the Earth; its blood is the underground water streams"*. Body temperature and blood pressure are considered preliminary indicators of the body behavior and, though simple to take, they can tell a lot about the patient's condition. Although temperature and blood pressure share importance, physicians start with temperature first because it is easy to measure and fast to yield answers. In the same manner, temperature measurements can help to gain information about groundwater systems. Actually, groundwater temperature can be measured easily and rapidly, because waterproof temperature loggers are now inexpensive and widely available (Stonestorm and Blasch 2003).

Heat-flow theory has contributed to the development of groundwater hydrology (Anderson, 2005). It is well known that Darcy's law has the same form as Fourier's law for heat flow. Even some analysts (Groenevelt, 2003) believed that Darcy was probably aware of Fourier's work soon after it was published, and well before he conducted his famous laboratory experiments in 1856 (Darcy, 1856).

The similarity between Darcy's law and Fourier's law for heat flow by conduction has motivated scientists to make use of analytical solutions of heat flow for developing solutions for groundwater flow problems. For example, Theis (1935) went to an analytical solution of the heat flow equation in developing his famous model for transient groundwater flow to a pumping well (Freeze, 1985).

Temperature measurements have been frequently exploited in groundwater studies, within different groundwater themes such as: 1) Geothermal behavior of groundwater systems 2) Surface Water - Groundwater Interaction. 3) Determining and constraining hydraulic

parameters of aquifers, and 4) Groundwater effect on surface soil temperature.

1.1.1 Geothermal behavior of groundwater systems

In order to pave the way to utilize temperature in groundwater movement studies, Mink (1964) investigated and described the thermal regime of a well-known flow pattern of groundwater in a tropical environment in a Hawaiian island. He traced the temperature increase in this system starting from 19.7 °C in the recharge area in the high terrain up to 21 °C in the recharge area near the sea. He attributed the increase in temperature to the absorption of heat from volcanic activity and normal terrestrial heat flow, flow friction and return irrigation water.

The basic equations for heat transport in a fully saturated medium were given by Suzuki (1960), Stallman (1965) and Bredehoeft and Papadopoulos (1965). Suzuki (1960) presented an analytical solution of the one-dimensional transient heat-flow equation and used it to estimate infiltration rate depending only on temperature measurements. Stallman (1965) showed how Suzuki's solution could be used to analyze the temperature profile and calculate vertical velocity of infiltrating water. Similarly, Bredehoeft and Papadopoulos (1965) introduced a one-dimensional steady-state analytical heat transport model to calculate vertical leakage through a confining bed under constant temperature boundary conditions.

Analytical solutions to these equations for simplified groundwater systems were subsequently developed by several authors. And with the introduction of large memory computers general numerical solutions to complex groundwater system became available and were widely used.

Parson (1970) conducted a numerical simulation of the groundwater thermal regime in a glacial complex and numerical modeling of a hypothetical groundwater basin. The two models suggested that groundwater flow had a significant effect on the subsurface temperature field and that effect depended on the magnitude and direction of flow velocity. He distinguished between the recharge areas where the climate influence largely determines the water table temperature and the discharge areas (like springs) where the convective heat transfer within the medium probably determines the water table temperature. He ascribed the temperature distribution of the groundwater thermal regime to terrestrial heat flow, thermal and hydraulic properties of the saturated medium, subsurface

hydrodynamics and the climate history as well as present climate conditions. Similarly, Cartwright (1970) successfully utilized temperature data to gain insight into basin-scale groundwater flow, and to locate areas of both recharge and discharge in the basin.

Many other researchers continually investigated the vertical and horizontal groundwater movement in aquifers using temperature measurements of water using both analytical and numerical solutions (Kilty and Chapman, 1980; Wade and Reiter, 1994; Tanigushi et al., 1999; Ferguson et al., 2003; Ferguson and Woodbury, 2005). Manning and Kip Solomon (2005) utilized temperature together with other environmental tracers (Noble gas recharge temperatures, groundwater ages) and combined with heat and fluid flow modeling to characterized bulk fluid circulation in a mountain block. Bense et al. (2008) conducted numerical analysis of groundwater temperature and found that thermal anomalies designated preferential flow along faults in unconsolidated sedimentary aquifers. Recently, Saar (2011) presented a review of coupled groundwater and heat transfer and discussed temperature depth profiles and heat discharge at springs to deduce hydraulic parameters and processes.

1.1.2 Surface water- groundwater interaction

Using heat as a tracer, several scientists studied and modeled the interconnection between surface water and groundwater (Andrews and Anderson, 1979; Hunt et al. 1996; Townley and Trefry, 2000; Constantz et al., 2003). In fact, heat has merit over chemical tracers: The temperature signature is natural and its measurement is quick, cheap and ready to construe (Stonestrom and Constantz 2003). Estimating groundwater discharge to streams is important in describing subsurface flow and can be useful in calibrating numerical groundwater models, especially where enough pressure data is not available (Becker 2004).

To locate anomalies in sediment temperature Lee (1985) designed a device to be dragged along lakebeds, and used it successfully to detect an artificially created seepage area in soft bottom sediment below eight meters of lake water. Silliman and Booth (1993) used temperature measurements of both the sediment and the overlying water to locate inflows - outflows in both creeks and streams. They found that temperature proved to be an excellent tool for that purpose. Similarly, Evans et al. (1995) used thermal profiles within river beds to quantify groundwater discharge to the river.

Extending the earlier work by Stallman (1965), Silliman et al. (1995) presented a simple mathematical formulation to estimate the downward flux passing through creek sediments. Constantz (1998) demonstrated that simultaneous analysis of stream temperatures and stream flows provides insight into both spatial and temporal patterns in stream-groundwater interaction. And Frayer et al. (2000) found that thermal monitoring can be useful for delineating gaining and losing reaches of streams because temporal variability in stream temperature along gaining reaches should be less than along losing reaches.

Conant (2004) used streambed temperature mapping jointly with other methods to delineate the pattern of groundwater discharge in a sandy streambed. He measured the temperature (in both winter and summer) of stream water, groundwater, shallow streambed (Plan view mapping) and vertical profiles of streambed temperature.

Hatch et al. (2006) presented a method for determining streambed seepage rates using time series thermal data. Their method is based on quantifying changes in phase and amplitude of temperature variations between pairs of subsurface sensors. Constantz (2008) reviewed the use of heat as a tracer of shallow groundwater flow and discussed temperature-based methods for estimating streambed water exchanges. Bianchin et al. (2010) used Temperature measurements, coupled with independent hydraulic head measurements to investigate groundwater-surface water interaction beneath a large tidally influenced river.

Recent studies continued to use temperature measurements to determine rates of streambed seepage (Cardenas, 2010; Hatch et al., 2010; Lautz, 2010; Shanafield et al., 2010; Gerecht et al., 2011). In a different approach, Schuetz and Weiler (2011) used ground-based thermographic systems to detect localized groundwater inflows into small streams. They suggested that infrared radiation temperatures of surface water can be used for the instant recognition and quantification of local groundwater inflow.

It should be mentioned here that using temperature as a tracer has also some limitations and difficulties. Firstly, there should be enough temperature fluctuations within water body so the sensors can detect the differences in temperature and distinguish between the variant fluxes (Anderson, 2005; Hatch et al 2006; Westhoff et al., 2011a;b). And secondly, minimum values of hydraulic permeability are needed to observe advective heat transfer (Saar, 2010). Lower permeability causes heat-conduction-dominated systems; this in turn prevents the

inversion of temperature fields for groundwater flow patterns detection.

Yet, the first limitation can be overcome by heating the water system. Furthermore, the advent of the new technology - Distributed Temperature Sensing (Selker et al., 2006; Tyler et al., 2009; Steele-Dunne et al., 2010) - made it possible to have higher accuracy in temperature measurements and would decrease this problem (Lowry et al 2007; Matheswaran et al., 2011).

1.1.3 Determining and constraining hydraulic parameters

Limiting uncertainty in groundwater models requires accurate determination of the spatial and temporal variations in hydraulic parameters of the aquifer such as the conductivity and permeability (Su et al., 2004). These parameters often vary significantly over space, and it is not easy to take enough measurements for adequately mapping their spatial variation within an aquifer (Woodbury and Smith, 1988; Painter et al., 2007). Besides, heads information are not usually enough to specify unique values of model parameters; for instance, different combinations of hydraulic conductivity and recharge can result in identical spatial distribution of the simulated head (Bravo et al., 2002).

Macfarlane et al. (2002) showed that hydraulic properties can be estimated by observing heated water flow between wells. Changes in the temperature profile recorded in observation wells specify the flow path of the heated water, i.e. the tracer.

One method to face data limitation or uncertainty in groundwater models is to exploit additional data set such as subsurface temperature which is sensitive to spatial variation in hydraulic conductivity and apply joint inversion. The basic idea of joint inversion is to exploit the sensitivity of water temperature to hydro-geologic parameters (Woodbury and Smith, 1988). The efficiency of this method was demonstrated by Su et al. (2004) who combined groundwater temperature with well water levels to estimate the spatial variation of hydraulic conductivities in a shallow aquifer, and Bravo et al. (2002) who proved that the estimates of hydraulic conductivity and groundwater flow could be better constrained by simultaneous inversion of temperature and water level data.

Other investigators (Bravo et al., 2002; Burow et al., 2005) found that joint inversion of head and temperature data is effective to

estimate simultaneously hydraulic conductivity and water flow. Constantz et al. (2003) showed that hydraulic conductivities can be estimated by matching simulated groundwater temperature to the observed groundwater temperatures. And Su et al. (2004) combined hydro-geologic data with measured vertical temperature profiles to constrain a series of two dimensional, transient simulations of groundwater flow and heat transport.

Recently, Hatch et al. (2010) used time-series analysis of streambed thermal records to assess seepage rates changes and hydraulic conductivity in streambed with time, as a function of channel discharge and connected changes in sediment conditions. Saar (2010) reviewed and discussed studies that inferred hydraulic permeability using temperature depth profiles (geotherms) and heat discharge at springs. He emphasized that the optimal permeability should range between 5×10^{-17} and $10^{-15} m^2$ to observe advective heat transfer and related geotherm perturbations.

1.1.4 Groundwater effect on surface soil temperature

The idea of exploiting temperature measurement in groundwater flow studies was furthered by other investigators to study the thermal effect of groundwater on soil temperature and to locate shallow aquifers by detecting thermal anomalies at land surface. This method offers some promise as a rapid, inexpensive, and fairly reliable means of locating shallow linear unconsolidated aquifers during the summer and winter months (Becker 2006).

The effect of groundwater on soil temperature has been noted as early as the 1930's, (van den Bouwhuysen, 1934). In one of the pioneering investigations, Kappelmeyer (1957) successfully used near surface soil temperatures (1.5 m depth) to overcome the problem of finding fissures, cracks and similar features, provided that convective heat transport from depth to surface occurred through these features (Figure 1.1). Since then, studies have been using soil temperature at shallow depths (0.5-2 m) to locate aquifers and delineate their flow systems.

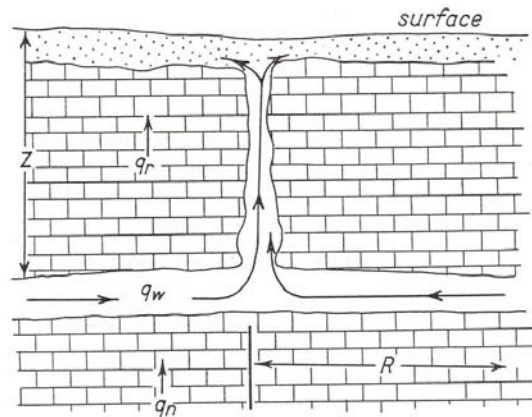


Figure 1.1: Heating of water rising from depth to surface (After Kappelmeyer, 1957).

Cartwright (1968) made use of temperature measurement at a 0.5 m depth to find thermal anomalies caused by shallow alluvial aquifers located at a depth of about 5 m (Figure 1.2). He has shown that the high specific heat of water makes shallow aquifer acts as a heat sink in summer and a heat source in winter and affects the near surface soil temperature.

According to Cartwright (1968), the effect of a shallow aquifer on the overlying material can be illustrated in Figure 1.3 which shows graphically the heat flow through a wall affected by the presence of an internal projecting rip. This would be similar to an aquifer in the zone affected by surface temperature fluctuations where, during the cold and hot months, the aquifer maintains a temperature at some greater depth.

Finally, Cartwright (1968) used a simple mathematical model to describe heat transport between soil-air interface and aquifer-overburden interface. Though his model was the earliest to describe this process, it included a major shortcoming: both land surface and groundwater had predefined standing temperatures (Dirichlet boundary condition). Obviously, this prevented any thermal interaction between the aquifer and the land surface.

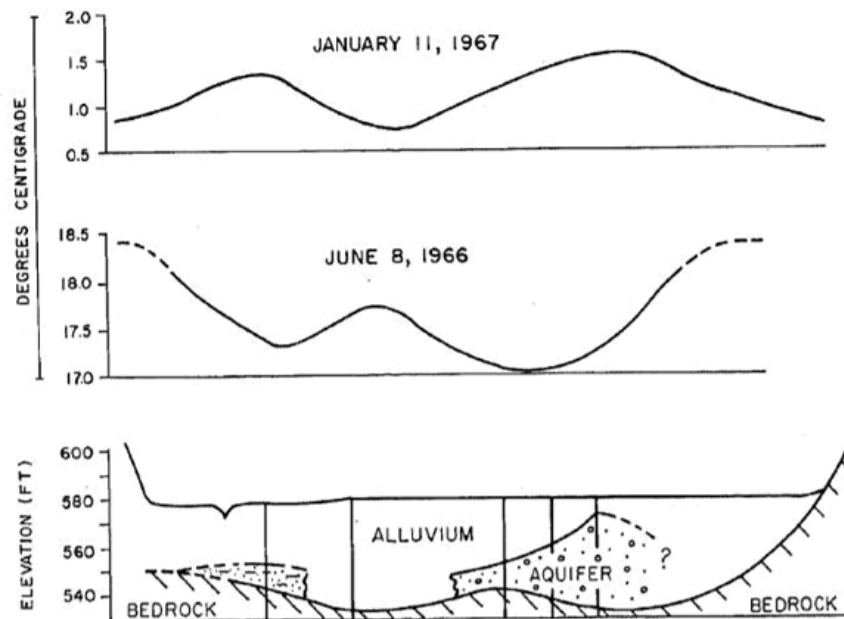


Figure 1.2: Geologic cross section and horizontal thermal profiles at both wintertime and summertime. The shown profiles have been taken at spacing of 15 meters at a depth of 50 centimeters in east-central Illinois, USA (After Cartwright, 1968).

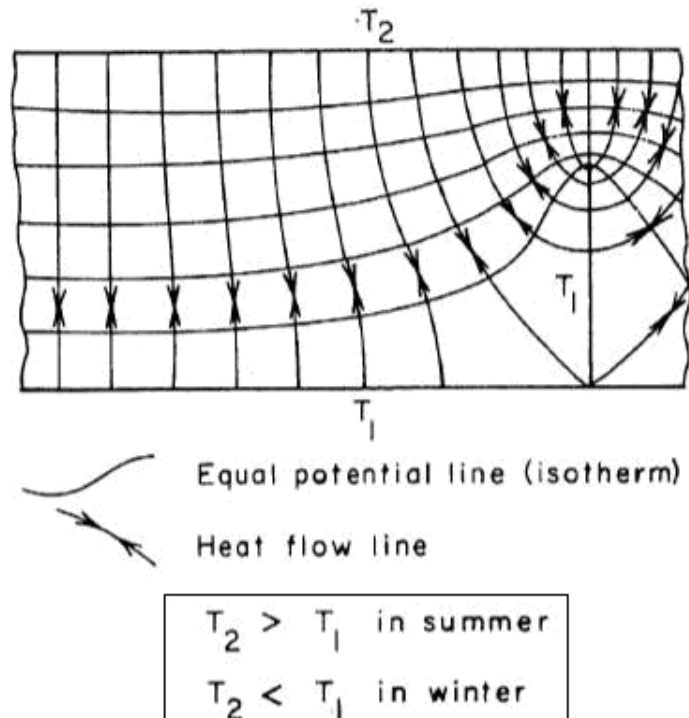


Figure 1.3: Isotherms and flow lines for steady heat conduction through a soil (After Ingersoll et al., 1948, p.203 cited in Cartwright, 1968).

Birman (1969) attributed the small amplitude of annual shallow-earth temperature wave to the presence of shallow groundwater. A year later, Krcmar and Masin (1970) reported that the most important results of geothermic measurements had been the investigation for circulation of both cold and hot underground waters.

Studies of geothermal prospecting for groundwater were continued by Cartwright (1971; 1974). Specifically Cartwright (1974) studied the use of soil temperature measured at 1 m depth to describe the flow of small, shallow groundwater systems. Afterwards, and along the same line, several studies such as: Olmsted et al., 1986; Bense and Kooi, 2004 and Takeuchi, 1980; 1981; 1996; Yuhara, 1998 cited by Furuya et al., 2006, used thermal prospecting to locate shallow aquifers and to delineate their flow systems.

By the advent of remote sensing technologies, scientists were motivated by the accomplishments that had been realized by the in-situ measurements to employ thermal remote sensing in locating and

delineating shallow groundwater systems. The new tool (i.e. remote sensors) provided radiant temperatures of extensive areas. Studies that consider remote sensing capability to detect groundwater effect on land surface temperature are addressed within the following section.

1.2 Groundwater and remote sensing

In spite of the fact that groundwater lies underground and remote sensing devices can not normally penetrate the ground, remote sensing proved efficacy in groundwater studies. Remote sensing has been utilized within various groundwater themes such as: 1) Geologic mapping and lineaments tracing, 2) Model boundary conditions defining, 3) Vegetation Classification, 4) Gravity measurements, 5) Precipitation and evapotranspiration estimation and 6) Groundwater thermal effect on land surface temperature.

1.2.1 Geologic mapping and lineaments tracing

Geologic maps derived from remote sensing have been used widely for groundwater studies. They were helpful in giving valuable information regarding hydraulic conductivity and possible water bearing geological formations. Notable application of remote sensing in groundwater studies is detecting of lineaments which may be a sign for faults and fractures (Mabee and Hardcastle, 1997; Travaglia, 1996; Moore et al., 2002; Shaban et al., 2006). Faults and fractures are basically linear features and hence can be recognized using simple visual interpretation of satellite images (Meijerink et al., 2007). Such geological information is helpful in constructing more realistic conceptual models of groundwater reservoirs; besides, lineaments on the surface have been known as potential channels for groundwater flow in fractured aquifers and hence addressed for locating production wells (Mulwa et al., 2005; Brunner et al., 2007).

1.2.2 Defining boundary conditions

Defining suitable model boundary conditions is essential in building of numerical groundwater models. Those boundary conditions may be rivers and streams, lakes and wetlands, springs and seepage regions. Those features can be delineated on remotely sensed imageries. Land topography is a key boundary condition to groundwater models. With the continuous advancement in remote sensing technology more accurate digital elevation models (DEM) are being produced (Becker, 2006; Meijerink et al., 2007).

1.2.3 Vegetation classification

The presence, speciation, and expansion of plant cover are determined by water and nutrients availability. Hence, vegetation cover classification may offer important signs for groundwater presence and quality (Becker, 2006). This is especially true in arid environments where groundwater discharge may be the only source of water for flora (Nichols, 1994; Klijn and Witte, 1999). For example, Batelaan et al. (1998) utilized remote sensing data in classifying vegetation to study natural ground water discharge in a nature reserve. Multi-spectral remote sensing data are available at low cost and can be used for producing spectral classification and vegetation indexes which are important information regarding groundwater vegetation-groundwater interactions. Since it is possible to obtain a spectral signature for vegetation species, growth and health, groundwater discharge in arid regions can be usually monitored by remote sensors (Meijerink et al., 2007).

1.2.4 Gravity measurements

The NASA Gravity Recovery and Climate Experiment (GRACE) satellites were launched in March 2002. Using GRACE is a recent development that proved to be a good tool for observing changes in water storage within large scale aquifers (Swenson et al., 2003). The basic principle of measuring changes in the mass of the groundwater body is based on consequent changes in the gravity field which is measured by the two GRACE satellites (Rodell and Famiglietti, 2002; Seo et al., 2006). Although GRACE spatial resolution is very low, a time series of gravity could be interpreted into a temporal variation of water storage. In a practical application, Rodell et al. (2007) proved that GRACE is useful to estimate the change in terrestrial water storage, which includes groundwater, soil moisture and snow. The change in groundwater storage can be solely estimated by using supplementary information of soil moisture and snow conditions. They suggested that GRACE may be the only hope for groundwater variations' assessment in regions with limited or poor data availability.

Recently, Chen et al. (2010) used GRACE data to observe a decrease in terrestrial water storage in the southern La Plata river basin of South America over the period 2002-2009. The GRACE data were consistent with accumulated precipitation data from satellite remote sensing, vegetation index changes derived from Terra satellite observations and with the available groundwater level data.

1.2.5 Precipitation and evapotranspiration estimation

Another application of remote sensing data for groundwater studies is the estimation of net recharge to aquifers. For flat terrain net recharge over long time is the long term average residual between precipitation and evapotranspiration. Both can be derived from remote sensing data. For example, Herman et al. (1997) utilized remote sensing for estimating accumulated precipitation for African continent. In their method remotely sensed cloud top temperatures were used jointly with orographic data and numerical simulations. On the other hand evapotranspiration can be derived from multispectral satellite data via surface energy balance systems such as SEBAL (Bastiaanssen, 1995) and SEBS (Su, 2002).

1.2.6 Groundwater effect on land surface temperature

By the advent of remote sensing technologies, scientists were motivated by the accomplishments that had been realized by the in-situ measurements (see section 1.1.4) to employ thermal remote sensing in locating and delineating shallow groundwater systems. The new tool (i.e. remote sensors) provided radiant temperatures of extensive areas.

A key factor to explore groundwater via remote sensing is to trace the influence of groundwater on the land surface. Perhaps the most promising effect groundwater has on land surface is the heat signature. Saturated soils have a greater heat capacity than dry soils, suggesting that remote thermal sensing might be used to estimate depth to water table. The existence of thermal infrared sensors on board of many satellites combined with the potential groundwater effect on surface temperature has led several researchers to look for relation between the depth and areal extension of aquifers and radiometric temperatures (Huntley, 1978).

The majority of investigations that used remote sensing for detecting shallow groundwater effect on surface temperature was conducted between the late 60's (Chase, 1969) and the early 80's (Heilman and Moore, 1982). These studies were accompanied with relevant in-situ measurements and modeling efforts; Quiel (1975) measured the radiant temperature of gravel with varying depth of the groundwater table. He concluded that the influence of groundwater on surface temperature is insignificant if it is deeper than 0.2 m (diurnal damping depth of dry gravel). His conclusion is striking but understandable because gravel allows for a very small capillary rise; consequently, it does not affect the moisture state and the thermal properties of the section above water table. Furthermore, Quiel's

study considered only the penetration of the daily temperature variation and totally neglected the yearly temperature oscillation.

The latter was also neglected in the numerical model built by Huntley (1978), who conducted an important theoretical and practical investigation for aquifer detection using remote sensing. The diurnal numerical model he developed was simple (numerical faculties were not as advanced as it is today), but it was the last and the most detailed model that dealt with this phenomenon. His study concluded that it is impractical to estimate groundwater depth directly using thermal infrared imagery. Actually, his investigation underestimated the effect of groundwater on surface temperature mainly due to two reasons. Firstly, his study neither distinguished hot from cold groundwater nor separated very deep from shallow groundwater. For that reason, the measured subsurface soil temperatures and the depths of groundwater brought forth poor correlation. Secondly, his model was not sophisticated enough to simulate the inter-connection among energy balance components at land surface. Moreover, it did not consider the effect of groundwater on soil moisture and thus the thermal properties of the vadose zone.

To our knowledge, the study by Chase (1969) was one of the earliest attempts to investigate remote sensing capability for mapping the thermal effect of shallow groundwater. In this regard, he found that the (2.5–5.6 μm) band was informative and promising.

This early work was followed by the investigation of Myers and Moore (1972) that made use of seasonal flights with thermal radiometers flown over the Sioux Basin in eastern South Dakota. Soil temperature data (8.0-14.0 μm) were obtained from predawn missions flown on May 7, July 21, August 26 and October 12, 1971. The August 26 imagery showed a broad cool area within the flood plain. This cool area extended over farms with a diversity of land use. Furthermore, a high correlation was found between soil temperature and the aquifer thickness. Their study concluded that late August or early September was the best period for thermal detection of shallow aquifers.

In agreement with the review paper by Becker (2006), and the book by Meijerink et al. (2007), the latest study that we could trace in the literature regarding the investigation of the shallow groundwater effect on land surface temperature was the study of Heilman and Moore (1982). In this study they correlated radiometric temperatures (10.5-12.5 μm) from five scenes captured between 5 June and 4 September, 1978 by the Heat Capacity Mapping Mission, with water table depths measured on these dates. After empirical correction for

vegetation effect, they found that the daytime thermal scene of 4 September had the best correlation. They have demonstrated that radiometric temperature measurements from satellites can be correlated with depth to shallow groundwater if proper deliberations are given to the effect of vegetation. Furthermore they suggested, similar to Huntley (1978), developing a procedure for differentiating groundwater influence from that of soil moisture.

To complete the view, it may be worth mentioning here that some remote sensing investigations utilized the thermal effect of shallow water table in influencing snow cover, like delaying and shortening the period of its occurrence over lowlands relative to the surrounding highlands within a watershed (Falconer et al., 1981), or reducing its reflectance and emissivity (Bobba et al., 1992). Where such phenomena occur, visible to near infrared imageries may be more informative than thermal infrared ones.

1.3 Problem statement

Not only do shallow water table conditions characterize low lands in many drainage basins (Freeze and Cherry, 1979), but it has become a general feature in many of the world's large-scale irrigation systems in various countries, i.e. USA, Mexico, China, India, Pakistan, Australia, etc. (Dregne et al., 1996; Rahman, 2008; Umali, 1993; Middleton and Thomas, 1997; Wichelns, 1999; World Bank, 1992; Xiong et al., 1996). Shallow water table is common in such areas due to high recharge rates, low assimilative capacity of unconfined aquifers and, often, low drainage rates (Wichelns, 1999; Northey et al., 2006).

The possibility of utilizing thermal measurements of operational satellites in observing the depth and the areal extent of shallow groundwater can be of great value in supporting groundwater flow models and in improving the management of vast irrigation systems. Besides, these measurements would be useful in observing the effect of shallow groundwater on surface energy balance, and in bringing that effect within land surface models and climate studies on more solid basis.

Despite the humble faculties of earth observation technology during that early period (section 1.2.6), keen investigations were conducted with regards to tracing shallow groundwater effect on land surface temperature. Nowadays, there are plenty of satellites orbiting the earth and continuously collecting valuable data about the planet surface (Bosilovich et al., 2008). Hence it is quite odd that in spite of

the revolutionary development achieved in this technology, there is hardly any study that researched the utilization of this wealth of data in shallow groundwater studies. Furthermore, this data has not been effectively utilized in mapping shallow groundwater effect on land surface temperature and surface energy balance components thus far.

Prior to any real success in the application of remote sensing techniques in shallow groundwater studies, and prior to solid integration of aquifers within coupled land surface models, it is essential to appreciate the basic physical principles involved in the process. In fact, the question whether shallow groundwater affects land surface temperature or not is still put forth. Furthermore, questions as: when and how this effect takes place or whether it is possible to utilize currently operational satellites in its detection, have not been adequately answered until now.

1.4 Research objective

The main objective of this research is:

To explore and describe the different aspects and basic physical principles involved in the process of shallow groundwater effect on land surface temperature and surface energy balance, and to investigate the potential of remote sensing to delineate this effect.

1.5 Outline of the thesis

The basic principles of shallow groundwater effect on land surface temperature and surface energy balance are presented in Chapter 2. Chapter 3 describes the investigated study area, field measurements and the numerical models and algorithms used in this study.

Chapter 4 explains the preliminary findings of the in-situ groundwater effect reconnaissance, the relationship between soil temperature close to the surface (5 and 10 cm) and water table depth was investigated. The shallow groundwater effect on surface temperature was simulated using a simple one dimensional transient heat transport model, which was built within Flex PDE environment.

Chapter 5 deals with the thermodynamic effect of shallow groundwater. Numerical modeling that progressed in complexity were built to explore how the presence of groundwater, through its distinctive thermal properties within the yearly depth of heat

penetration, affects directly land surface temperature and the entire surface energy balance system thereby.

Chapter 6 portrays the pattern and the magnitude of the combined shallow groundwater effect using numerical simulations that take into consideration the majority of the aspects, through which shallow groundwater affects land surface temperature and the various components of surface energy balance.

Chapter 7 supports the findings and conclusions of Chapter 6 by a practical investigation of the potential of remote sensing for delineating groundwater effect in the study area. The interrelationship between water table depths measured in the field and land surface temperatures retrieved from MODIS images was investigated. The spatial distribution of shallow groundwater effect on surface energy balance components, soil moisture, evaporative fraction and daily evaporation in this area at the day of image acquisition was reconnoitered as well.

Finally, Chapter 8 summarizes and concludes the findings of this research.

2 Theoretical Background

2.1 Shallow groundwater systems

Generally, groundwater is defined as water under positive pressure in the saturated zone of earth materials (Dingman, 2002). Within the context of this study, 'shallow' groundwater means that water table is with the yearly depth of heat penetration and close enough to influence soil moisture at land surface. In such systems, water can move upward from the water table into the vadose zone, driven by surface tension forces. This results in a saturated to nearly saturated zone of negative pressure above the water table (i.e. capillary fringe or tension-saturated zone) which may range in height from about 10 mm for gravel, to 1.5 m for silt and even to several meters for clay (Dingman, 2002).

The effect of shallow groundwater on soil moisture in the vadose zone may further extend above the capillary fringe to the land surface. This is not only due to surface-tension forces, but also due to its effect on the infiltration rate, as a result of air compression and counterflow in bounded soil columns (Grismer et al. 1994; Salvucci and Entekhabi, 1995).

2.2 The energy balance at land surface and heat transfer within soil matrix

At land surface, energy fluxes interact instantaneously with each other in accordance with the prevailing meteorological conditions and the specific thermal and radiative characteristics of soil surface. The surface temperature represents the state variable that continuously adjusts to changes in hydraulic and meteorological forcing in such a way that the energy balance is always being preserved:

$$R_n = LE + H + G \quad (2.1)$$

LE (Wm^{-2}) is latent heat flux that is used for evaporation (in this study we consider bare soil conditions). H (Wm^{-2}) is sensible heat flux which expresses the heat exchange between land surface and the air above it; G (Wm^{-2}) is ground heat flux, that is, the heat that enters the ground or migrates upward to the surface. R_n (Wm^{-2}) is the net radiation, which is the outcome of the radiation irradiated by the sun K_{in} and the sky (εL_{in}) onto the land surface, minus the radiation which is reflected (αK_{in}) or emitted by the land surface ($\varepsilon \sigma T_s^4$), as:

$$R_n = (1 - \alpha) K_{in} + \varepsilon L_{in} - \varepsilon \sigma T_s^4 \quad (2.2)$$

where a , ε are land surface albedo and emissivity respectively, T_s is land surface temperature (K) and σ is Stefan-Boltzmann constant (5.6697 E-8). Soil albedo, α , changes according to soil moisture, θ , as (Idso et al., 1975):

$$\alpha = \alpha_d \exp[-\alpha_a \theta] \quad (2.3)$$

where α_d is dry soil albedo and α_a is an empirical coefficient.

Sensible heat flux is related to temperature gradient between the soil surface and the atmosphere. Following Campbell (1977), we write:

$$H = \rho_a c_a \frac{(T_s - T_a)}{r_H} \quad (2.4)$$

where ρ_a , c_a and T_a are air density (kgm^{-3}), specific heat ($Jkg^{-1}^{\circ}C^{-1}$) and temperature ($^{\circ}C$) at the measurement reference height (z_{ref}); T_s is the temperature ($^{\circ}C$) of soil surface, and r_H is the resistance to surface heat transfer (sm^{-1}) corrected for atmospheric stability.

Latent heat flux is associated with water vapor transfer from soil surface to the atmosphere, as:

$$LE = -L \frac{(\rho_{vs} - \rho_{va})}{r_v} \quad (2.5)$$

where L is the latent heat of vaporization (Jkg^{-1}), E is vapor flux ($kg s^{-1} m^{-2}$), ρ_{vs} and ρ_{va} are vapor density (kgm^{-3}) of soil surface and air at the reference height. r_v (sm^{-1}) is the resistance value for vapor transfer.

Ground heat flux G is a function of thermal conductivity k_s and soil temperature gradient, $\partial T/\partial z$, and expressed by:

$$G = -k_s \frac{\partial T}{\partial z} \quad (2.6)$$

Heat transfer and temperature variation within soil matrix can be simply described by the common diffusion equation:

$$\frac{\partial(k_s \partial T)}{\partial^2 z} = VHC \frac{\partial T}{\partial t} \quad (2.7)$$

where k_s is the thermal conductivity ($Wm^{-1}^{\circ}C^{-1}$), T is temperature ($^{\circ}C$), z is depth (m), VHC is the volumetric heat capacity ($J m^{-3}^{\circ}C^{-1}$) and t is time (s).

Values of thermal conductivity and volumetric heat capacity can be calculated by using the method of de Vries (de Vries, 1963; Wierenga and de Wit, 1970). According to this method and depending on the physical properties of the soil components (i.e. air, water, minerals and organic matter) thermal conductivity can be expressed as:

$$k_s = \frac{\sum_{i=0}^n \phi_i x_i k_i}{\sum_{i=0}^n \phi_i x_i} \quad (2.8)$$

And volumetric heat capacity can be described as:

$$VHC = \sum_{i=0}^n VHC_i \cdot X_i \quad (2.9)$$

where X_i is the volumetric fraction of each soil component, k_i ($Wm^{-1}^{\circ}C^{-1}$) is its thermal conductivity, ϕ_i is its shape factor, VHC_i ($Jm^{-3}^{\circ}C^{-1}$) is its volumetric heat capacity and n is the number of the soil components.

2.3 Shallow groundwater effect

Shallow groundwater affects thermal properties of the region below its water table. Moreover, it alters soil moisture of the zone above its water table which results in affecting its thermal properties, the magnitude of evaporation, albedo and emissivity. Hence shallow groundwater affects land surface temperature and the surface energy balance in two different ways: direct and indirect (Figure 2.1).

2.3.1 The direct effect

The direct way (henceforth referred to as thermodynamic effect) is through its distinctive thermal properties which make groundwater acts as a heat sink in summer and a heat source in winter, and affects heat propagation within soil profile. Among the studies that investigated the thermodynamic effect are the work of Kappelmeyer (1957), Birman (1969), Cartwright (1968, 1974), Bense and Kooi,

(2004), Furuya et al. (2006) and also works by Takeuchi (1980, 1981, 1996) and Yuhara (1998) cited by Furuya et al. (2006).

2.3.2 The indirect effect

On the other hand, the indirect way of groundwater effect is through its effect on soil moisture above water table and its related effects (i.e. evaporation, soil thermal properties of vadose zone, land surface emissivity and albedo). A number of studies partly considered the indirect effect of shallow groundwater in terms of its effect on soil moisture of the vadose zone and at land surface (York et al., 2002; Liang and Xie, 2003; Chen and Hu, 2004; Yeh et al., 2005; Fan et al., 2007; Gulden et al., 2007; Niu et al., 2007; Lo et al., 2008; Yuan et al., 2008; Jiang et al., 2009).

Studies that dealt with the thermodynamic effect explored that effect on soil temperature at some depth under land surface. By their deep measurements, they aimed at eliminating the indirect effect. Consequently they missed out considering that effect on temperature and energy fluxes at land surface. On the other hand, studies that considered the indirect effect were centered on the effect of soil moisture in terms of its mass on the water budget and evapotranspiration at land surface. The various aspects of this effect were not considered entirely in those studies. Actually, there was hardly any sole study that conceptually and numerically discriminated the thermodynamic effect from the effect of soil moisture.

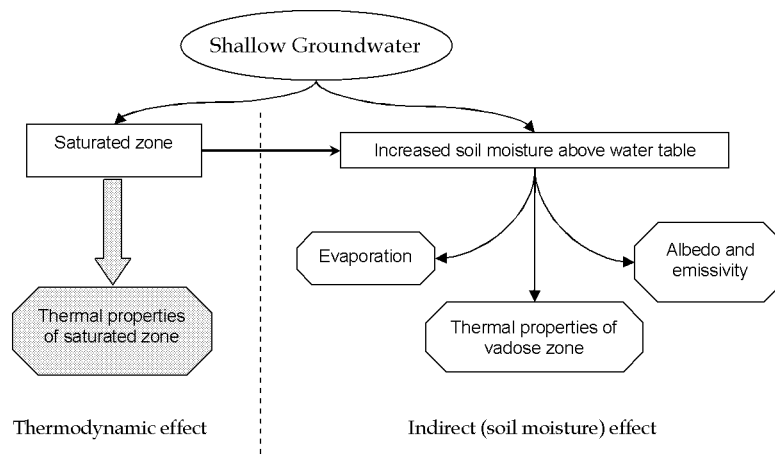


Figure 2.1: Schematic description of the two different effects of groundwater

2.3.3 The combined effect

The combined effect is the upshot of the direct and indirect effects. Figure 2.2 is a sketch of how shallow groundwater affects the different components of the energy balance at land surface. The component that prospers most when the soil moisture rises by shallow groundwater presence is latent heat flux (LE). Thus, more energy is spent for evaporation leaving less energy to heat the soil surface. Consequently, the cooler soil surface induces smaller thermal exchanges between the top surface soil and both the air above (sensible heat flux, H) and the subsurface soil beneath (ground heat flux, G).

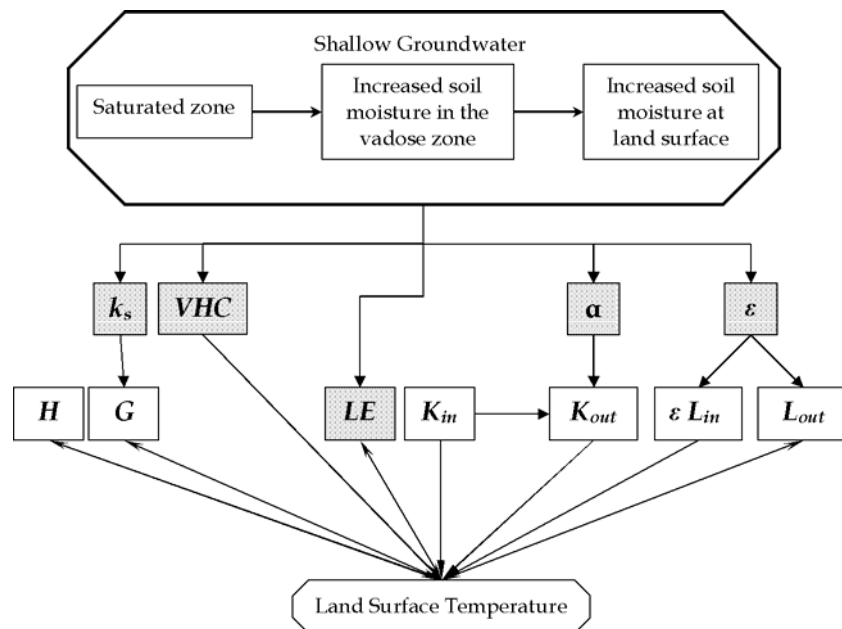


Figure 2.2: Schematic description of shallow groundwater effect on land surface temperature and the different components of surface energy balance.

Furthermore, the presence of shallow groundwater, since it affects soil moisture, affects thermal properties of both saturated and unsaturated zones (equations (2.8 and 2.9)). Through its effect on thermal conductivity and volumetric heat capacity of the soil profile, groundwater alters the propagation of heat in the subsurface (equation (2.7)) and thereby affects soil temperature and ground heat flux (equation (2.6)). Whereas the change in thermal conductivity affects the intensity of ground heat flux and both diurnal and annual heat penetration depths, the change in volumetric heat

capacity alters the amount of heat that can be stored in soil layers. As a result, both amplitude and phase of diurnal and annual waves of ground heat flux and soil temperature are affected.

Net radiation, R_n , (equation (2.2)) has three components that are likely to be influenced by the wetness of land surface, namely; the reflected shortwave radiation (aK_{in}) and both absorbed and emitted longwave radiation (ϵL_{in} and $\epsilon\sigma T_s^4$). The first component (aK_{in}) is controlled by albedo (equation (2.3)), while the last two are dependent on emissivity; both albedo and emissivity vary with soil moisture. Nevertheless, soil emissivity may have a minor effect since it is involved in two components of comparable magnitude acting in opposite directions, i.e. ϵL_{in} and $\epsilon\sigma T_s^4$ (equation (2.2)).

3 Materials and Methods

To reach the goal of this study, three paths were followed: in situ measurements, numerical simulations and remote sensing data manipulations.

3.1 Study area and field measurements

3.1.1 Study area description

Al-Balikh river basin is in northern Syria (Figure 3.1), with a total area of 370 km^2 . The basin is located eastern Euphrates reservoir which supplies the basin by water for irrigation. The measurements covered an area of about 186 km^2 , between latitude $36^\circ 02'$ to $36^\circ 13'$ N and longitude $38^\circ 46'$ to $39^\circ 03'$ E. Al-Balikh river originates in the spring of 'Ayn al-Arus' (Syria) and flows due south and joins the Euphrates near Ar-Raqqa city. Large parts of the river have been canalized recently.

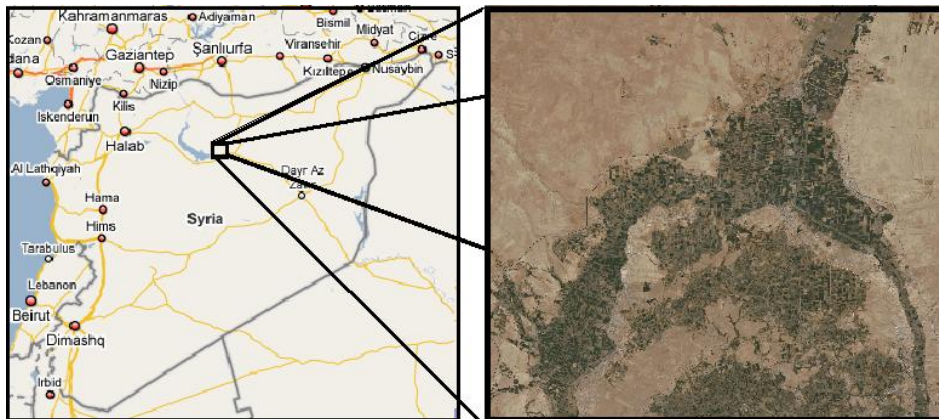


Figure 3.1: Study area location within Al-Balikh river basin in northern Syria.

Many investigation and consulting firms addressed this area before constructing a complete irrigation and drainage system. Among those companies are: Nedeco (The Netherlands) in 1963, Sir Alexander Gibb and Partners (England) in 1966, and Sogeria (France) in 1976. The project of reclamation these lands started in 1970; Irrigation canals, pumping stations, leveling, and drainage network have been established some 40 years ago. After accomplishing Euphrates dam in 1973, the area has entered into service. The entire area is now under service by canals and drainage systems; however the performance is somewhat poor in some places. The area is equipped with a dense

network of piezometers to monitor water level and drainage efficiency. However the large number of piezometers (around 198) makes it difficult to conduct their reading frequently; they are read only four times per year.

According to Alkhaier (2003) the agro-ecological conditions are very uniform over the study area; topography, climate, geology and soils conditions are relatively invariant. The study area represents a flat region of reclaimed agricultural fields. Hence, there is no considerable topographic relief within the area under consideration. Somewhat poorly drained soils are predominant in this area, and in many places, shallow water tables exist all year round. Water table depth in the area ranges between 1 and 10 m.

The geologic map (Figure 3.2) shows that major parts of the study area are composed of Quaternary alluvium (loams, sandy loams, gravel, mud, pebbles and sands). Generally, soils of the surface layer can be classified as silty clay; furthermore clayey and gypsum horizons may be encountered at different shallow depths throughout the basin. This was clear from the soil investigation conducted within this study and the investigation by Alkhaier (2003), and agrees well with information retrieved from approximately 95 borehole records conducted by the General Organization for Land Reclamation, Ar-Raqqa, Syria (Figure 3.3).

The area is characterized by steppe climate (Köppen climate classification), which is a semi-dry climate with an average annual rainfall of less than 200 mm. Free water surface evaporation in the region is high, and reaches up to 14 mm daily during summer period. This means that crops in the entire area are almost fully dependent on irrigation. The weather data were obtained from the nearby weather station (Ar-Raqqa, 35° 57' N, 39° 00' E). Climate chart of the region is shown in Figure 3.4. In this area, air temperature usually has a high contrast between day and night.

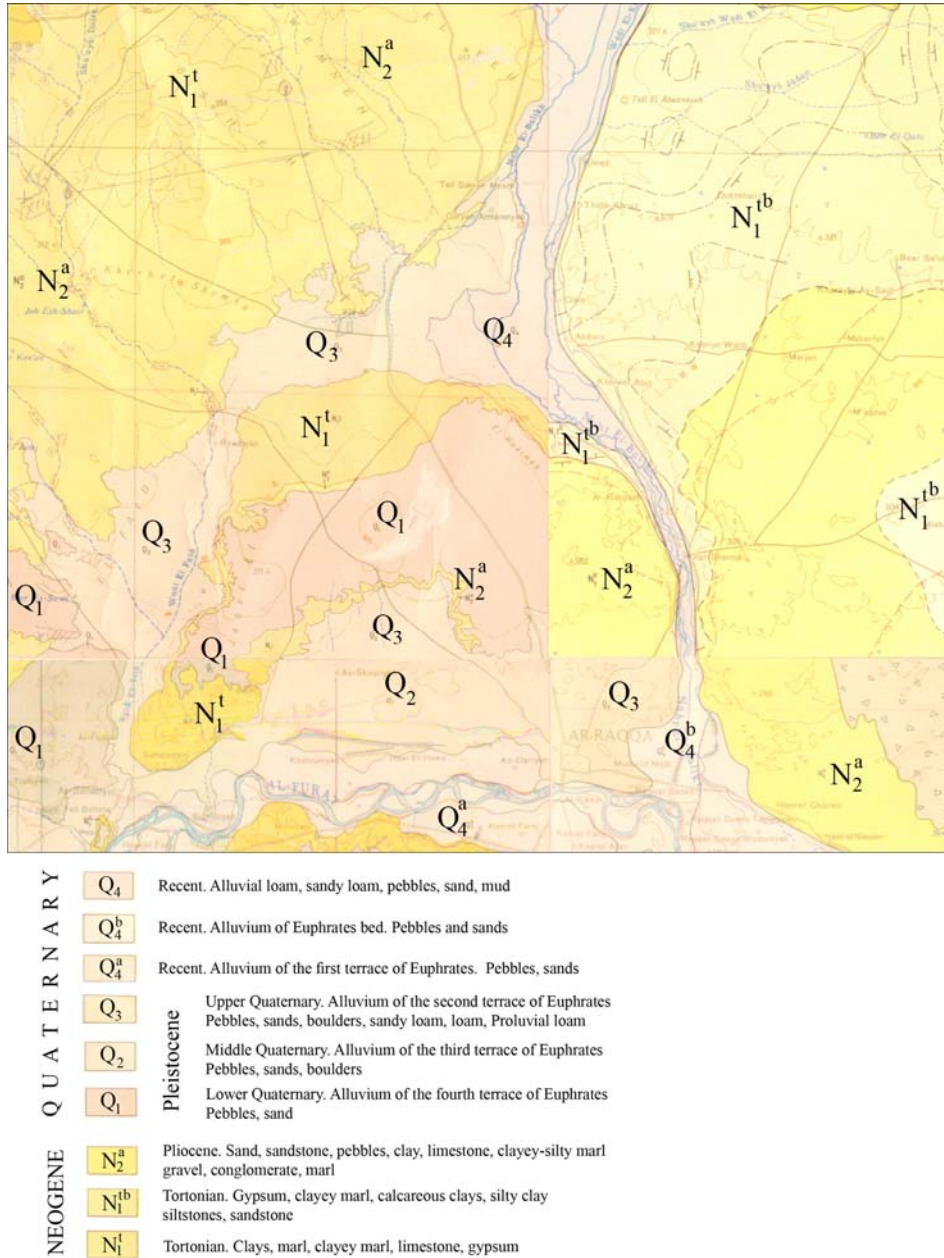


Figure 3.2: Geological map of the study area by the ministry of industry department of geological and mineral research, 1963, the map is a part of a scanned 4 tableaux plats mosaic.



Figure 3.3: Scenes from the study area. Drilling a piezometer. The soil core of a borehole. A sample of a boreholes conducted by the General Organization for Land Reclamation, Ar-Raqqa, Syria.

The main crop cultivated is cotton, which is often planted in rotation with wheat (Alkhaier, 2003). The following cropping systems are observed (Figure 3.5):

1. Cotton, not in rotation.
2. Cotton in the first year, immediately followed by wheat in autumn. After harvesting the wheat in spring the land is left fallow until the third year when cotton is planted again (two years rotation).
3. Wheat in the first year. The land then is left fallow for the rest of the year and the next year until autumn when wheat is planted again (two years rotation).
4. Cotton in the first year. The land thereafter is fallow for one year till next autumn when wheat is planted. After the harvesting of the wheat, the land is left fallow for another year and in the spring of the fourth year, cotton is planted again (three years rotation).

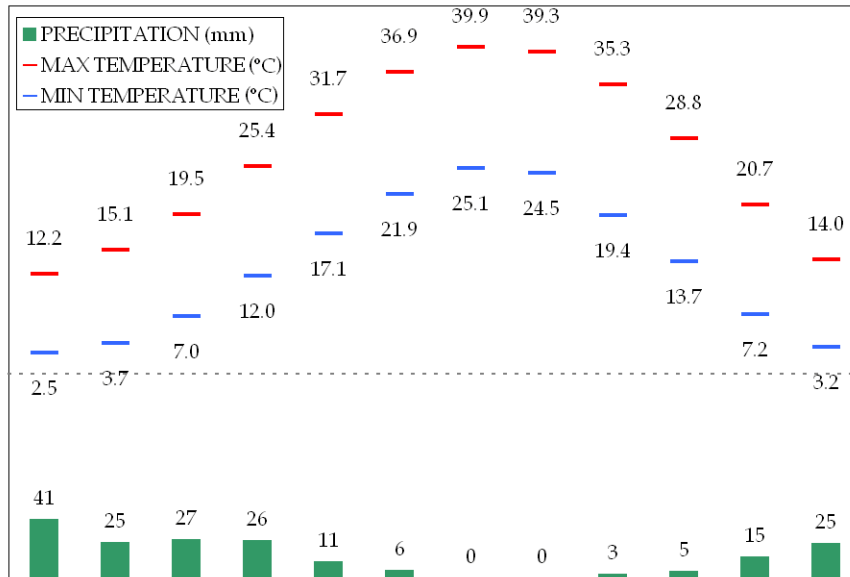


Figure 3.4: Climate chart of the region.

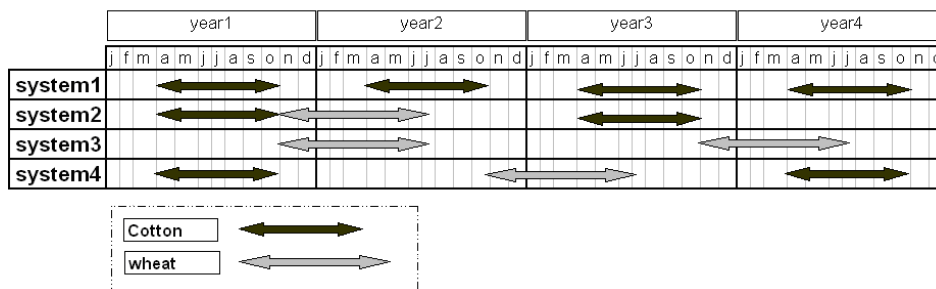


Figure 3.5: Four cropping systems in the area (After Alkhaier, 2003).

3.1.2 Field measurements

During this study, the area has been visited several times. Field measurements and data collection conducted within the study area included soil moisture measurements, water table depth readings, soil composition analysis, geologic maps and weather data collection.

In January 2007, surface soil moisture and water table depth readings were conducted at about 90 locations. Water table depth which was measured manually using a simple sounding device (Figure

3.6, right). Additionally, some soil samples were brought to the laboratory at the General Organization for Land Reclamation for texture analysis and soil moisture verification. Soil moisture of the upper 5 cm was measured in-situ using Stevens' Hydra probe (Figure 3.6, left). The Stevens' Portable Hydra probe has an Instantaneous sensor response. The Stevens' Portable Hydra Reader acquires, displays, and logs data directly from the Hydra Probe Sensor and converts raw Hydra Probe voltages directly into soil moisture, salinity, and temperature readings without requiring additional processing or calibration.



Figure 3.6: **Left:** Soil moisture measurements device (Stevens' Portable Hydra Reader and Stevens' Hydra probe). **Right:** water table depth reading device.

In January 2008, seven locations were chosen for continuous temperature measurements. In each location, two temperature loggers (HOBO Pendant Temperature and Light Data Logger, 64K model) were deployed in the soil at two different depths (approximately 5 and 10 cm). The loggers recorded temperature every ten minutes for almost six days duration. Upon loggers' deployment, water table depths were measured, soil samples of the upper 5 cm were taken to the laboratory for texture analysis and soil moisture determination.



Figure 3.7: Two temperature loggers (HOBO Pendant) deployed in the soil at two different depths (approximately 5 and 10 cm).

3.2 Numerical simulations

To get a detailed insight into the processes that play a role in groundwater effect on land surface temperature and surface energy balance, variant numerical experiments have been conducted. In this study two numerical tools were used: FlexPDE and SHAW.

3.2.1 FlexPDE

FlexPDE (PDE Solutions, Inc.) is a scripted finite element model builder and numerical solver. After the user writing a script, FlexPDE performs the operations necessary to turn a description of a partial differential equations system into a finite element model, solve the system, and present graphical and tabular output of the results.

FlexPDE performs the entire range of functions required for solving partial differential equation systems: an editor for writing scripts, a mesh generator for building finite element meshes, a finite element solver to find solutions, and a graphics system to plot results (Figure 3.8).

The problem of heat transfer within soil profile was programmed within FlexPDE environment. Several scenarios were investigated to explore the effect of shallow groundwater on land surface temperature and ground heat flux. This is explained in the following chapters.

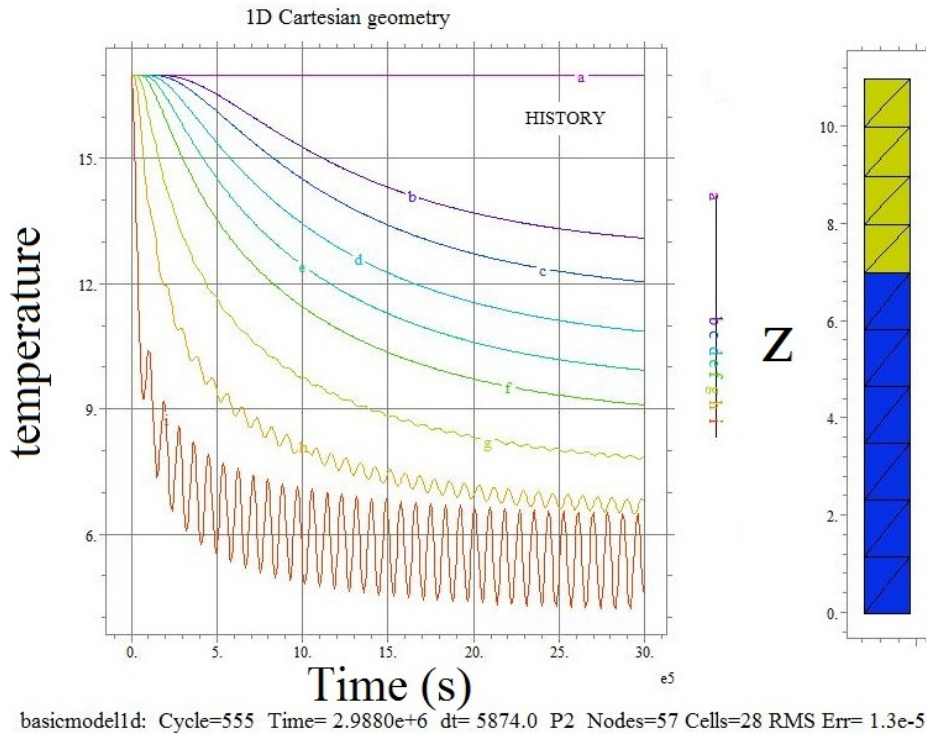


Figure 3.8: A sample of FlexPDE graphical output of temperature at diverse depths within the soil profile.

3.2.2 SHAW

The Simultaneous Heat and Water (SHAW) model originally was developed to simulate soil freezing and thawing (Flerchinger and Saxton, 1989). It simulates heat, water and solute transfer within a one-dimensional profile which may include the effects of plant cover, dead plant residue, and snow. Its ability to simulate heat and water movement through plant cover, snow, residue and soil for predicting climate and management effects on soil freezing, snowmelt, runoff, soil temperature, water, evaporation, and transpiration has been established. SHAW can provide useful information for evaluating management and climate effects on biological and hydrological processes, i.e. seedling germination, insect populations, soil freezing, water infiltration, runoff, and groundwater seepage.

The physical system described by the SHAW model consists of a vertical, one-dimensional profile extending from the vegetation canopy, snow, residue, or soil surface to a specified depth within the

soil (Figure 3.9). The system is represented by integrating detailed physics of a plant canopy, snow, residue and soil into one simultaneous solution.

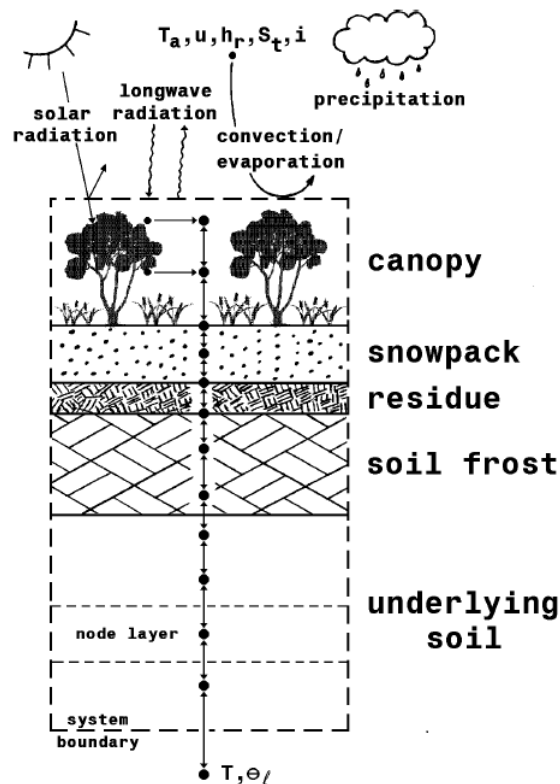


Figure 3.9: Physical system described by the SHAW model. (T_a is temperature, u is wind speed, h_r is relative humidity, S_t is solar radiation, i is precipitation, T is soil temperature, and θ_l is water content.) (After Flerchinger, 2000)

The ability of SHAW to represent shallow groundwater conditions made it suitable for the purpose of this study. Since it can simulate only one-dimensional profile, several simulations were run to investigate the different scenarios of water table level within soil profile. The mathematical representation details of the physical system of SHAW are demonstrated in subsequent chapters.

By simulating water and energy fluxes within soil profiles under actual forcing weather conditions, SHAW was useful in investigating the various features of groundwater effect on land surface

temperature and surface energy balance, and in highlighting the chief factors within this effect.

3.3 Remote sensing data manipulations

The final path in this study involves using remote sensing data of the study area to inspect the spatial and temporal patterns of shallow groundwater effect on land surface temperature and surface energy balance.

3.3.1 Satellite data

Being rich in spectral bands with moderate spatial resolution, and providing free-of-charge images four different times per day, MODIS (Moderate-resolution Imaging Spectroradiometer) instrument was chosen to be exploited in this study. MODIS provides a broad range of land, sea, and atmosphere observations to study global change and valuable data sets to study various environmental problems.

MODIS is a payload scientific instrument launched into Earth orbit by NASA in 1999 on board the Terra Satellite, and in 2002 on board the Aqua satellite. Together the instruments image the entire Earth every 1 to 2 days. MODIS captures images of 36 spectral bands ranging in wavelength between 0.4 μm and 14.4 μm . The numerous bands of MODIS have three spatial resolutions: 250 m, 500 m, and 1000 m, and provide valuable data regarding land cover type and dynamics, vegetation indices, land surface temperature, emissivity and albedo.

MODIS data and products are available at no charge from the archive of LP DAAC (Land Processes Distributed Active Archive Center), provided that they are cited properly in the published research. MODIS products are distributed in Hierarchical Data Format for Earth Observing System (HDF-EOS). The MODIS Reprojection Tool Swath (MRTSwath) was developed to process MODIS swath products, specifically those archived at LP DAAC (MOD11_L2, MYD11_L2, MOD14, and MYD14). It is available freely to all registered users from the LP DAAC Tools Website. MRTSwath provides the capability to transform HDF-EOS swath format to a uniformly gridded image that is geographically referenced according to user-specified projection and resampling parameters.

After transforming MODIS data from HDF-EOS swath format to a projected GeoTIFF image and resampling for appropriate spatial resolution, they can be imported to the Integrated Land and Water Information System (ILWIS) for further processing.

3.3.2 ILWIS

ILWIS (Integrated Land and Water Information System) is a Geographic Information System (GIS) with Image Processing capabilities. It includes a complete package of image processing, spatial analysis and digital mapping. It has been developed by the International Institute for Aerospace Survey and Earth Sciences (ITC), Enschede, The Netherlands, and it is freely available as open source software.

Being a GIS and Remote Sensing package, ILWIS allows managing and handling geo-spatial and remote sensing data. Useful information can be generated about the spatial and temporal processes that take place at the earth surface. Further, it can be an important tool for land use and urban planning, natural hazards management, pollution analysis, and many other processes that have spatial and temporal patterns.

ILWIS can be used for transforming MODIS raw data to radiance or reflectance, and for computing brightness temperature, albedo, emissivity, vegetation indexes and land surface temperature. It can be also used to calculate surface energy balance maps using available remote sensing algorithms such as Surface Energy Balance System (SEBS).

3.3.3 SEBS

To explore the effect on the variant surface energy balance components SEBS was applied using MODIS data of the study area. SEBS is an advanced remote sensing algorithm developed by Su (2001) for estimating atmospheric turbulent fluxes using satellite earth observation data.

It consists of: a set of tools for determining the land surface physical parameters from spectral reflectance and radiance, an extended model for determining the roughness length for heat transfer, and a new formulation for estimating the evaporative fraction on the basis of energy balance at limiting cases. After estimating all terms of the surface energy balance using SEBS, additional important physical information can be retrieved easily, such as evaporative fraction, daily evaporation and surface soil moisture.

SEBS requires three sets of input information: 1) Land surface albedo, emissivity, temperature, fractional vegetation coverage and

leaf area index, and the height of the vegetation. 2) Air pressure, temperature, humidity, and wind speed at a reference height. 3) Incoming solar radiation and longwave radiation.

In SEBS, the friction velocity, sensible heat flux and the Obukhov stability length are obtained by solving the system of non-linear equations. All calculations use the Monin-Obukhov Similarity (MOS) functions given by Brutsaert (1999).

4 Exploring Shallow Groundwater Effect on Surface Soil Temperature Using Field Measurements and a Simple Numerical Model*

* Based on:
Alkhaier, F., R. J. Schotting, and Z. Su (2009), A qualitative description of shallow groundwater effect on surface temperature of bare soil, *Hydrology and Earth System Sciences*, 13, 1749–1756.

4.1 Introduction

Whether or not shallow groundwater affects land surface temperature is important in many aspects. Land surface temperature is a key factor in solving surface energy balance and affects all its components (i.e. latent, sensible and ground heat fluxes). Besides, land surface temperature is the straightforward means through which thermal remote sensing can detect the presence, depth and areal extent of groundwater perching at shallow depths.

In spite of the numerous studies which dealt with heat transfer and temperature distribution within the soil profile and at land surface, a few have investigated the effect of shallow groundwater on the behavior of surface soil temperature.

The objective of this chapter is to explore the effect of shallow groundwater on land surface temperature using in situ measurements and to examine the reason behind this effect with a simple numerical model. A detailed numerical model that can simulate the energy balance components and solve this balance for land surface temperature and soil moisture is beyond the scope of this chapter.

In this chapter the relationship between soil temperature close to the surface (5 and 10 cm) and water table depth was investigated by correlating the daily minimum, maximum and average soil temperature readings to water table depth. To simulate the effect of shallow groundwater on land surface temperature, a one dimension transient heat transport model was built using FlexPDE (PDE Solutions, Inc.), a scripted finite element model builder and numerical solver.

In the numerical simulation of this chapter the groundwater existence within the soil profile is expressed by the distinctive values of both thermal conductivity and volumetric heat capacity of the saturated soil. Saturated soils naturally have high values of both.

4.2 Methods and materials

4.2.1 Field measurements

In January 2008 (winter time in Syria) seven locations (Figure 4.1) with dissimilar water table depths were chosen for measurements. In each location, two temperature loggers were deployed in the soil at two different depths (approximately 5 and 10 cm). The loggers

recorded temperature every ten minutes for almost six days duration. However, taking into account only the full 24- hour days restricted the data to five days (from 16 to 21 January). Table 4.1 presents the weather data for the experiment period and for some days before.



Figure 4.1: Study area with observation locations (Google Earth image).

Upon loggers' deployment, water table depths were measured, soil samples of the upper 5 cm were taken to the laboratory for texture analysis and soil moisture determination.

Table 4.1: The weather data for the experiment period and for some days before: Minimum and maximum air temperature ($^{\circ}\text{C}$), average relative humidity (%), average air pressure (mb), rain (mm) and average wind speed (ms^{-1}).

	Min T $^{\circ}\text{C}$	Max T $^{\circ}\text{C}$	RH %	P Mb	Rain mm	Wind ms^{-1}
13-Jan	-9	7	68.5	974.5	0	2.5
14-Jan	-8	8	69.5	977	0	1.5
15-Jan	-9	8	66	978.5	0	1.9
16-Jan	-10	9	63.5	978	0	1.8
17-Jan	-11	8	68.5	979	0	1.5
18-Jan	-9	11	65.5	981	0	1.5
19-Jan	-9	12	63.5	977	0	0.8
20-Jan	-9	14	63.5	973.5	0	0.6
21-Jan	-8	14	66	973.5	0	0.6

To omit the effect of soil moisture difference on soil temperature among the measurement locations, soils at the loggers' locations were watered until saturated immediately before the last day of the experiment. The temperature of the applied water was just above the freezing point, as it was taken from the nearby irrigation canals where water froze at the surface of these canals.

To explore the relationship between groundwater depth and temperature oscillations of soil at land surface, correlation coefficients were calculated between, on one hand, the maximum, minimum and average daily soil temperatures, and the average water table depths for a year backward, on the other. Further on, the p-values (Schervish, 1996) were calculated to test the significance of the above resultant correlations. In addition, the maximum, minimum and average daily temperatures at the different sites of measurement for two days (day 3, as a representative of the four dry days, and day 5, the wet day) were plotted against the average water table depths. Also, soil moisture values of the upper 5 cm at the different locations were plotted against average water table depths.

4.2.2 Numerical simulations

Daily ground heat flux, G (Wm^{-2}), can be described analytically under periodic forcing assumption (Horton and Wierenga, 1983; Santanello and Friedl, 2003) as:

$$G_{daily} = k_s A_1 \sqrt{\frac{2\pi}{\alpha p_1}} \sin\left(\frac{2\pi t}{p_1} + \frac{\pi}{4}\right) \quad (4.1)$$

This can be extended to describe the yearly ground heat flux by:

$$G_{yearly} = k_s \left[A_1 \sqrt{\frac{2\pi}{\alpha p_1}} \sin\left(\frac{2\pi t}{p_1} + \frac{\pi}{4}\right) + A_2 \sqrt{\frac{2\pi}{\alpha p_2}} \sin\left(\frac{2\pi t}{p_2} + \frac{\pi}{4}\right) \right] \quad (4.2)$$

where k_s and α are average soil thermal conductivity ($Jm^{-1}s^{-1}^{\circ}C^{-1}$) and average thermal diffusivity (m^2s^{-1}). A_1 and A_2 ($^{\circ}C$), respectively, are the daily and yearly temperature amplitudes at land surface respectively, p_1 is one day and p_2 is one year expressed in the time unit of the equation (s).

As soon as heat penetrates the soil its transfer can be described by the heat diffusion equation (equation 2.7).

FlexPDE, a scripted finite element model builder and partial differential equations numerical solver, has been utilized to simulate heat transfer (equation 2.7) in one dimension of the soil profile. Supposing that groundwater existence within the soil profile does not affect the energy balance at land surface, the same ground heat flux, G (equation 4.2), was applied as an upper boundary condition (Neumann boundary condition) at the top of two different profiles:

- The first profile has no groundwater. So, it has a single value of thermal conductivity and another single value for volumetric heat capacity (please note that the simulation was simplified by assuming that the soil profile is homogenous with invariant soil thermal properties).
- The second profile has shallow groundwater perching at different depths (one, two, three, four and five meters, respectively) from land surface downwards. Therefore, it has two different sections with different values of both thermal conductivity and volumetric heat capacity. Values of thermal conductivity and volumetric heat capacity of the unsaturated part of the second profile were given exactly the same values of the first (dry) profile.

The lower boundary condition at ten meters depth (approximately the yearly penetration depth of heat) was set as a fixed temperature of 22 °C (Dirichlet boundary condition), which is the annual deep soil temperature of the region.

The simulations were run for one year duration, after one year of pre-simulation to reach the actual initial boundary condition. The resultant land surface temperature of the two profiles was then compared to each other.

4.3 Results

4.3.1 Results from field measurements

Table 4.2 presents the correlation coefficients between, on one hand, the maximum, minimum and average daily temperatures at the two depths (5 and 10 *cm*) and the average water table depths for a year before, on the other. And Table 4.3 contains the p-values corresponding to the correlation coefficient of Table 4.2.

Table 4.2: Correlation coefficients between the min, max and average daily temperatures at the two depths (5 and 10 cm) and average water table depths.

	Minimum temperature		Maximum temperature		Average temperature	
	5 cm	10 cm	5 cm	10 cm	5 cm	10 cm
day1	0.03	-0.07	-0.85	-0.78	-0.69	-0.69
day2	0.06	-0.14	-0.85	-0.77	-0.73	-0.76
day3	0.08	-0.11	-0.83	-0.75	-0.70	-0.77
day4	0.04	-0.28	-0.71	-0.67	-0.72	-0.78
day5	0.22	-0.03	-0.75	-0.66	-0.55	-0.68

It is clear that the correlation coefficients values of the minimum temperatures are very low and have contradicting signs (negative and positive) between 5 and 10 cm, while those for maximum and average temperatures are high and have negative sign. Another remark can be elicited here that the values of the correlation coefficients did not change significantly in the last day when the soils were saturated.

Table 4.3: P-values for the Correlation coefficients of Table 4.2.

	Minimum temperature		Maximum temperature		Average temperature	
	5 cm	10 cm	5 cm	10 cm	5 cm	10 cm
day1	0.95	0.89	0.02	0.04	0.09	0.09
day2	0.89	0.77	0.02	0.04	0.06	0.05
day3	0.86	0.81	0.02	0.04	0.08	0.04
day4	0.93	0.54	0.08	0.10	0.07	0.04
day5	0.63	0.95	0.05	0.11	0.20	0.09

Studying the p-values in Table 4.3, it can be noticed that the high correlation coefficients for the maximum and average temperatures have very small values of p-values. The observation that most of these values are smaller than 0.10, and many are smaller than 0.05, indicates that those high values of correlation coefficients are statically significant. At the same time it can be noticed that the p-values corresponding to the low values of correlation coefficients for the minimum temperatures are large, which is understandable as there is no correlation for those minimum temperatures.

To inspect the relationship between soil temperature oscillations and water table depth schematically, the maximum, minimum and average daily temperatures plotted against the average water table depths at the different measurement sites for the third day (chosen randomly out of the four dry days) are shown in Figure 4.2, and for the last day (wet day) in Figure 4.3. Depending on these figures, one can recognize that the deeper the water table is the lower the maximum and average values of soil temperature are. Whereas, the relationship between the minimum temperatures and the water table depth might hardly exist.

Exploring Shallow Groundwater Effect on Surface Soil Temperature Using Field Measurements and a Simple Numerical Model

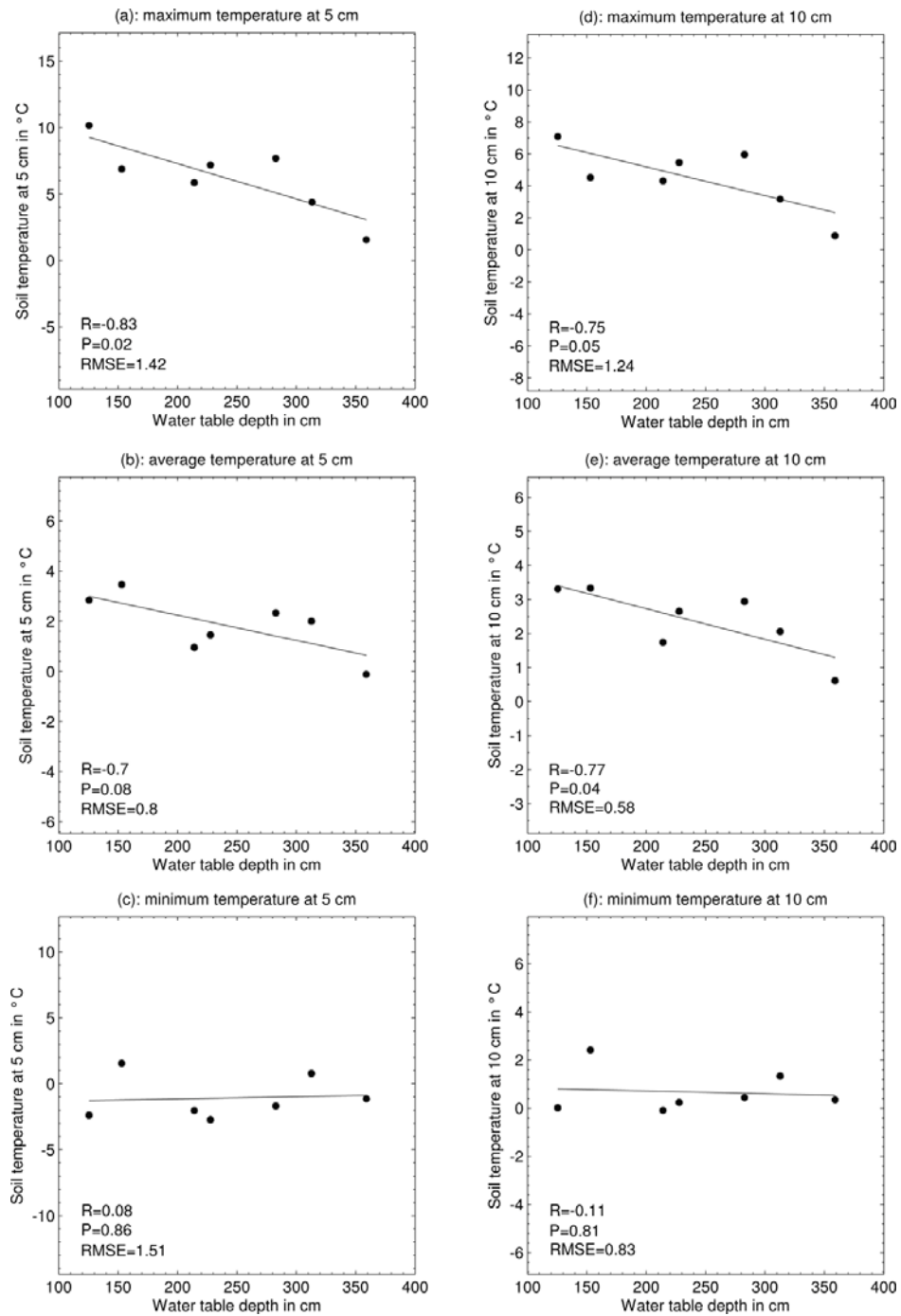


Figure 4.2: Min, max and average temperature vs. water table depth of the third day for temperature measurements at 5 and 10 cm depth.

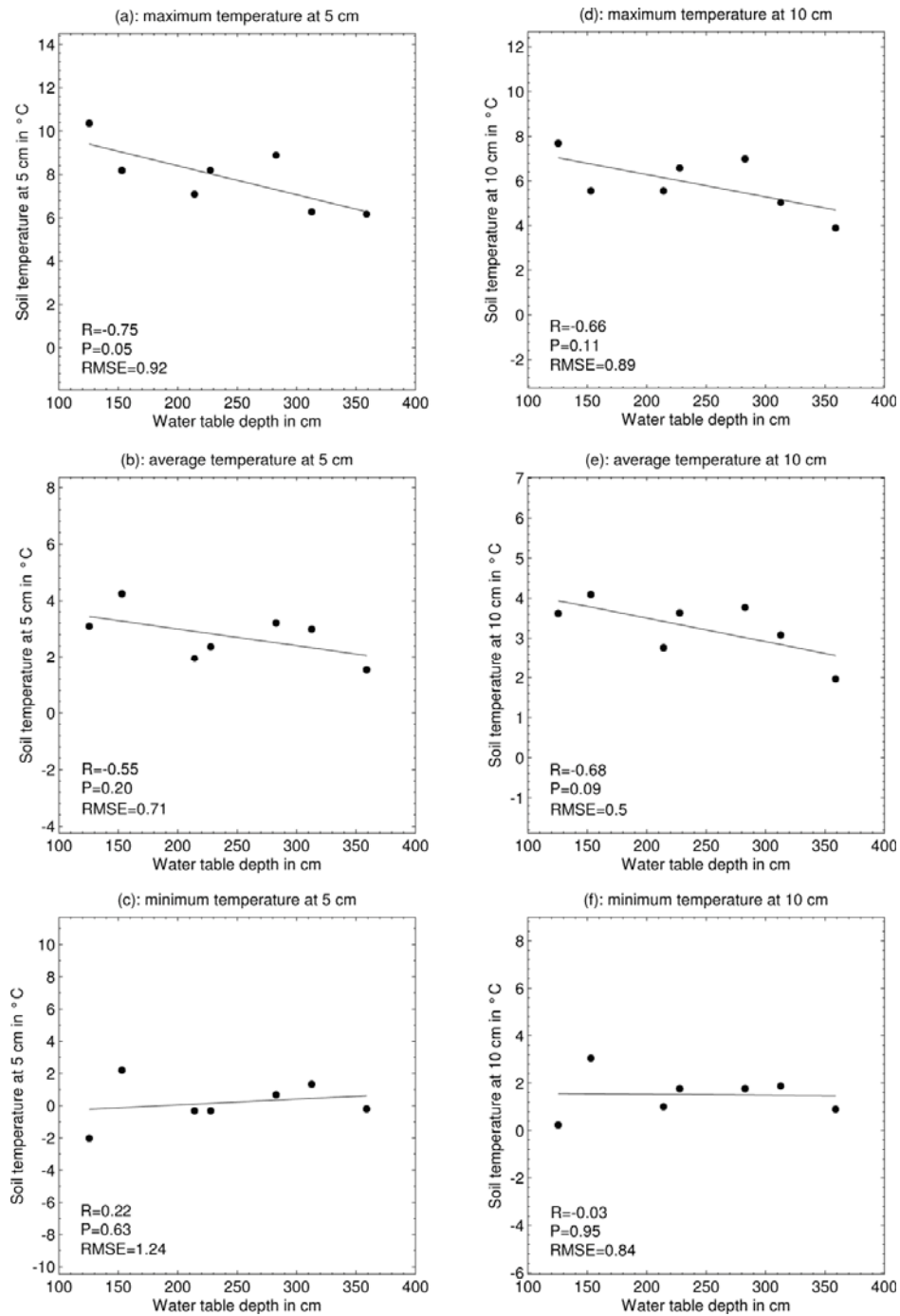


Figure 4.3: Min, max and average temperature vs. water table depth of the last day (wet soil) for temperature measurements at 5 and 10 cm depth.

For both figures, it is clear that the maximum temperature has the highest correlation coefficient followed by the average temperature, while the minimum temperature has very low correlation coefficient. Moreover, there is no drastic change in the correlation coefficients before and after wetting the soils.

Figure 4.4 shows the relationship between volumetric soil moisture of the upper 5 cm measured at the seven different locations and the average water table depth. It can be seen that soil moisture decreases when the depth to groundwater increases.

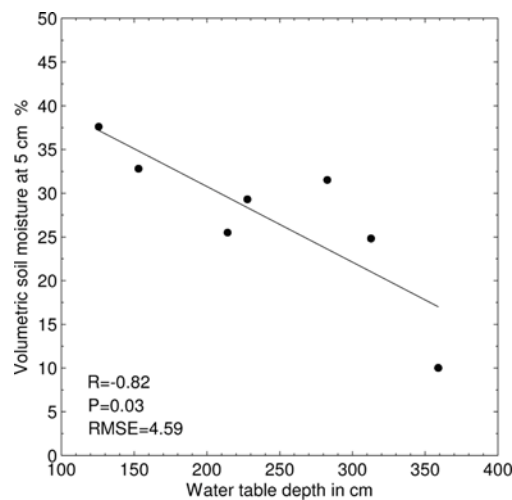


Figure 4.4: Soil moisture of the upper 5 cm vs. water table depth.

4.3.2 Results from numerical simulations

Values of thermal conductivity ($Jm^{-1}s^{-1}^{\circ}C^{-1}$) and volumetric heat capacity ($Jm^{-3}^{\circ}C^{-1}$) of the dry and saturated sections of the simulated profiles, calculated using equations (2.8) and (2.9) are shown in Table 4.4.

Table 4.4: Soil thermal properties used in the simulations.

	Thermal Conductivity ($Jm^{-1}s^{-1}^{\circ}C^{-1}$)	Volumetric Heat Capacity ($Jm^{-3}^{\circ}C^{-1}$)
Dry Soil	0.72	1.21E+06
Saturated Soil	1.27	3.10E+06

To give the reader an impression of the range and the shape of the simulated land surface temperature oscillation investigated in this hypothetical numerical experiment, Figure 4.5 presents the land surface temperature of the dry profile for the simulated year which begins in October. It can be observed that the lowest temperatures occur in February and the highest temperatures occur in August.

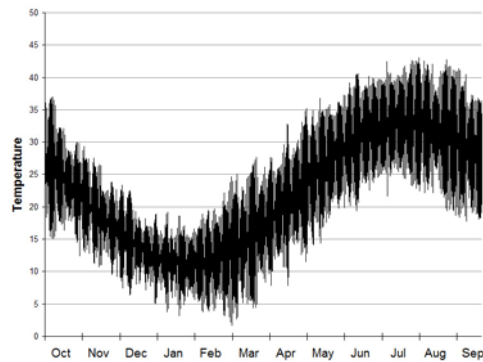


Figure 4.5: Land surface temperature oscillations of the simulated year.

The difference between the simulated values (land surface temperature of the profile with groundwater perching at one meter, minus the land surface temperature of the dry profile) is shown in Figure 4.6.

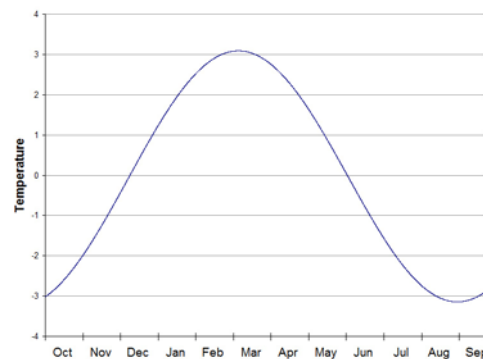


Figure 4.6: The difference between the simulated land surface temperatures of the two profiles (land surface temperature of the profile with groundwater perching at one meter, minus the land surface temperature of the dry profile).

Several remarks can be elicited from this graph, firstly, there is no oscillation in the values of difference, meaning that the land surface temperatures of the two simulations are shifting up or down without changing their daily amplitudes. Secondly, the difference is positive in months from January to May, and reaches its maximum value of 3 °C in March. Thirdly, the difference is negative in months from July to November and reaches its minimum value of -3 °C in September, and finally there are two months (namely December and June) when the difference is at lower values.

Values of maximum differences between the dry profile and the simulated profiles with different water tables are 1.5 °C for 2 m depth, 0.8 °C for 3 m depth, 0.4 °C for 4 m depth and 0.2 °C for 5 m depth. Naturally, these water depths include the capillary rise value.

4.4 Discussion and conclusions

In this chapter, it can be observed that shallow groundwater affects land surface temperature. This is evidenced firstly, by the statistically significant high correlation between daily maximum and average soil temperatures and water table depth (Tables 4.2 and 4.3, Figures 4.2 and 4.3), and secondly, by the difference in simulated land surface temperatures caused by groundwater perching within the relevant soil profile (Figure 4.6).

It is difficult and expensive to measure land surface temperature in situ for different locations simultaneously. However, in terms of the fact that the heat diffusion equation (equation 2.7) is the governing equation of heat transfer in the soil, the recorded temperatures at 5 and 10 cm can be considered as filtered signals of the temperatures at land surface. Further on, the obtained correlations can be safely considered valid for land surface temperature because of the homogeneity of the soil and meteorological conditions in the region.

There are still other potential factors behind these correlations. For instance, elevation difference can influence both soil temperature and groundwater depth and lower elevation can be related to higher air temperature and shallower groundwater depth. However, the study area is flat and limited. The difference in elevation among the seven locations is less than five meters, and the furthest distance among them is less than seven kilometers (Figures 4.1). That is why any effect of the difference in elevation or air temperature can be ignored.

Although both field measurements and numerical simulations show that shallow groundwater affects the temperature oscillation at land

surface, their results are not exactly the same. While the simulated land surface temperature difference (Figure 4.6) shows no daily oscillation i.e. groundwater existence shifts equally the whole daily temperature curve up (in winter) or down (in summer) without affecting the amplitude of the curve, field measurements show that the amplitudes of temperature curves are affected by shallow groundwater. That is lucid from the different values of correlation coefficients of the minimum, maximum and average daily temperature with water table depth (Table 4.2).

The dissimilarity between the two results is due to the simplicity of our numerical experiment. Firstly, it did not include and solve for the energy balance at land surface: Instead, the same ground heat flux was applied as a boundary condition in both cases: with and without groundwater. In fact, when shallow groundwater affects land surface temperature it affects all the components of the energy balance including ground heat flux. Secondly, it did not take into account the soil moisture effect: Not only does shallow groundwater affect land surface temperature directly by influencing heat flow within soil due to its distinctive thermal properties, but also it affects land surface temperature indirectly by increasing soil moisture due to capillary rise and vapor transport within soil pores. This is apparent in Figure 4.4, where soil moisture values increase with decreasing water table depth.

Soil moisture affects soil temperature in different and contradicting aspects. These effects fall into five categories: soil surface albedo, soil emissivity, evaporation, soil thermal conductivity and volumetric heat capacity. Firstly, increasing soil moisture decreases albedo which in turn increases the absorbed radiation during day time; hence, this increases daytime temperature. Secondly, soil emissivity increases with increasing soil moisture, which in turn increases the upward emission thus decreases surface temperature. Thirdly, the increase of soil moisture increases actual evaporation which accordingly decreases temperature. Fourthly, the increase of soil moisture increases soil thermal conductivity which eases heat transfer down and up within the surface soil and thereby decreases the absolute values of daily maximum and minimum temperatures. Finally, the increase of soil moisture increases soil volumetric heat capacity which increases the energy required for raising or lowering soil temperature, and in a similar manner to that of the third effect, it decreases the absolute values of the daily maximum and minimum temperatures.

On the last day of the experiment all locations were wetted until saturation. Consequently, the difference in soil moisture effects among the different locations was almost vanished. However, the relationship between soil temperature and water table depth (Tables 4.2 and 4.3, Figures 4.2 and 4.3) was not affected considerably. This clarifies the direct effect of groundwater on land surface temperature.

An unexpected phenomenon is worth mentioning here. Despite the general awareness that in daytime, wet soil must have lower temperature than dry one (due to its higher actual evaporation and higher heat capacity), the correlation between water table depth and maximum temperature was negative (Figures 4.2 and 4.3) and so was it for soil moisture (Figure 4.4). This means that the observed maximum temperature was higher for wetter soils. The reason behind this counterintuitive behavior of soil temperature will be discussed and explained later after conducting more realistic and comprehensive numerical simulations and remote sensing measurements.

In summary, it can be concluded that shallow groundwater affects land surface temperature on yearly basis. As mentioned in many previous studies it acts like a heat sink in summer and a heat source in winter. However, due to the complex processes that take place at land surface (radiations and fluxes interactions) its effect is not simple to describe. Many studies avoided this complexity by going with their measurements deep into the soil to correlate groundwater existence to soil temperature. And the other studies which dealt with land surface temperature had different opinions and contradicting results. Through the results of this chapter, it is shown that shallow groundwater has a clear impact on land surface temperature. This impact will be useful in two fields: first, in utilizing thermal satellite remote sensing in groundwater studies and second, in land surface energy balance studies (land surface models and climate models).

In this chapter it was shown qualitatively that shallow groundwater affects land surface temperature. Besides, the developed model was simple and turned out to be of limited value in explaining and justifying the reason behind the effect of shallow groundwater on land surface temperature. Thus, it was recommended to use a more sophisticated model that takes into account the variant factors which contribute to determining land surface temperature and the magnitude of that effect. Such a model is used in the following chapters.

5 The Thermodynamic Effect of Shallow Groundwater on Temperature and Energy Balance at Bare Land Surface*

* Based on:

Alkhaier, F., G. N. Flerchinger, and Z. Su (2011), The Thermodynamic Effect of Shallow Groundwater on Temperature and Energy Balance at Bare Land Surface, in: "Heat Analysis and Thermodynamic Effects", A. Ahsan (Ed.), InTech, 394 p. ISBN 978-953-307-585-3. pp. 19-34.

5.1 Introduction

It was demonstrated in Chapter 2 that Shallow groundwater affects land surface temperature and the surface energy balance in two different ways: direct and indirect (Figure 2.1). The direct way (the thermodynamic effect) is through its distinctive thermal properties which make groundwater acts as a heat sink in summer and a heat source in winter, and affects heat propagation within soil profile. The indirect way is through its effect on soil moisture above water table and its related effects (i.e. evaporation, soil thermal properties of vadose zone, land surface emissivity and albedo).

It was observed that studies that dealt with the thermodynamic effect (for example, Kappelmeyer, 1957; Cartwright, 1968, 1974, etc...) explored that effect on soil temperature at some depth under land surface. By these measurements, they aimed at eliminating the indirect effect. As a result they totally neglected groundwater effect on temperature and energy fluxes at land surface. On the other hand, studies that considered the indirect effect (such as, York et al., 2002; Liang and Xie, 2003; Chen and Hu, 2004, etc...) were centered on the effect of soil moisture in terms of water mass and passed over the effect on soil thermal properties. Furthermore, some studies which considered groundwater effect to be utilized in remote sensing applications (for instance: Huntley, 1978; Heilman and Moore's, 1982; Alkhaier et al., 2009) were faced with the problem of separating the direct effect of groundwater from that of soil moisture, there was hardly any sole study that conceptually or numerically differentiated the thermodynamic effect from the indirect effect.

In the previous chapter (Chapter 4), the in situ measurements demonstrated a clear relationship between soil temperature and groundwater depth. However, there was a doubt about the cause of the noticed effect; was it due the indirect effect throughout soil moisture or was it because of the thermodynamic effect of the groundwater body. Furthermore, it was suggested building a comprehensive numerical model that simulates the effect of shallow groundwater on land surface temperature and on the different energy fluxes at land surface.

For a better understanding the groundwater effect, this chapter explains one step towards quantifying its diverse aspects. It centers on the thermodynamic effect which was separated out numerically from the indirect effect. It undertook to answer these questions: does shallow groundwater affect land surface temperature and surface energy balance at land surface regardless of its effect on soil

moisture above water table? What are the magnitude and the pattern of that effect? And is that effect big enough to be detected by satellites?

With the aid of numerical modeling which progressed in complexity, it is shown in this chapter how the presence of groundwater, through its distinctive thermal properties within the yearly depth of heat penetration, affects directly land surface temperature and the entire surface energy balance system thereby. By applying different kinds of boundary conditions at land surface and changing the level of water table within the soil column, the differences in temperature and the energy fluxes at land surface were observed.

5.2 Numerical experiments

Two numerical experiments were implemented in this chapter. The first was simple and conducted using FlexPDE (PDE Solutions Inc.), a simulation environment which makes use of finite element technique to solve differential equations. The aim behind this experiment was to 1) prove that the thermodynamic effect of groundwater does indeed reach land surface and 2) to show that it is not appropriate to simply assign one type of boundary condition at land surface, and to explain that solving the entire surface energy balance at land surface is inevitable to realize groundwater effect. The entire surface energy balance system was simulated in the second experiment which was implemented using a well known land surface model code (Simultaneous Heat and Water model, SHAW, Flerchinger, 2000).

Initially, the common features among the different experiments are portrayed; afterwards, the specific conditions for each experiment are described. Although the experiments were implemented within different numerical environments, they were performed using similar 1-D soil profiles. The lower boundary condition in all simulations was set at a depth of 30 *m* (deeper than the yearly penetration depth of heat) as a fixed temperature which is the mean annual soil temperature. Each experiment involved five simulations that were performed first for a profile with no groundwater presence, then for cases where groundwater perched at 0.5, 1, 2 and 3 meters respectively.

Groundwater presence within the soil column was introduced virtually through assigning different values of both thermal conductivity and volumetric heat capacity of saturated soil to the region below the imaginary water table. Rest of the soil in the profile was assigned the values of thermal properties for dry soil.

In the first experiment, water transfer was not considered at all; heat transfer was the only simulated process. In the second experiment water movement and soil moisture transfer were simulated normally, because SHAW simulates both heat and water transfers simultaneously and its forcing data include rainfall. Yet, the code of SHAW was adjusted in a way that soil thermal properties were independent from soil moisture, and were fixed and predefined as the values adopted in the simulations of the first experiment. In that way groundwater was not present actually within soil profile in SHAW simulation rather than it did exist virtually through the different thermal properties of the two imaginary zones (saturated and dry zones). By this, the harmony among the two experiments was guaranteed and also separating the thermodynamic effect from the effect of soil moisture was ensured.

The same soil thermal properties of virtually saturated and dry zones within soil profiles were used in all simulations. Values of thermal conductivity were adopted as the values for standard Ottawa sand measured by Huntley (1978), who conducted similar modeling experiment. Volumetric heat capacity values were calculated using the expression of de Vries (1963). Accordingly, the used values for thermal conductivity in all simulations were 0.419 and 3.348 ($J m^{-1} s^{-1} C^{-1}$), and the used values for volumetric heat capacity were 1.10E+06 and 3.10E+06 ($J m^{-3} C^{-1}$) for dry and saturated sections respectively.

The first experiment comprises two different simulation setups. In the first simulation setup, land surface temperature was assigned as a boundary condition and the change in ground heat flux caused by groundwater level change within soil profile was observed. In the second simulation setup, ground heat flux was applied as a boundary condition at land surface and the change in land surface temperature was observed. The results of the two simulations suggested the indispensability of examining the effect of shallow groundwater on both temperature and ground heat flux simultaneously. To do so, it was necessary to free both of them and simulate the whole energy balance at land surface for scenarios with different groundwater levels. This was accomplished in the second experiment. All simulations were run for one year duration, after three years of pre-simulation to reach the appropriate initial boundary conditions.

5.2.1 Experiment 1

The experiment was conducted within FlexPDE environment. In one dimension soil column, heat transfer was simulated assuming

conduction the only means of heat transport. Consequently, the sole considered governing equation was the diffusion equation (equation (2.7)).

Analytically, yearly land surface temperature can be described by expanding equation (7) of Horton and Wierenga, (1983) to include both the daily and the yearly cycles and by setting the depth z to zero, hence:

$$T = \bar{T}_{avr} + A_1 \sin\left(\frac{2\pi t}{p_1}\right) + A_2 \sin\left(\frac{2\pi t}{p_2}\right) \quad (5.1)$$

where \bar{T}_{avr} ($^{\circ}\text{C}$) is the average soil temperature at all depths. A_1 and A_2 ($^{\circ}\text{C}$) are the daily and yearly temperature amplitudes at land surface respectively, p_1 is one day and p_2 is one year expressed in the time unit of the equation (s).

Similarly, yearly ground heat flux at land surface can be expressed by equation (4.2) which results by expanding equation (10) of Horton and Wierenga (1983) to include both daily and yearly cycles and by setting the depth, z , to zero.

In the first simulation, land surface temperature (equation (5.1)) was applied as a Dirichlet boundary condition at land surface of profiles with variant groundwater depth. As a result, FlexPDE provided the simulated ground heat flux for the different situations in terms of groundwater presence and level. Afterwards, the resultant ground heat flux values of the profile with no-groundwater were subtracted from those of the profiles with groundwater at different depths, and the differences were observed.

On the contrary, in the second simulation ground heat flux (equation (4.2)) was applied as a forcing flux (Neumann boundary condition type) at land surface. Consequently, FlexPDE provided the simulated land surface temperature for the different situations in terms of groundwater presence and level. Then, land surface temperature values of the profiles with no-groundwater were deducted from those of the profiles with groundwater at different depths, and the differences were observed.

5.2.2 Experiment 2

To observe the thermodynamic effect of shallow groundwater on both land surface temperature and ground heat flux, all at once, the complete balance system at land surface was solved. SHAW was used to conduct this experiment because it presents heat and water transfer processes in detailed physics, besides, it has been successfully used to simulate land surface energy balance over a wide range of conditions and applications (Flerchinger and Cooley, 2000; Flerchinger et al., 2003, 2009; Flerchinger and Hardegree, 2004; Santanello and Friedl, 2003; Huang and Gallichand, 2006).

SHAW model simulates a vertical, one-dimensional profile which may extend from the top of possibly existing vegetation canopy, plant residue, snow, or soil surface down to a certain depth within the soil. This system is represented by detailed physics. Hereinafter, some of SHAW's fundamental equations are presented. For further details the reader is referred to SHAW technical documentation (Flerchinger, 2000).

Surface energy balance and both water and heat transfer within the soil profile are expressed in SHAW as follows: Surface energy balance is represented by the equations described in Chapter 2 (equations (2.1-2.6)). The resistance value for vapor transfer r_v (sm^{-1}) is assumed to be equal to the resistance to surface heat transfer, r_H , which is calculated from:

$$r_H = \frac{1}{u_* k} \left[\ln \left(\frac{z_{ref} - d + z_H}{z_H} \right) + \psi_H \right] \quad (5.2)$$

where u_* is the friction velocity (ms^{-1}):

$$u_* = u k \left[\ln \left(\frac{z_{ref} - d + z_m}{z_m} \right) + \psi_m \right]^{-1} \quad (5.3)$$

u is wind speed (ms^{-1}), k is von Karman's constant, d is the zero plane displacement, z_m and z_H are the surface roughness parameters for momentum and temperature respectively, ψ_m and ψ_H are the stability correction functions for momentum and heat transfer respectively. Atmospheric stability is expressed as the ratio of thermally induced to mechanically induced turbulence (Campbell, 1977):

$$stable = \frac{k z_{ref} g H}{\rho_a c_a (T_a + 273.16) u_*^3} \quad (5.4)$$

where g is the gravitational acceleration (ms^{-2}).

when $stable > 0$ (stable conditions):

$$\psi_H = \psi_m = 4.7 \times stable \quad (5.5)$$

and when $stable < 0$ (unstable conditions):

$$\psi_m \approx 0.6 \times \psi_H = 0.6 \times \left[-2 \ln \left(\frac{1 + \sqrt{1 - 16 \times stable}}{2} \right) \right] \quad (5.6)$$

Ground heat flux, $G = -k_s \partial T / \partial z$, is a function of thermal conductivity, k_s , and soil temperature gradient, $\partial T / \partial z$, and computed in SHAW by solving for a surface temperature that satisfies surface energy balance, which is solved iteratively and simultaneously with the equations for heat and water fluxes within the soil profile.

The governing equation for temperature variation in the soil matrix within SHAW considers, next to heat conduction, latent heat of water freezing and ice thawing, convective heat transfer by liquid water flux and latent heat transfer by vapor:

$$VHC \frac{\partial T}{\partial t} - \rho_i L_f \frac{\partial \theta_i}{\partial t} = \frac{\partial (k_s \partial T)}{\partial^2 z} - VHC_w \frac{\partial q_l T}{\partial z} - L \left(\frac{\partial q_v}{\partial z} + \frac{\partial \rho_v}{\partial t} \right) \quad (5.7)$$

where ρ_i is ice density (kgm^{-3}); L_f is the latent heat of fusion (Jkg^{-1}); θ_i is the volumetric ice content (m^3m^{-3}); VHC and VHC_w are the volumetric heat capacity of soil matrix and water respectively ($Jm^{-3}C^{-1}$); q_l is the liquid water flux (ms^{-1}); q_v is the water vapor flux ($kgm^{-2}s^{-1}$) and ρ_v is the vapor density (kgm^{-3}). Soil thermal properties are calculated according to de Vries (1963): equations (2.8-2.9).

The governing equation for water movement within soil matrix is expressed in SHAW by extending the traditional Richards equation to include the dynamic change in volumetric ice content and water vapor flux within the soil pores:

$$\frac{\partial \theta_l}{\partial t} + \frac{\rho_l}{\rho_i} \frac{\partial \theta_l}{\partial t} = \frac{\partial}{\partial z} \left[k_h \left(\frac{\partial \psi}{\partial z} + 1 \right) \right] + \frac{1}{\rho_l} \frac{\partial q_v}{\partial z} + U \quad (5.8)$$

where θ_l is the volumetric liquid water content ($m^3 m^{-3}$), ρ_l is the liquid water density ($kg m^{-3}$); k_h is the unsaturated hydraulic conductivity ($m s^{-1}$); ψ is the soil matric potential (m) and U is a source/sink term ($m^3 m^{-3} s^{-1}$).

The moisture characteristic equation is expressed as (Brooks and Corey, 1966; Campbell, 1974):

$$\psi = \psi_{ae} \left(\frac{\theta_l}{\phi} \right)^{-b} \quad (5.9)$$

where ψ_{ae} is air entry potential (m), b is a pore size distribution parameter, and ϕ is soil porosity ($m^3 m^{-3}$). Unsaturated hydraulic conductivity is computed from:

$$k_h = k_h^* \left(\frac{\theta_l}{\phi} \right)^{(2b+3)} \quad (5.10)$$

where k_h^* is saturated hydraulic conductivity (ms^{-1}).

Vapor flux in soil pores takes place because of the gradient in vapor density. The latter is the result of both water potential gradient, q_{vp} , and temperature gradient, q_{vT} , (Campbell, 1985) so:

$$q_v = q_{vp} + q_{vT} = -D_v \rho_v \frac{dh_r}{dz} - \xi D_v h_r s_v \frac{dT}{dz} \quad (5.11)$$

where D_v is vapor diffusivity within the soil matrix ($m^2 s^{-1}$); h_r is relative humidity within the soil matrix; ξ is an enhancement factor; s_v ($kg m^{-3} C^{-1}$) is the slope of the saturated vapor pressure curve ($d\rho_v / dT$).

The one-dimensional state equations describing energy and water balance are written in implicit finite difference form and solved using an iterative Newton-Raphson technique for infinitely small layers.

Atmospheric forcing above the upper boundary (land surface) and soil conditions within the soil profile define heat and water fluxes within the system. Consequently, the input to the SHAW model includes a) meteorological data and general site information, b) soil composition and hydraulic parameters and c) initial soil temperature and moisture.

The forcing weather data were obtained from Ar-Raqqa weather station. The simulations were run for the year 2004 after three years (2001-2003) of pre-simulation to reach appropriate initial conditions for soil profile. The daily input data includes minimum and maximum temperatures, dew point, wind speed, precipitation, and total solar radiation.

Since the groundwater was virtually presented within soil profile, and since the thermal properties were predefined, the type of the simulated soil is of minor importance. Basically, SHAW calculates thermal conductivity and volumetric heat capacity according to the method of de Vries (de Vries, 1963). However for the sake of separating the thermodynamic effect of groundwater from the indirect one, the FORTRAN code of SHAW are adjusted so the model uses the same values as used in the first experiment.

The output of the model includes surface energy fluxes, water fluxes together with temperature and moisture profiles. After solving for energy balance at the top of the different profiles, the resultant land surface temperature, and surface heat fluxes of the no-groundwater profile were subtracted from their correspondents of the profiles with the groundwater perches at 0.5, 1, 2 and 3 m.

5.3 Results

5.3.1 Experiment 1

By applying land surface temperature (equation (5.1)) as an upper boundary condition, then changing the thermal properties of the soil profile (due to the variation in the imaginary groundwater level), there was a considerable difference in the resultant simulated ground heat flux at land surface. The differences between ground heat flux of the no-groundwater profile and those of the profiles with different water table depths are shown in Figure 5.1a.

In wintertime, when the daily upshot of ground heat flux is usually directed upward (negative sign) and heat is escaping from the ground, ground heat flux of the profile with half meter groundwater

depth was higher (in negative sign) than that of the no-groundwater profile. The difference in ground heat flux between the two profiles reached its peak value of almost -28 Wm^{-2} in February. The differences in ground heat fluxes between the no-groundwater profile and the profiles with groundwater at 1, 2 and 3 m depth behaved similarly but had smaller values of the peaks and roughly one month of delay in their occurrence between one and the next.

Quite the opposite, in summertime, when the daily product of ground heat flux is usually downward (positive) and earth absorbs heat, ground heat flux of the profile with groundwater at half meter depth was also higher (but in positive sign) than that of the no-groundwater profile, and reached similar peak value of about 28 Wm^{-2} in August. Again, the differences in ground heat flux between the no-groundwater profile and the profiles with groundwater at 1, 2 and 3 m depth behaved similarly with a delay in occurrence of the yet lower-values peaks.

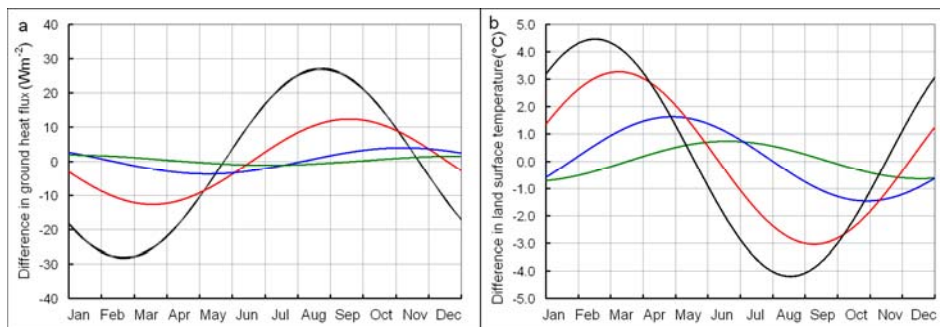


Figure 5.1: **a)** Ground heat flux (Wm^{-2}) of the no-groundwater profile subtracted from those of profiles with water table depth of half meter (black), one meter (red) two meters (blue) and three meters (green). **b)** The same as (a) but for land surface temperature ($^{\circ}\text{C}$).

Figure 5.1b shows the differences among the simulated land surface temperatures resulting from applying the same values of ground heat flux (equation (4.2)) at the surface of the profiles with different thermal properties due to variant levels of groundwater.

In wintertime, land surface temperature of the profile of half meter depth of groundwater was higher than that of the no-groundwater. The difference between the two, reached its peak of about $4 \text{ }^{\circ}\text{C}$ in February. Subsequently, the differences between land surface temperature of the profiles of 1, 2 and 3 m and that of the no-

groundwater profile had lower peak values with a delay of almost a month between each other.

On the contrary, land surface temperature of the profile of half meter depth of groundwater was lower than that of no-groundwater in summer. The difference in temperature between the two profiles reached its peak value of about 4 °C in August. Again, the differences between land surface temperature of the profiles with groundwater at 1, 2 and 3 m depth and that of the no-groundwater profile had lower peak values with a delay in their occurrence of about a month between one another (Figure 5.1b).

5.3.2 Experiment 2

With comprehensive consideration of surface energy balance and using real measured forcing data, SHAW showed more realistic results. The scattered dots in Figures 5.2-5.6 represent the differences between the no-groundwater profile and those with groundwater in terms of hourly values of the different variables which have been affected by the presence of groundwater within soil profile. The solid line drawn through the scattered dots in each figure represents the first harmonic which was computed by Fourier harmonic analysis.

Figure 5.2 demonstrates the surface temperature of the profile with no-groundwater subtracted from temperatures of the profiles with groundwater at 0.5, 1, 2 and 3 m depth. Land surface temperature of the profile with groundwater at half meter depth reached a value of about 1 °C higher than that of the no-groundwater profile in winter (Figure 5.2a). Similarly, land surface temperatures of the profiles of 1, 2 and 3 m groundwater-depth respectively reached values of roughly 0.5, 0.2 and 0.1 °C higher than that of the no-groundwater profile (Figures 5.2b-5.2d). In summer, land surface temperature of the profiles with groundwater at depths 0.5, 1, 2 and 3 m were lower than that of the no-groundwater profile by about 1, 0.5, 0.3 and 0.2 °C respectively.

The Thermodynamic Effect of Shallow Groundwater on Temperature and Energy Balance at Bare Land Surface

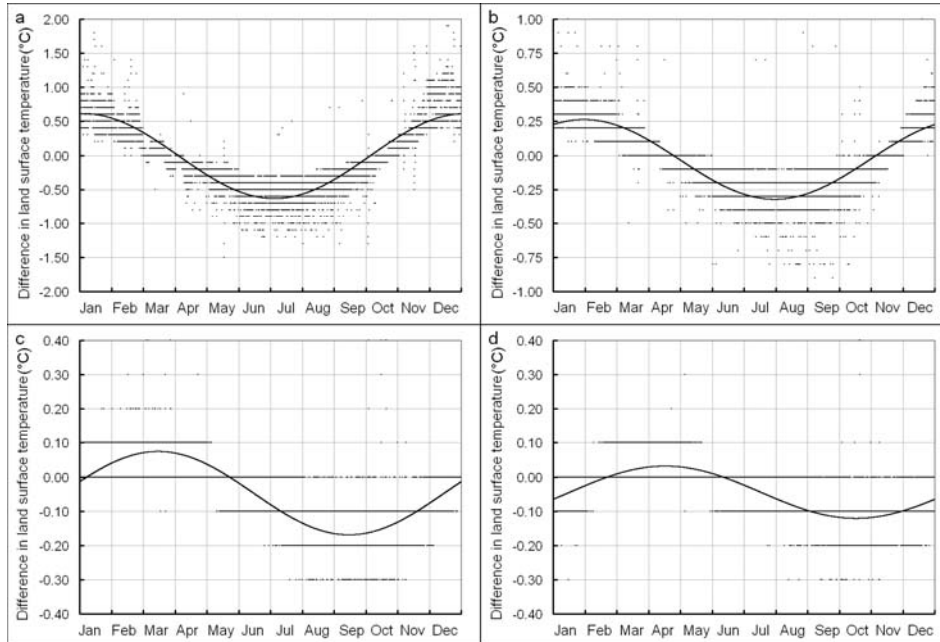


Figure 5.2: Land surface temperature ($^{\circ}\text{C}$) of the no-groundwater profile subtracted from those of profiles with groundwater at **a)** 0.5 m depth **b)** 1 m depth **c)** 2 m depth **d)** 3 m depth. Solid lines are first harmonics.

Simultaneously, ground heat flux was also influenced by the presence of groundwater as shown in Figure 5.3 which shows ground heat flux of the profile with no-groundwater subtracted from ground heat fluxes of the profiles with groundwater at 0.5, 1, 2 and 3 m depth. In wintertime, ground heat flux of the profile with half meter depth was higher (in negative sign) than that of the profile with no-groundwater by more than 11 Wm^{-2} , and also higher by about the same value (but in positive sign) in summertime (Figure 5.3a). In the same way, ground heat fluxes of the profiles with groundwater at 1, 2 and 3 m depth were higher than that of the no-groundwater but with smaller peak values and with shifts in the phase (Figures 5.3b-5.3d).

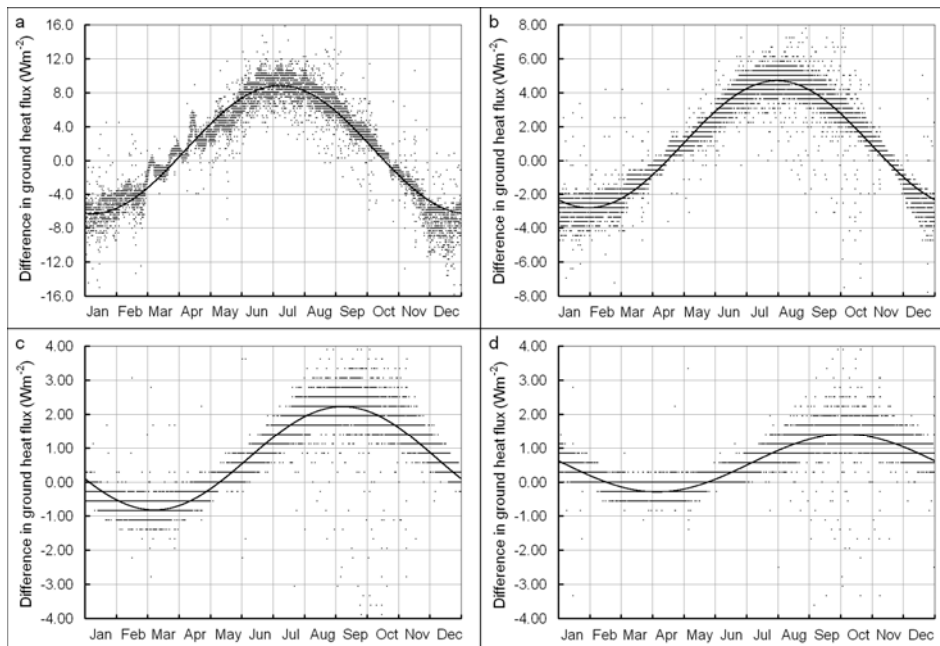


Figure 5.3: Ground heat flux (Wm^{-2}) of the no-groundwater profile subtracted from those of profiles with groundwater at **a)** 0.5 m depth **b)** 1 m depth **c)** 2 m depth **d)** 3 m depth. Solid lines are first harmonics.

Similarly, Figure 5.4 illustrates clear differences in sensible heat flux among the profiles of variant groundwater depths. In wintertime, sensible heat flux of the profile with groundwater at half meter depth reached a value of about $8 Wm^{-2}$ higher than that of the profile with no-groundwater. Quite the opposite in summertime, sensible heat flux of the profile with groundwater at half meter depth reached a value of about the same magnitude lower than that of the profile with no-groundwater (Figure 5.4a). Figures 5.4b-5.4d show that sensible heat fluxes of the profiles with groundwater at 1, 2 and 3 m depth were higher than that of the no-groundwater in wintertime but with smaller magnitudes and with shifts in the phase. In summertime, sensible heat fluxes of the profiles with groundwater at 1, 2 and 3 m depth were lower by similar magnitudes than that of the no-groundwater.

The Thermodynamic Effect of Shallow Groundwater on Temperature and Energy Balance at Bare Land Surface

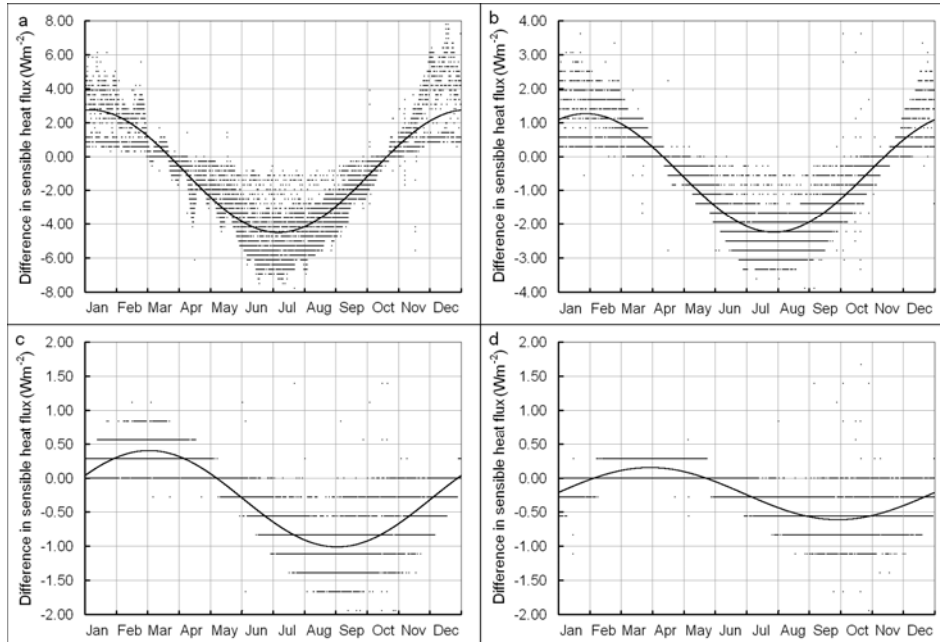


Figure 5.4: Sensible heat flux of the no-groundwater profile subtracted from those of profiles with groundwater at **a)** 0.5 m depth **b)** 1 m depth **c)** 2 m depth **d)** 3 m depth. Solid lines are first harmonics.

Unlike ground and sensible heat fluxes, latent heat fluxes showed very small differences among the different profiles (Figure 5.5). In spite of the immense amount of chaotic scattering, one can still see a small positive trend in winter and negative one in summer.

The last constituent of energy balance system which was investigated and altered by the presence of groundwater was the outgoing long-wave radiation (Figure 5.6). The differences looked similar to those of sensible heat flux in terms of diurnal shape and peak values but in reverse direction. Outgoing long-wave radiation of the no-groundwater profile was bigger in negative sign than that with groundwater in winter and smaller in summer.

The first harmonics sketched along of the scattered dots in Figures 5.2-5.6 demonstrated the periodic nature of the differences and were useful in pointing to the occurrence time of the differences' peaks both in winter and summer.

To have a closer look at the hourly variations (scattered dots in Figures 5.2-5.6), we zoomed in into hourly data of surface

temperature and energy fluxes for two profiles: the no-groundwater profile and the profile with 50 cm groundwater depths within two different days (Figure 5.7). The first day was in winter (23 December, Figure 5.7 left side) and the second one was in summer (24 July, Figure 5.7 right side).

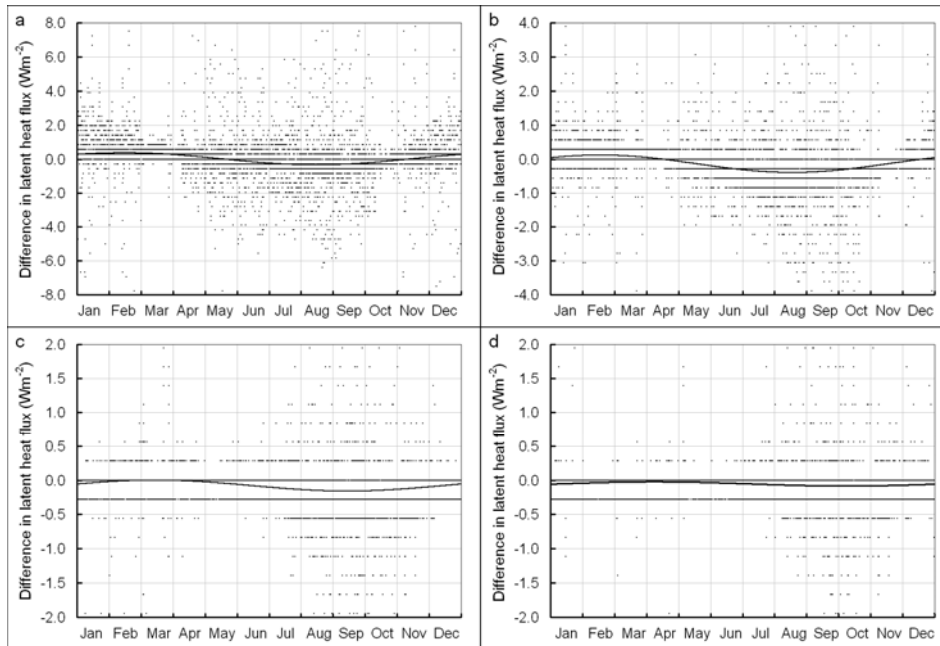


Figure 5.5: Latent heat flux of the no-groundwater profile subtracted from those of profiles with groundwater at **a)** 0.5 m depth **b)** 1 m depth **c)** 2 m depth **d)** 3 m depth. Solid lines are first harmonics.

In the winter day, land surface temperature of the no-groundwater profile was lower than that with groundwater all day long (Figure 5.7a). Therefore, the difference was positive. However, during nighttime the difference in land surface temperature was highest (about 1.2 °C). During daytime when the sun radiated solar energy on land surface, the difference diminished to 0.5 °C. After sunset the difference started to rise again. Oppositely, in the summer day (Figure 5.7b) land surface temperature of the no-groundwater profile was higher than that with the groundwater all day long; as a result, the difference was negative. Again, the difference was big at night (-1 °C) and moderated to -0.4 °C in daytime hours.

Figure 5.7c illustrates that in the winter day, ground heat flux of the no-groundwater profile was smaller (in negative sign) than that of the

The Thermodynamic Effect of Shallow Groundwater on Temperature and Energy Balance at Bare Land Surface

profile with groundwater during nighttime but greater than it was (in positive sign) in daytime. Hence, the difference remained negative in sign day and night. However, the difference was larger at day than it was at night. Conversely, in the summer day (Figure 5.7d) ground heat flux of the no-groundwater profile was bigger (in negative sign) than that of the profile with groundwater during nighttime, but smaller than it was (in positive sign) during daytime. Hence, the difference remained positive in sign during day and night, and again the difference was larger by day than it was at night.

Sensible heat flux of the no-groundwater profile was smaller than that of the profile with groundwater during day and night in the winter day. Therefore, the difference was positive all day long (Figure 5.7e). However, the difference was small at night (about 1 Wm^{-2}) and increased during the day up to more than 6 Wm^{-2} . In contrast, in the summer day (Figure 5.7f) sensible heat flux of the no-groundwater profile was bigger than that of the profile with groundwater day and night. Therefore, the difference was negative all day long. And again the difference was small at night (about -1 Wm^{-2}) and increased during the day to more than -6 Wm^{-2} .

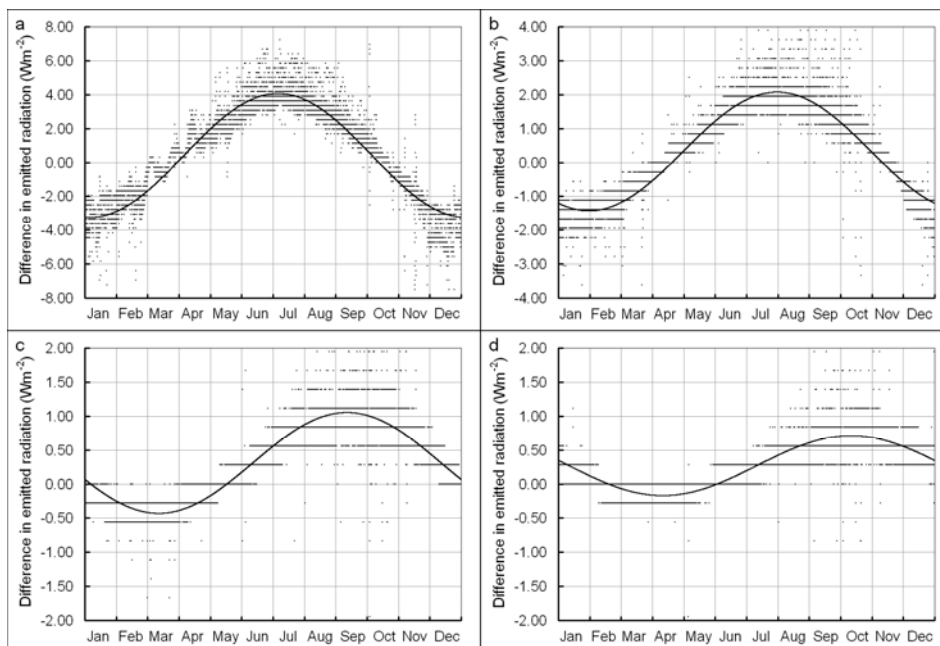


Figure 5.6: Outgoing longwave radiation (Wm^{-2}) of the no-groundwater profile subtracted from those of profiles with groundwater at a) 0.5 m depth b) 1 m depth c) 2 m depth d) 3 m depth. Solid lines are first harmonics.

Unlike the previous two heat fluxes, latent heat flux showed very small difference between the two profiles, both in winter and summer days. In the winter day (Figure 5.7g) the difference in latent heat flux between the two profiles was around zero during nighttime. During daytime, latent heat flux of the profile with groundwater started to be larger than that of the no-groundwater. Oppositely, during the summer day (Figure 5.7h) latent heat flux of the profile with groundwater was smaller than that of the no-groundwater during daytime.

The Thermodynamic Effect of Shallow Groundwater on Temperature and Energy Balance at Bare Land Surface

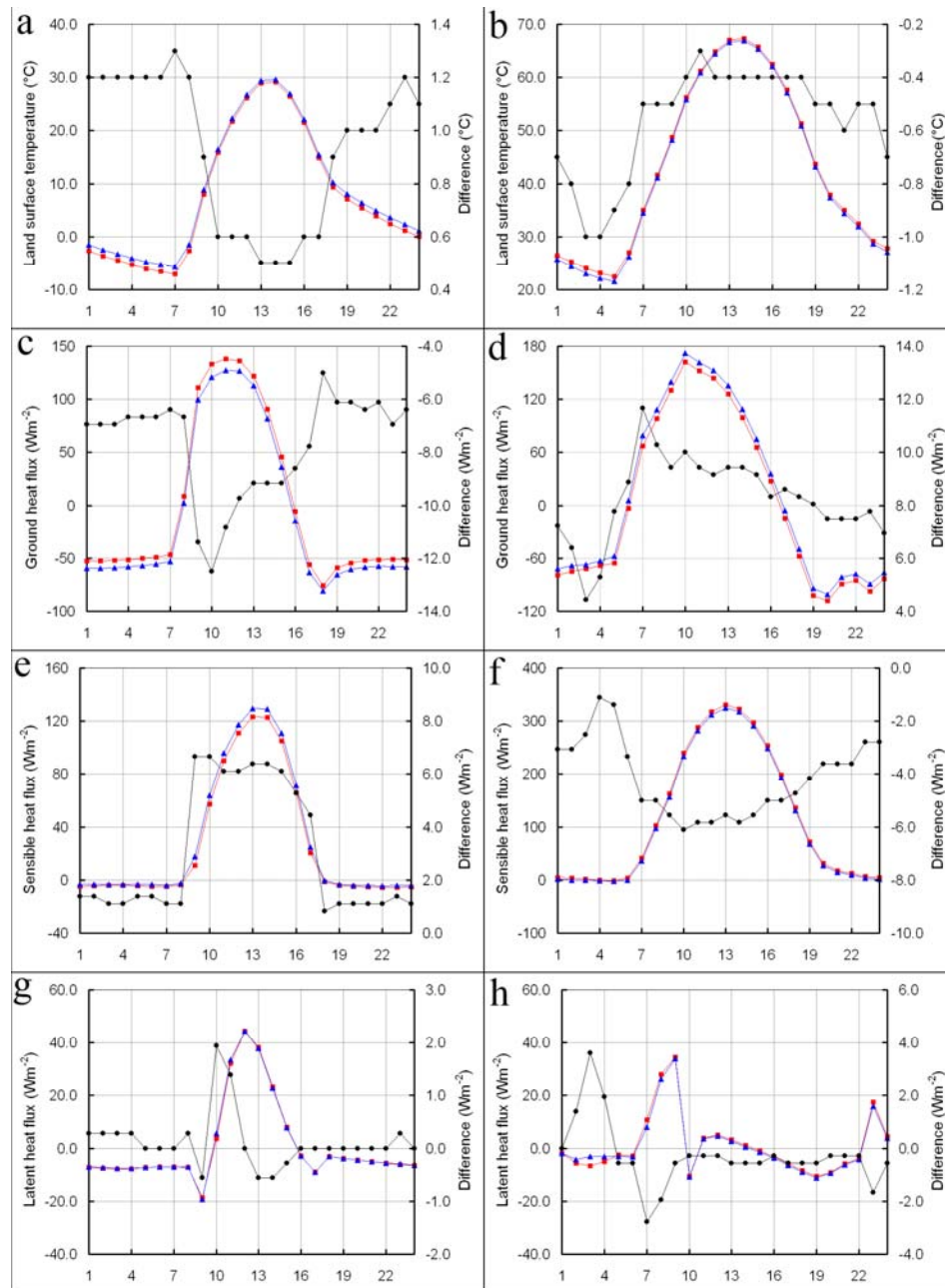


Figure 5.7: Hourly values of temperature and energy fluxes of two profiles 1) with no-groundwater (red), 2) with groundwater at 50 cm depth (blue) and 3) the difference between them [(2)-(1)] (black), for two days: 23 Dec (left side) and 24 Jul (right side).

5.4 Discussion

In this chapter it was shown that the presence of groundwater within the yearly depth of heat penetration affects directly, and regardless of its effect on soil moisture above water table, both land surface temperature and ground heat flux, thereby affecting the entire surface energy balance system. The numerical experiments demonstrated that when land surface temperature was applied as an upper boundary condition and the water table depth was changed, a significant difference in ground heat flux at land surface was obtained. On the contrary, when ground heat flux was applied as forcing boundary condition at land surface, a considerable difference in land surface temperature was obtained by changing water table depth. Consequently, when solved for the complete energy balance system at land surface, the thermodynamic effect of groundwater was demonstrated in simultaneous alteration of land surface temperature, ground heat flux, sensible heat flux, latent heat flux and outgoing longwave radiation at land surface.

The key reason behind this thermodynamic effect is the contrast in thermal properties within the soil profile. Resulting from the presence of groundwater, this contrast affects first and foremost heat penetration into the soil (equation (5.7)) which is chiefly pronounced via soil temperature and soil heat flux. Consequently, the largest difference should be marked for ground heat flux and land surface temperature.

When groundwater comes closer to land surface, it increases land surface temperature in winter and decreases it in summer (Figure 5.2). In this way it acts as a heat source in wintertime and a heat sink in summertime. As a result, shallow groundwater increases the intensity of ground heat flux both in wintertime and summertime (Figure 5.3). In wintertime, it increases the upward ground heat flux which leads to further energy released from the ground. Contrarily, in summer it increases the downward ground heat flux allowing the earth to absorb more energy from the atmosphere.

In the second experiment it was observed a lower magnitude of temperature difference (Figure 5.2) than that observed in the first experiment (Figure 5.1b). Actually, the observed difference in land surface temperature in the first experiment (Figure 5.1b) was due to the fact that land surface temperature was the single parameter which was subject to change, since the first experiment did not take into account the entire surface energy balance system. The big differences observed in the first experiment simulations were distributed among sensible and latent heat fluxes together with

emitted long-wave radiation as explained by the second experiment (Figures 5.4-5.6).

Whilst sensible heat flux mitigates land surface temperature through the reciprocal swap of heat with air above land surface, latent heat flux exploits the gained heat in more evaporation. Finally, outgoing longwave radiation continuously alleviates land surface temperature by emitting energy into the atmosphere. Therefore, the increase in land surface temperature in wintertime increases the amount of energy exchange between land surface and the air above it (i.e. sensible heat flux) due to the increment in temperature contrast between both of them. Contrarily, the decrease in land surface temperature in summer decreases sensible heat flux (Figure 5.4). Similarly the increase in land surface temperature in winter enhances evaporation, and its decrease in summer reduces evaporation (Figure 5.5). Yet the effect on evaporation was the smallest. Finally the increase in land surface temperature in winter increases energy emission from soil in the form of longwave radiation, and its decrease in summer causes yet smaller amount of emission (Figure 5.6).

Bearing in mind the convoluted interactions among energy fluxes and radiations at land surface, it is very difficult to describe how the groundwater thermodynamically affects each of them separately. Though, keeping in mind the instantaneous nature of those interactions, a simplified conception of the thermodynamic effect can still be furnished as in Figure 5.8. Since the different soil thermal properties within the soil profile alter vertical heat transfer in both vertical directions (equation (5.7)), ground heat flux and soil temperature are the first two components to be directly affected by the thermodynamic effect. Consequently, land surface temperature affects sensible heat flux (equation (2.4)), latent heat fluxes (equation (2.5)) and the outgoing longwave radiation. The latter affects the net radiation available for the three fluxes, hence it affects again sensible and latent heat fluxes. On the other hand, ground heat flux also affects sensible and latent heat fluxes by reducing the energy left for them from the net radiation. Obviously, incoming, reflected short-wave radiation and incoming long-wave radiation stay outside the thermodynamic effect of groundwater.

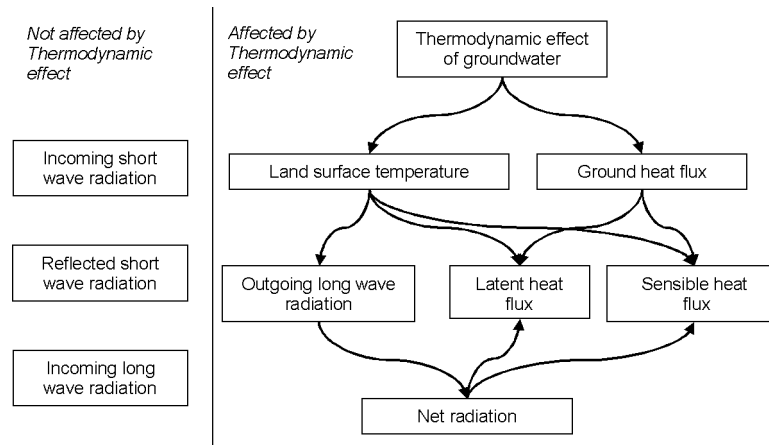


Figure 5.8: Schematic description of groundwater thermodynamic effect on land surface temperature and the different components of surface energy balance.

The small difference in latent heat flux compared to the difference in other fluxes (Figure 5.5) can be justified by two reasons: Firstly, latent heat flux was originally small in this experiment due to the dry conditions in the considered area, and secondly, latent heat flux, unlike ground and sensible heat fluxes, is not a main function of land surface temperature; Whereas ground heat flux is a key function of land surface temperature and temperature of the soil beneath (equation (2.6)), and sensible heat flux is a primary function of land surface temperature and temperature of the air above (equation (2.4)), latent heat flux is a function of vapor density contrast between land surface and the atmosphere (equation (2.5)), and not a primary function of land surface temperature.

When groundwater depth increased, it was observed that the differences' peaks experienced a delay of about a month between one depth and the next (Figures 5.1-5.6). Similarly, it was also observed that the differences' peaks had lower values when groundwater went deeper. The delay and the lower values can be justified by the fact that the closer the groundwater is to land surface the stronger and sooner its effect takes place on the penetrated ground heat flux.

The first experiment was simple and could not be compared to real world; therefore the observed differences in Figures 5.1a and 5.1b were sketched by neat lines without hourly fluctuations. On the contrary, the simulations in the second experiment were closer to reality and produced hourly variations presented by the scattering dots around the first harmonic lines within Figures 5.2-5.6. Samples

of such hourly variations were presented in Figure 5.7. In both winter and summer days, the difference in land surface temperature was highest during nighttime and decreased in the daytime (Figures 5.7a and 5.7b). That was due to the fact that sensible and latent heat fluxes were stronger during daytime and had small magnitude during nighttime, in this way, they reduced the difference in land surface temperature in daytime in favor of their own differences (Figures 5.7e-5.7h).

In contrary to land surface temperature difference behavior, the difference in ground heat flux had high values in the night and had even higher values in daytime. This is explained by that the earth subsurface is the primary source of energy that drives the upward ground heat flux during nighttime, on the other hand, during daytime solar radiation provides the earth with higher amounts of energy and makes the difference in downward ground heat flux more pronounced (Figures 5.7c and 5.7d).

In general it is found that the magnitude of the thermodynamic effect on land surface temperature and surface energy balance system was small, but when considering the indirect effect, there will be two possibilities: 1) the two effects work in the same direction, then the thermodynamic effect will increase the intensity of the combined effect, or 2) the two effects work in opposite directions and then the thermodynamic effect will decrease the intensity of the combined effect. In this way, highlighting this aspect of groundwater effect was necessary to complete the view. As a result, it is important to study the combined effect. The latter is studied in the following chapter (Chapter 6) in which the majority of the aspects through which shallow groundwater affects land surface temperature and the various components of surface energy balance system are taken into consideration.

5.5 Conclusions

In summary, it can be concluded that shallow groundwater - regardless of its indirect effect generated via its effect on soil moisture above water table - does indeed affect directly the components of the energy balance system at land surface by its distinctive thermal properties. This thermodynamic effect is primarily obvious on land surface temperature, ground heat flux, sensible heat flux and outgoing long-wave radiation.

In terms of seasonally prospective, the thermodynamic effect on all these components is mostly pronounced in winter and summer.

Whereas, in terms of hourly prospective, the difference in land surface temperature and outgoing longwave radiation is higher during nighttime, and the difference in ground and sensible heat fluxes is higher during daytime.

In spite of its small magnitudes, highlighting the different features of the thermodynamic effect is important to make the understanding of the combined effect of groundwater more complete. The importance of the thermodynamic effect comes from its interaction with the indirect effect which originates from soil moisture above water table; this interaction may increase or decrease the upshot of the combined effect.

Finally, it is important to give emphasis to the fact that in this chapter the thermodynamic effect was separated numerically from the indirect effect of groundwater on land surface temperature and surface energy balance system. However, in real world these two effects can not be separated naturally and the image can not be complete without considering the combined effect. Nevertheless, this thermodynamic effect on land surface has not been established before and it clearly offers a more clear view of groundwater effect which is promising for enhancing the related surface energy balance studies and remote sensing applications.

The Thermodynamic Effect of Shallow Groundwater on Temperature and Energy Balance at Bare Land Surface

6 The Combined Effect of Shallow Groundwater on Temperature and Energy Balance at Bare Land Surface*

* Based on:

Alkhaier, F., G. N. Flerchinger, and Z. Su (2011), Shallow groundwater effect on land surface temperature and surface energy balance under bare soil conditions: Modeling and description, *Hydrology and Earth System Sciences Discussions*, 8, 8639-8670, doi:10.5194/hessd-8-8639-2011.

6.1 Introduction

Investigating the effect of shallow groundwater on land surface temperature and surface energy balance has two-fold benefits. Firstly, it provides solid ground for optimal utilization of thermal remote sensing in observing the areal extent of shallow groundwater and developing future satellite designs. Secondly, it contributes to establishing the basis in which this effect can be included in climate research, weather forecast, and water management studies.

Recently, there have been keen attempts to include groundwater systems in land surface models (i.e. models that simulate the interactions between soil, vegetation and the atmosphere). York et al. (2002), the earliest to include aquifers within coupled land surface models, triggered a series of investigations that approached the coupling between groundwater and land surface models using different schemes and techniques (Liang and Xie, 2003; Chen and Hu, 2004; Maxwell and Miller, 2005; Gulden et al., 2007; Fan et al., 2007; Niu et al., 2007; Jiang et al., 2009). Careful inspection of these works shows that their focal point was limited to the mass effect of the linkage between the surface and the subsurface domains via moisture flux. In this way, the main interest was the influence of groundwater, as an extra source of water for evaporation, on water budget at land surface. Specifically, Niu et al. (2007) developed a simple groundwater model (SIMGM) which considers unsaturated soil water and evaluated the model against the Gravity Recovery and Climate Experiment (GRACE) terrestrial water storage change data. Therefore, these studies did not yield a complete prospective of shallow groundwater effect. The temporal patterns of that effect on surface temperature, net radiation, and surface heat fluxes (latent, sensible and ground heat fluxes) were not portrayed. More importantly, utilizing thermal remote sensing in these efforts or reversely, utilizing their findings in detecting shallow groundwater via thermal remote sensing was beyond the scope of these studies.

In the previous chapter (Chapter 5) the thermodynamic effect of shallow groundwater was investigated. The Fortran code of SHAW was adjusted in a way that soil thermal properties were fixed and independent from soil moisture. Further on, groundwater was not actually present within soil profile rather than it did exist only virtually through the different thermal properties of the two imaginary zones (saturated and dry zones).

In this chapter the combined effect is explored (Figures 2.1 and 2.2): In contrast to the SHAW simulations in the previous chapter,

groundwater is actually present within soil profile and affects soil moisture above water table. The SHAW code was left intact so the soil thermal properties were changing every time step according to the soil moisture content (equations (2.8-2.9)).

To know when and how groundwater effect takes place or whether it is possible to utilize currently operational satellites in its detection, comprehensive numerical simulations were implemented in this chapter. In these simulations, the majority of the aspects through which shallow groundwater affects land surface temperature and the various components of surface energy balance were taken into consideration. In the following chapter (Chapter 7), the findings and conclusions of this chapter are supported by further investigating the possibility of utilizing remotely sensed temperatures as a practical application in featuring that effect.

With respect to the numerical simulation implemented in this chapter, two soil profiles -one having shallow groundwater-were exposed to the same meteorological forcing. The different responses of both profiles were then spotlighted with regards to surface soil moisture, surface soil temperature and surface energy balance components.

Hereinafter, the numerical modeling experiments that had been implemented for portraying the expected pattern and magnitude of groundwater effect are described.

6.2 Methodology

The simulations were implemented for two different soil profiles that were put under the same forcing meteorological conditions. Though the two profiles were alike in terms of soil composition and profile depth, they differed in one aspect which was the presence of groundwater. One profile had water table perched at 2 meters from land surface (hereafter referred to as the "GWP") whereas the other profile had no groundwater (hereafter designated to as the "NOGWP").

To maintain simplicity, the following assumptions were adopted: 1) both heat and water transfers took place only in the vertical direction 2) the soil was homogeneous in both soil profiles and 3) water table in GWP was stagnant during the simulation period.

All simulations were run for one year duration, after three years of pre-simulation in order to reach proper initial boundary conditions

The Combined Effect of Shallow Groundwater on Temperature and Energy Balance at Bare Land Surface

(i.e. soil moisture and temperature profiles). The time step was chosen to be one hour.

The weather input data in this study was artificially generated by the weather generator model GEM (Generation of weather Elements for Multiple applications) for Medford, Oregon, USA, which has Mediterranean climate (Köppen climate classification). This climate was chosen because it is temperate climate and characterized by two distinctive seasons: warm dry summer and cool wet winter. Figure 6.1 shows monthly averaged data for minimum and maximum temperatures and precipitation of the year under consideration.

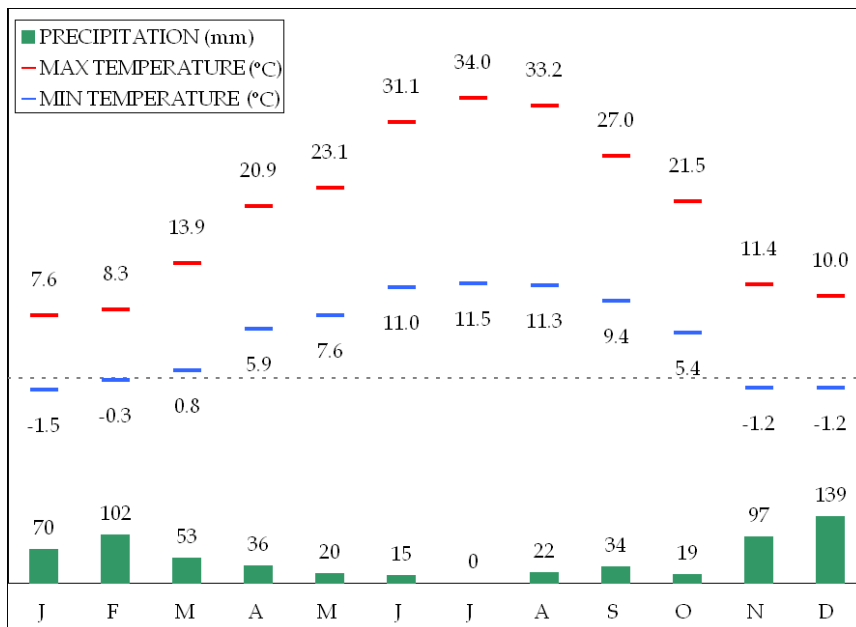


Figure 6.1: Monthly averaged data for minimum and maximum temperatures and precipitation for the simulation year.

The soil of both profiles was chosen to be loam, which is medium-textured soil and contains a relatively even mixture of sand, silt, and clay (Brown, 2003). The soil texture composition and hydraulic parameters are listed in Table 6.1 (Clapp and Hornberger, 1978). The depth of both profiles was assigned to be 30 m to ensure that it is deeper than the common annual depth of heat penetration. The lower boundary condition at the bottom of both profiles was set as a fixed temperature (Dirichlet boundary condition) that is equal to the mean annual temperature at the simulated site. Matric potential of the bottom soil layer for the profile with shallow groundwater (GWP) was

set to maintain a water table at 2 meters below the soil surface. The lower boundary for the water flow of the profile with no water table (NOGWP) was assumed to be gravitational flow.

Table 6.1: Texture composition and physical properties of soil in the two profiles.

Property	Value	Unit
Sand percentage	40	%
Silt percentage	40	%
Clay percentage	20	%
Porosity ϕ	0.451	-
Bulk density ρ_b	1455	kgm^{-3}
Pore-size distribution index b	5.39	-
Air-entry potential ψ_{ae}	0.478	m
Saturated conductivity k_h^*	6.95E-6	ms^{-1}
Dry soil albedo α	0.2	-

After solving for heat and water fluxes within the soil simultaneously with the energy balance at soil surface for each profile, the model provided for each time step the parameters of our concern, i.e. soil moisture, soil temperature, net radiation and heat fluxes (latent, sensible and ground heat fluxes) at land surface. Temperature and moisture of the surface 2.5-cm soil layer within the model were taken as "surface" conditions. The different responses of both profiles were compared with respect to the above mentioned parameters.

6.3 Simulation results and discussion

At the surface of both NOGWP and GWP, Figure 6.2 presents monthly averaged values of a) soil moisture; b) soil temperature; c) net radiation; d) latent heat flux; e) sensible heat flux; and f) ground heat flux, for the simulated year.

The Combined Effect of Shallow Groundwater on Temperature and Energy Balance at Bare Land Surface

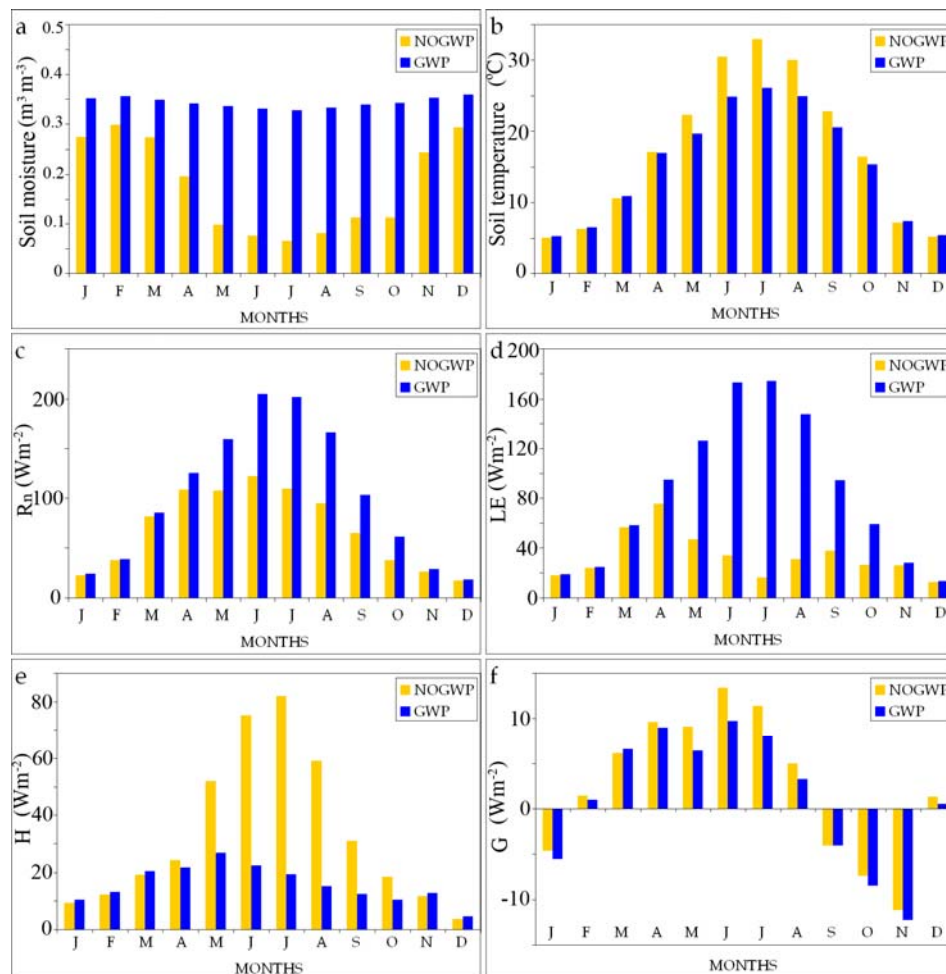


Figure 6.2: Monthly averaged values of surface soil moisture, surface soil temperature and surface energy balance components for the simulated year.

Surface soil moisture (Figure 6.2a) of GWP persisted at high levels all year round. This was due to the incessant water supply from the shallow water table. This supply was not provided for NOGWP which suffered moisture deficit in summer as a result of the increase in potential evaporation and the absence of frequent rainfalls.

Surface soil temperature (Figure 6.2b) of GWP was slightly higher than that of NOGWP in winter and noticeably lower in summer. The higher wintertime surface temperature of GWP can be ascribed to its higher volumetric heat capacity. This effect revealed itself despite the counteractive effects of evaporation and longwave radiation emission.

While the latent heat flux was exploiting the higher temperature in more evaporation, the longwave radiation was continuously alleviating land surface temperature by emitting energy into the atmosphere. Nevertheless, the latter two effects were minor in winter. In summertime, evaporation played a major role in cooling down the soil surface of GWP.

Net radiation (Figure 6.2c) of GWP was generally higher than that of NOGWP all through the year. The higher soil moisture of GWP resulted in lower surface albedo (equation (2.3)); this in turn induced smaller magnitude of reflected shortwave radiation which caused higher net radiation (equation (2.2)).

Latent heat flux (Figure 6.2d) of GWP was continually higher than that of NOGWP. While GWP had boundless supply of water, NOGWP lacked that supply to meet the demand of potential evaporation. This was especially apparent during the dry hot summer at what time the difference in LE between the two profiles was at its highest level.

Synchronized with soil temperature behavior, sensible heat flux (Figure 6.2e) of GWP was a little higher in winter and noticeably lower in summer.

In comparison to NOGWP, ground heat flux of GWP had the propensity to be weaker when it was positive and stronger when it was negative (Figure 6.2f). Since soil thermal conductivity k_s was always higher in GWP, the magnitude of soil temperature gradient $\partial T/\partial z$ controlled which profile had higher G (equation (2.6)). This indicates that NOGWP had higher ground heat flux only when its soil temperature gradient $\partial T/\partial z$ was significantly higher than it is in GWP. This happened mainly during the months when the profile depth was gaining heat, i.e. ground heat flux was downward (positive), and coincided with the months when surface temperature of NOGWP was considerably higher than that of GWP.

The yearly averaged values (Table 6.2) of the variables shown in Figure 6.2, indicates that in the long run, GWP had higher values for soil moisture, net radiation and latent heat flux and lower values for soil temperature, sensible heat flux and ground heat flux.

In GWP, the ample surface soil moisture, which was endowed by the nearby water table, increased the albedo. This in turn made the net radiation higher. Latent heat flux was also higher due to the abundant soil moisture which facilitated satisfying potential evaporation demand. This demand could not be met in NOGWP, and

The Combined Effect of Shallow Groundwater on Temperature and Energy Balance at Bare Land Surface

the extra available energy was spent for increasing soil temperature. The increased soil surface temperature brought on higher magnitudes of sensible and ground heat fluxes.

Ground heat flux in both profiles was small, even though GWP had higher soil thermal conductivity. Thermal conductivity affects heat flux intensity in both vertical directions, thus its effect fades away in the long run. Under this condition, soil temperature gradient $\partial T/\partial z$ becomes the sole governor of ground heat flux magnitude (equation (2.6)). Given that deep soil temperatures eventually come into equilibrium with surface and climate conditions, the deep temperatures are very close to the average annual temperature of the soil surface. As a result, the yearly upshot of ground heat flux in both profiles is very close to zero.

Table 6.2: The yearly averaged values of surface soil moisture, surface soil temperature and the surface energy balance components for the simulated year.

Variable/ Unit	SM m^3m^{-3}	T_s $^{\circ}C$	R_n Wm^{-2}	LE Wm^{-2}	H Wm^{-2}	G Wm^{-2}
NOGWP	0.18	17.1	68.70	33.44	32.74	2.52
GWP	0.34	15.2	100.42	83.52	15.67	1.24

To get a bird's eye view of the instantaneous behavior of the two profiles in terms of the variables under consideration, it is good to zoom into two-hourly averaged data for three days: one typical winter day (January 3), one typical summer day (July 16) and one wet summer day (June 19).

In the winter day (Figure 6.3), both profiles were comparably wet, though surface soil moisture of GWP was slightly higher (Figure 6.3a). This emphasizes that the two profiles react in a different way to rain incidents in terms of their soil moisture. Surface temperature of GWP was a little higher while temperature was decreasing and to some extent lower while temperature was increasing (Figure 6.3b). This can be explained by the difference in volumetric heat capacity between the two profiles; wetter soil has higher volumetric heat capacity and needs more time to warm up or cool down. Net radiation of GWP was slightly higher day and night (Figure 6.3c). During nighttime, the higher negative net radiation of GWP was due to the higher outgoing longwave radiation. The effect of the lower albedo of GWP appeared during daytime through a small increment in its positive net radiation. Similarly, ground heat flux of GWP was a little

higher most of the time (Figure 6.3f). Both latent and sensible heat fluxes of GWP remained somewhat higher day and night except for a few hours after noon (Figures 6.3d and 6.3e).

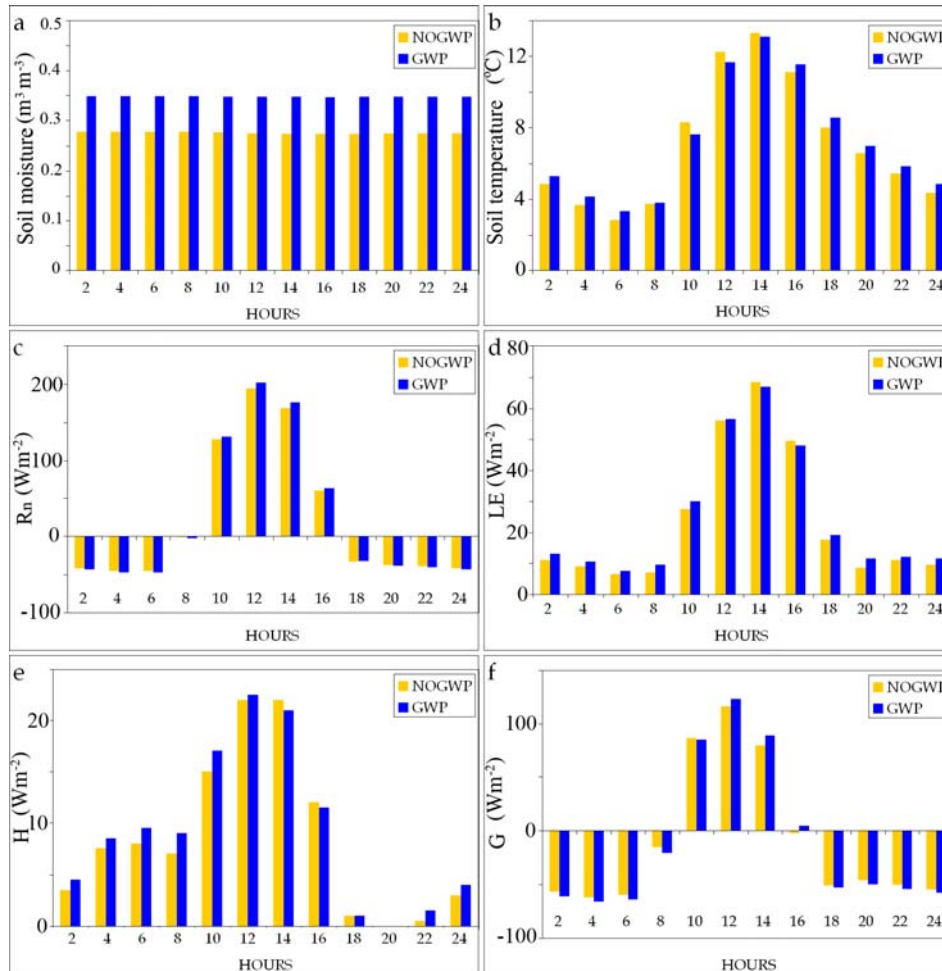


Figure 6.3: Surface soil moisture, surface soil temperature and surface energy balance components for the two profiles in a winter day (January 3 of the simulated year).

In this winter day, the low atmospheric demand for moisture (i.e. potential evaporation), the low temperature contrast between day and night and the comparable wetness status of the two profiles made the differences between them small in terms of the discussed parameters. On the contrary, the summer day demonstrated large and clear differences (Figure 6.4).

The Combined Effect of Shallow Groundwater on Temperature and Energy Balance at Bare Land Surface

The high potential evaporation rapidly consumed the available soil moisture in both profiles (Figure 6.4a). However, the deficit in soil moisture of GWP was compensated by upward fluxes of both water and vapor from the water table. This resulted in considerably higher soil moisture and latent heat flux in this profile (Figures 6.4a and 6.4d). Land surface temperature and hence sensible heat flux of GWP were remarkably lower both day and night (Figures 6.4b and 6.4e). Net radiation of GWP was higher during daytime, but a little lower in nighttime (Figure 6.4c). Finally, ground heat flux of GWP tended to be stronger than that of NOGWP most of the time (Figure 6.4f). The higher thermal conductivity of GWP induced clearly stronger ground heat flux during nighttime. During daytime, the higher surface temperature of NOGWP imposed higher soil temperature gradient $\partial T/\partial z$ and resulted in comparable ground heat flux values between the two profiles.

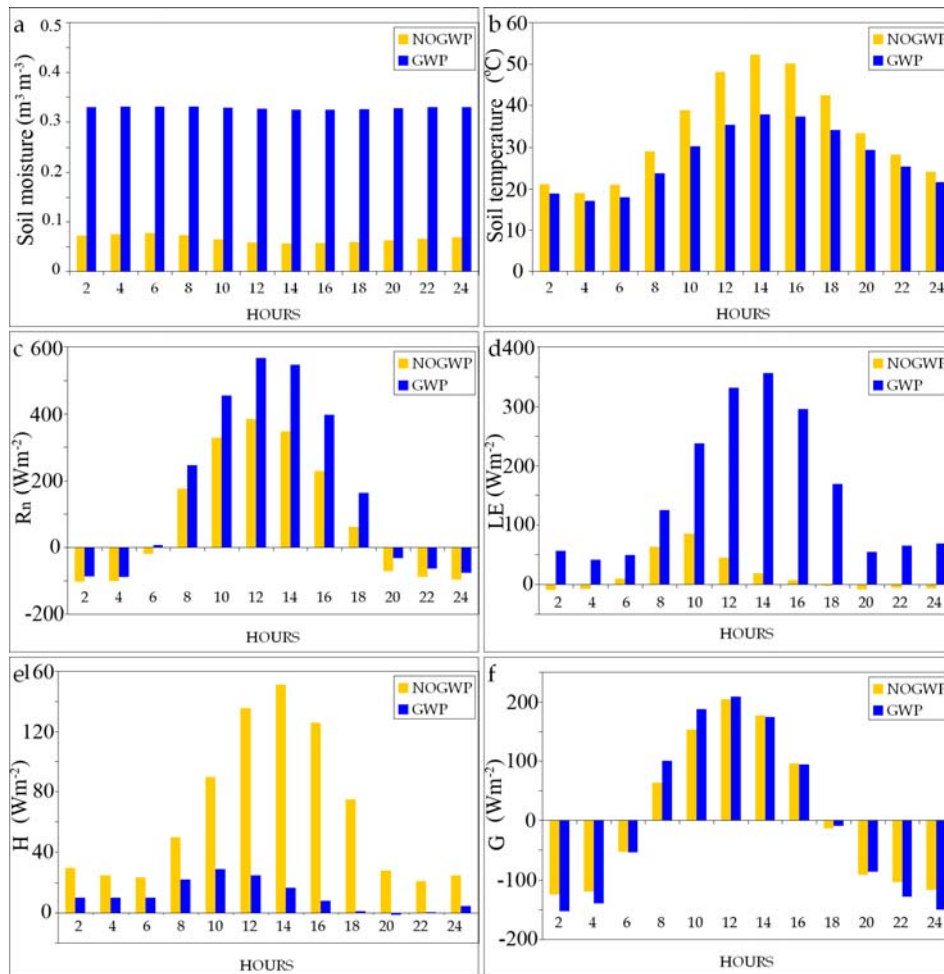


Figure 6.4: Surface soil moisture, surface soil temperature and surface energy balance components for the two profiles in a summer day (July 16 of the simulated year).

It may be useful to observe what happened after it had rained in summer (Figure 6.5). The rain temporarily compensated the moisture deficit in NOGWP, thus the change occurred chiefly in this profile. The differences between the two profiles became smaller regarding land surface temperature, net radiation, latent heat and sensible heat fluxes. This recalls the situation of the winter day (Figure 6.3), but with more pronounced differences (difference of more than ± 1.5 °C in land surface temperature). The increased surface soil moisture of NOGWP after rainfall (Figure 6.5a compared to 6.4a) increased latent heat flux (Figure 6.5d) and decreased the surface albedo which caused the increment in daytime net radiation (Figure 6.5c). Surface

The Combined Effect of Shallow Groundwater on Temperature and Energy Balance at Bare Land Surface

soil temperature of NOGWP decreased and became comparable to that of GWP (Figure 6.5b). It is noticed here that the effect of the difference in volumetric heat capacity became clear again, particularly when surface temperature of GWP decreased slower during the decreasing phase. Harmonized with surface soil temperature, sensible heat flux of NOGWP decreased to become comparable to that of GWP (Figure 6.5e). Finally, ground heat flux of NOGWP decreased during daytime (downward flux), due to the cooling surface temperature which decreased soil temperature gradient $\partial T/\partial z$ (Figure 6.5f).

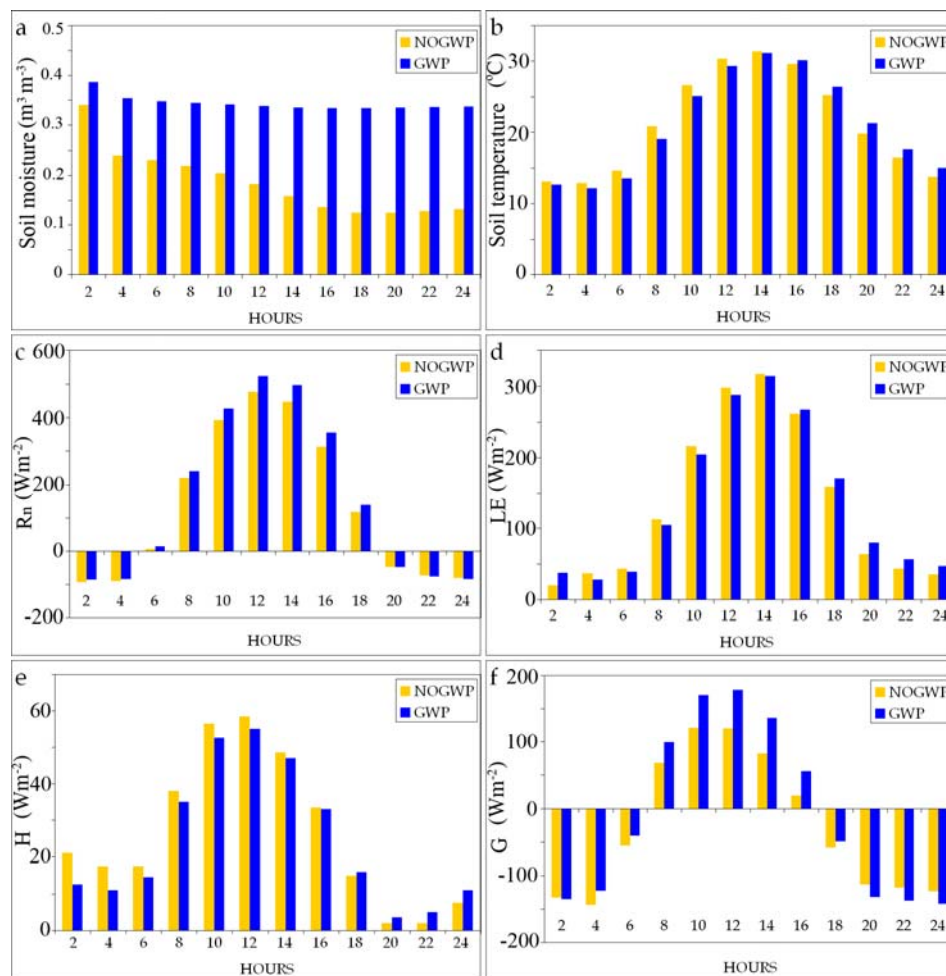


Figure 6.5: Surface soil moisture, surface soil temperature and surface energy balance components for the two profiles in a wet summer day (June 19 of simulation year).

The above results show that GWP is more capable of meeting the demand of potential evaporation. When evaporation is not that intense or precipitation provides both profiles with adequate amount of moisture, differences in latent heat flux are minor between the two profiles. Under such conditions, latent heat fluxes of the two profiles have approximately the same values.

On the other hand, latent heat flux plays a major role in differentiating between the two profiles when potential evaporation is sufficiently strong. Thus, large portion of the available energy for GWP is consumed by evaporation, leaving less energy to be spent in warming the soil surface. Consequently, the cooler surface soil causes smaller exchange of heat with the air above land surface (i.e. sensible heat flux) and with subsurface soil layers (i.e. ground heat flux).

Nevertheless, the increment of latent heat flux due to the excess of soil moisture is not the sole player within the course of shallow groundwater effect on surface temperature and surface energy balance. Actually, the results show that there are other factors that play a role in shaping and molding that effect. Due to its higher moisture, GWP has different values of volumetric heat capacity, thermal conductivity, albedo and emissivity (Figure 2.2). Accordingly, the two profiles differ in the absorbed and emitted amounts of energy, and also in heat fluency within the soil. In other words, both profiles respond differently to the atmospheric forcing.

The effect of volumetric heat capacity was clear in the temperature behavior when the difference in wetness between the two profiles was not severe, i.e. in the winter day and the rainy summer day (Figures 6.3 and 6.5). Under this condition, the profile with higher volumetric heat capacity (GWP) shows a delayed temperature response during both increasing and decreasing phases. On the other hand, the effect of thermal conductivity was clear in increasing the intensity of ground heat flux within GWP, and the effect of albedo was clear in increasing its net radiation. Finally, the effect of emissivity as aforementioned is minor due to its two fold connection to both incoming and outgoing longwave radiation. The latter two have generally comparable magnitudes and act in opposite directions. Actually, this effect cannot be traced in the figures presented in this study because SHAW adopts a constant value of emissivity of 1.0 and does not account for its moisture dependency.

The results show that the effect of shallow groundwater on surface soil temperature is definite. However, what can be learned regarding

differences large enough to be detectable via the currently operational satellites? It was noticed that the temperature differences in the winter day were small (about ± 0.5 °C), and might be difficult to be detected remotely (Figure 6.3). On the contrary, the differences in both summer days were big enough, and could be basically sensed using the currently operational thermal infrared sensors (Figures 6.4 and 6.5).

Concerning the best time of the day to detect groundwater effect, the presented results show that all day and night hours are suitable when the effect of latent heat flux is predominant (Figure 6.4). When the effect of volumetric heat capacity is predominant, most day and night hours are suitable except for the transition period when the temperature of the two profiles equalizes (Figures 6.3 and 6.5).

In this experiment, two meters was applied as water table depth; however the critical depth at which groundwater can still show its effect on land surface is different for each soil type. While the critical depth may be very small for groundwater within coarse well-drained soils as sands and gravels, it may reach up to several meters for groundwater within clayey soils.

6.4 Conclusions and recommendations

The purpose of this investigation was to explore the features of shallow groundwater effect on land surface temperature and surface energy balance components under bare soil conditions. It has been illustrated that areas dominated by shallow groundwater have wetter soil profile due to the upward water and vapor flux; consequently, they respond differently to the prevailing atmospheric forcing. Furthermore, fundamental processes that are noticeably different within the scope of this effect were brought to light.

Generally speaking, shallow groundwater areas reflect less shortwave radiation to the atmosphere due to their lower albedo and therefore, they get higher magnitude of shortwave radiation. When potential evaporation demand is high enough, a large portion of the energy received by these areas is spent on evaporation. This makes the latent heat flux predominant, and leaves less energy to heat the soil. Consequently, this induces lower magnitudes of both sensible and ground heat fluxes.

The higher soil thermal conductivity in shallow groundwater areas facilitates heat transfer between the top soil and the subsurface which promotes greater provisional heat transfer in both vertical

directions. That is to say, soil subsurface is more thermally connected to the atmosphere. Nevertheless, the continuous heat exchange between the surface and the subsurface makes the deep soil temperatures come into equilibrium with surface and climate conditions. As a result, the yearly upshot of ground heat flux in both profiles is very close to zero.

With regards to remote sensors' capability of detecting shallow groundwater effect on land surface temperature, it was found that this effect can be sufficiently clear to be sensed if at least one of two conditions are met: firstly, latent heat flux effect is predominant due to the high potential evaporation, or secondly, soil volumetric heat capacity effect is strong due to the big contrast in air temperature between day and night.

The recent advancement in the field of remote sensing models, e.g. Surface Energy Balance System (SEBS) (Su, 2002; van der Kwast et al., 2009; Ma et al., 2011) and Surface Energy Balance Algorithm for Land (SEBAL) (Bastiaanssen, 1995; Mohamed et al., 2004; Zwart and Bastiaanssen, 2006), has proved that satellite imagery is valuable tool in retrieving major components of surface energy balance. Wherever it is possible to delineate the effect of shallow groundwater on remotely sensed map of land surface temperature, it would be routinely feasible to highlight its effect on surface energy fluxes maps. The practical utilization of remote sensing data and SEBS in delineating shallow groundwater effect on land surface temperature and surface energy balance is illustrated in the next chapter (Chapter 7).

The numerical experiment in this study represents a special case; it was implemented for specific site, climate type, soil conditions and water table depth. In spite of that, it was helpful in highlighting the main aspects of shallow groundwater effect and in concluding important findings regarding shallow groundwater depth detection using thermal remote sensing. This is because the experiment involved 1) a soil type (loam) that contains a relatively even mixture of sand, silt, and clay, and 2) a climate that has various weather conditions; wet and cold in winter, and dry and hot in summer. However, the complex convoluted interactions among the different components of surface energy balance may differ from one region to another and from time to time, in accordance to the site specific conditions. Hence in areas where there is a doubt concerning the chances and conditions of groundwater depth detection using thermal remote sensing, it is advisable to implement numerical simulations that consider the specific conditions prevailing in the area under

*The Combined Effect of Shallow Groundwater on Temperature and Energy
Balance at Bare Land Surface*

investigation (i.e. site elevation and latitude, soil types and characteristics, climate type, water table depth, etc.).

7 Reconnoitering the Effect of Shallow Groundwater on Land Surface Temperature and Surface Energy Balance Using MODIS and SEBS*

* Based on:

Alkhaier, F., Z. Su, and G. N. Flerchinger (2011), Reconnoitering the effect of shallow groundwater on land surface temperature and surface energy balance using MODIS and SEBS, *Hydrology and Earth System Sciences Discussions*, 8, 8671-8700, doi:10.5194/hessd-8-8671-2011.

7.1 Introduction

Shallow groundwater usually characterizes low lands within watersheds. Besides, many newly reclaimed irrigation lands suffer shallow water table conditions owing to intense irrigation, low assimilative capacity and low drainage rates (Wichelns, 1999; Northey et al., 2006).

Groundwater flow models and the management of irrigation systems can be greatly supported by satellite thermal recurrent measurements, provided that these measurements were capable of detecting the depth and the areal extent of shallow groundwater. Under this condition, these measurements may have additional advantage in monitoring the shallow groundwater effect on surface energy balance, and in bringing that effect within land surface and climate models on more solid basis.

In Chapter 1, it was noted that even with the modest faculties of remote sensing technology between the late 60's and the early 80's, enthusiastic investigations were conducted for tracing shallow groundwater effect on land surface temperature remotely (Chase, 1969; Heilman and Moore, 1982). In spite of the radical progress achieved in remote sensing, there is hardly any noticeable research of utilizing this powerful tool in shallow groundwater studies. Furthermore, remote sensing data has not been effectively utilized in mapping shallow groundwater effect on surface energy balance components thus far.

In the previous chapter (Chapter 6) a detailed description of how shallow groundwater affects surface soil moisture, temperature and the various components of surface energy balance was presented. Furthermore, the optimum conditions under which this effect can be sufficiently clear to be detected using satellite measurements were discussed.

One objective of this chapter is to inspect the capacity of MODIS (Moderate-resolution Imaging Spectroradiometer) to detect the effect of shallow groundwater on surface temperature of an area within Al-Balikh River basin in northern Syria, using day and night images. Another objective is to reconnoiter the spatial distribution of shallow groundwater effect on surface energy balance components, soil moisture, evaporative fraction and daily evaporation in this area at the day of image acquisition.

The interrelationship between water table depths measured in the field and land surface temperatures retrieved from two MODIS images (day and night) shot within the timeframe of our field campaign was investigated. The Surface Energy Balance System algorithm (SEBS) was used to produce the maps of surface energy balance, evaporative fraction and daily evaporation. The spatial relationships of water table depths with these parameters were then inspected and analyzed. Hereinafter a brief description of collecting and handling both field measurements and remote sensing data are given.

7.2 Study area description and data collection

7.2.1 Field data

During a short period (January 13-17, 2007) a field campaign was conducted within Al-Balikh river basin in northern Syria supported by the General Organization for Land Reclamation, Ar-Raqqa. The campaign covered an area of about 186 km^2 , between latitude $36^{\circ} 02'$ to $36^{\circ} 13'$ N and longitude $38^{\circ} 46'$ to $39^{\circ} 03'$ E (Figure 7.1).

The study area represents a flat region of reclaimed agricultural fields. Hence, there is no considerable topographic relief within the area under consideration. The Digital Elevation Model retrieved from the ASTER Global Digital Elevation Model (GDEM, 30 m pixel resolution) shows that the flat study area level ranges between approximately 265 m and 285 m AMSL (Figure 7.2a).

The majority of the fields in the area were fallow. Few spots were planted by winter wheat and vegetables (Figure 3.5). Figure 7.2b shows the Normalized Difference Vegetation Index (NDVI) map at January 17, which was calculated using the MODIS red and near-infrared bands (250 m pixel resolution), centered at 645 nm and 858 nm respectively. The NDVI values within the study domain were low demonstrating the predominance of bare soil conditions.

Reconnoitering the Effect of Shallow Groundwater on Land Surface Temperature and Surface Energy Balance Using MODIS and SEBS

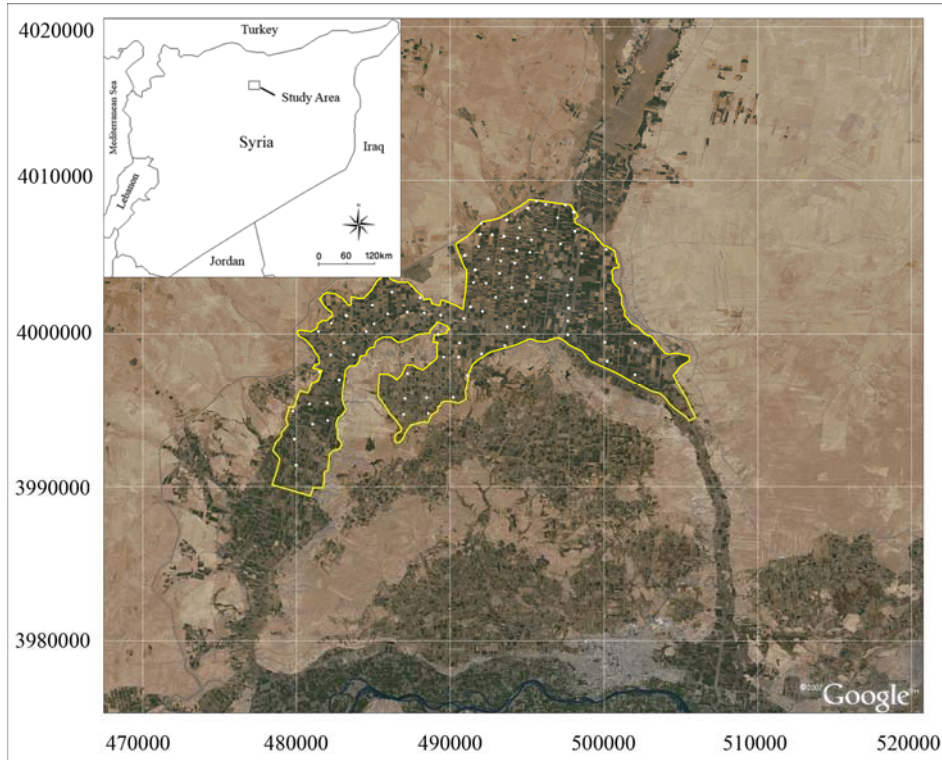


Figure 7.1: Study area location within Al-Balikh river basin in northern Syria (Google Earth image).

The field campaign days were mostly sunny. The prevalent wind was dry cold northerly wind with an average speed of 2.6 ms^{-1} . In this area, air temperature usually has a high contrast between day and night. During the field campaign period, air temperatures fell to $-5 \text{ }^\circ\text{C}$ in nighttime and rose to $14 \text{ }^\circ\text{C}$ in daytime.

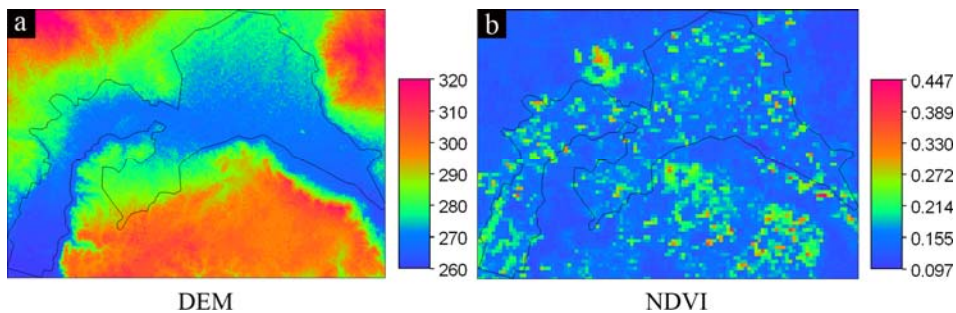


Figure 7.2: a) Digital Elevation Model (30 m pixel resolution), and b) NDVI map of the study area (250 m pixel resolution).

Somewhere between mid November and mid February, the main irrigation canal that supplies the whole area is usually blocked in favor of maintenance for about one and half months. A month before our field campaign the irrigation activity had been stopped. In this way, it was assured that there were no intense water table fluctuations in the period of our measurements.

Data of water table depth and surface soil moisture was collected from about 90 locations. Soil moisture of the upper 5 *cm* was measured in-situ using Stevens' Hydra probe. Additionally, some soil samples were brought to the laboratory for texture analysis and soil moisture verification. Water table depth which was measured manually using a simple sounding device ranged between 1 and 8 *m*. Raster maps of soil moisture and water table depth were generated starting from the point data by means of a moving average interpolation.

7.2.2 Remote sensing data

Two (day and night) MODIS level 1B images of January 17, 2007 were the clearest within the field work timeframe; hence they were used in this study. Using MODIS Reprojection Swath Tool (MRTSwath), each radiances-calibrated level 1B image was transformed from HDF-EOS swath format to a UTM projected GeoTIFF image and resampled for 1 km pixel size. Next, it was imported to the Integrated Land and Water Information System (ILWIS) for further processing and surface energy balance calculations. This included: raw data to radiance or reflectance transformation; brightness temperature computation and atmospheric correction. Within the framework of SEBS, land surface albedo, emissivity, temperature, vegetation indexes, surface energy fluxes, evaporative fraction and actual daily evaporation were then calculated.

7.3 Surface energy balance and related maps calculations

SEBS is an advanced remote sensing algorithm developed by Su (2001) for the estimation of atmospheric turbulent fluxes maps using satellite data. It has been extensively applied and validated with a variety of methods in different regions and climates (Su, 2002; Jia et al., 2003, 2009; Su et al., 2005; McCabe and Wood, 2006; McCabe et al., 2008; Pan et al., 2008; Badola, 2009; van der Kwast et al., 2009, Gibson, et al. 2011).

Calculating surface energy fluxes by means of SEBS involves using two types of data: spatially distributed variables (maps) and in-situ measured variables. The first type can be derived from remote sensing data and includes land surface albedo, emissivity, temperature, vegetation indexes and roughness height. The second type can be obtained from local weather stations and includes air pressure, temperature, humidity, wind speed and solar radiation.

SEBS algorithm is composed of: a set of equations to obtain land surface albedo, emissivity, temperature, vegetation indexes from satellite data; an extended model for calculating the roughness length for heat transfer; and a formulation for obtaining sensible heat flux by an iterative process. After estimating all four terms of the surface energy balance (equation (2.1)) using SEBS, additional important physical information can be retrieved easily, such as evaporative fraction, daily evaporation and surface soil moisture.

In SEBS, Net radiation, R_n , is calculated as the upshot of radiation at land surface (equation (2.2)), and Ground heat flux, G , is simply calculated as a ratio of net radiation, R_n , depending on the fractional canopy coverage f_c of the studied area:

$$G = R_n [0.05 + 0.265(1 - f_c)] \quad (7.1)$$

Sensible heat flux, H , is calculated using Monin–Obukhov similarity (MOS) theory. Within the Atmospheric Surface Layer (ASL), the bottom (10%) of the Atmospheric Boundary Layer (ABL) and above the roughness sub-layer, the similarity relationships for wind speed and temperature profiles can be expressed as:

$$u = \frac{u_*}{k} \left[\ln \left(\frac{z - d_0}{z_{z_{om}}} \right) - \Psi_m \left(\frac{z - d_0}{Ol} \right) + \Psi_m \left(\frac{z_{om}}{Ol} \right) \right] \quad (7.2)$$

$$\theta_s - \theta_a = \frac{H}{k u_* \rho_a c_a} \left[\ln \left(\frac{z - d_0}{z_{z_{oh}}} \right) - \Psi_h \left(\frac{z - d_0}{Ol} \right) + \Psi_h \left(\frac{z_{oh}}{Ol} \right) \right] \quad (7.3)$$

In which u is the average wind speed, θ_s and θ_a are the potential temperatures at land surface and at the reference height z respectively, u_* is wind friction velocity, k is von Karman's constant, d_0 is the zero plane displacement height, z_{om} and z_{oh} are the roughness heights for momentum and heat transfer respectively, Ψ_m

and Ψ_h are stability correction functions for momentum and heat transfer respectively, ρ_a and c_a are air density and specific heat correspondingly and Ol is the Obukhov length which is expressed as:

$$Ol = \frac{\rho_a c_a u_*^3 \theta_v}{k g H} \quad (7.4)$$

where θ_v is the virtual potential temperature near land surface and g is the gravitational acceleration.

Sensible heat flux, H , and latent heat flux, LE , are derived from equations (7.2-7.4) using an iterative process and controlled by two bounding limits (i.e. wet and dry conditions). Within the course of this iterative process, the relative evaporation, Λ_r , which is the ratio between the actual and the potential latent heat fluxes, LE and LE_{wet} , is calculated by:

$$\Lambda_r = \frac{LE}{LE_{wet}} = 1 - \frac{H - H_{wet}}{H_{dry} - H_{wet}} \quad (7.5)$$

where H_{wet} and H_{dry} are the sensible heat fluxes at the wet and the dry limits respectively. For further details the reader is referred to Su (2002 and 2005).

The evaporative fraction, Λ , which is the ratio between the energy consumed for actual evapotranspiration and the net available energy can be calculated from:

$$\Lambda = \frac{LE}{R_n - G} = \frac{LE}{LE + H} \quad (7.6)$$

Finally, the actual daily evaporation can be estimated as:

$$E_{daily} = 8.64 \times 10^7 \times \bar{\Lambda} \times \frac{\bar{R}_n - \bar{G}}{L \rho_w} \quad (7.7)$$

According to Su (2005), the evaporative fraction, $\bar{\Lambda}$, is conservative and can be approximated by the SEBS estimate (Λ). \bar{R}_n and \bar{G} are the daily values of net radiation and soil heat flux respectively, L is the latent heat of vaporization and ρ_w is water density. The daily

upshot of soil heat flux is small and can be neglected, and the daily net radiation, $\overline{R_n}$, is calculated by:

$$\overline{R_n} = (1 - \alpha) \overline{K_{in}} + \varepsilon \overline{L} \quad (7.8)$$

where $\overline{K_{in}}$ is the daily incoming radiation and \overline{L} is daily net longwave radiation.

The evaporative fraction proved to be a suitable indicator of soil moisture conditions. Using datasets from USA and Spain, Bastiaanssen et al. (2000) demonstrated that volumetric soil moisture can be estimated using a statistical relationship between evaporative fraction and soil moisture of the vadose zone. This relationship was later modified by Scott et al. (2003) to involve the degree of saturation (θ/θ_{sat}):

$$\frac{\theta}{\theta_{sat}} = \exp\{(\Lambda - 1)/0.42\} \quad (7.9)$$

where θ and θ_{sat} are the actual and the saturated volumetric soil moisture respectively. By validating the accuracy of this relationship with data from irrigated plains in Pakistan and Mexico, Scott et al. (2003) demonstrated that it is a kind of a standard relationship which can be applied to a wide range of soils.

To inspect the spatial relationships between groundwater depth map and the variant parameters' maps, the Cross operation in ILWIS was carried out between the relevant raster maps. The Cross operation performs an overlay of two raster maps by comparing pixels at the same positions in both maps and outputs all the combinations that occur between the values in both maps in an output cross-table. Afterwards, the results in each cross-table were plotted accordingly.

7.4 Results and discussion

7.4.1 Water table depth and soil moisture maps

The two raster maps showing the spatial distributions of water table depth and soil moisture were interpolated from the point data collected in the field (Figure 7.3). Areas in the vicinity to Al-Balikh River (the eastern area) and in Wadi Al-Faied (the south western area) have deeper water table (Figure 7.3a) and lower level of soil

moisture (Figure 7.3b), while the remaining area has shallower water table and higher level of soil moisture.

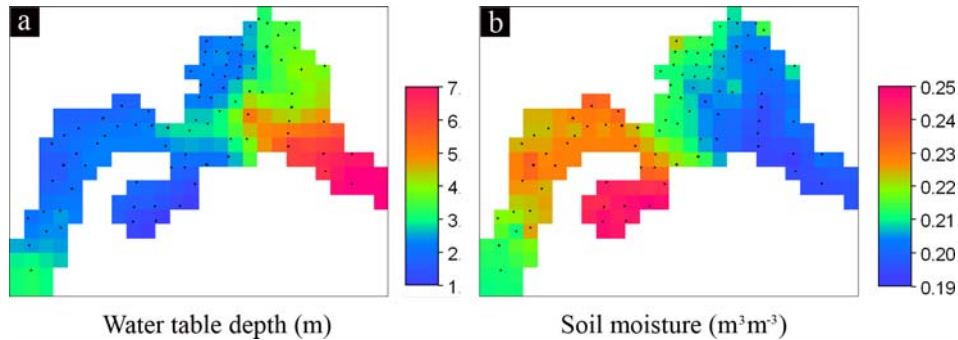


Figure 7.3: The interpolated raster maps for **a)** water table depth and **b)** soil moisture of the upper 5 cm. Locations of the point data collected in the field are also shown.

The deeper water table conditions in Al-Balikh River and Wadi Al-Faied are most likely attributable to the relatively better drainage conditions. A historical False Color Composite (FCC) image captured by the Multispectral Scanner System (MSS) sensor on board of Landsat 2 on August 08, 1975 (Figure 7.4), demonstrates that the areas with deeper water table correspond to very old cultivated land. On the other hand, the newly cultivated area had shallower water table demonstrating poorer drainage conditions.

The cross-relationship between water table depth and surface soil moisture is plotted in Figure 7.5, and explains that soil moisture clearly increased starting from a water depth of 4 m and up. Where the water table was deeper than 4 m, surface soil moisture seems not to be affected by water table level.

Reconnoitering the Effect of Shallow Groundwater on Land Surface Temperature and Surface Energy Balance Using MODIS and SEBS

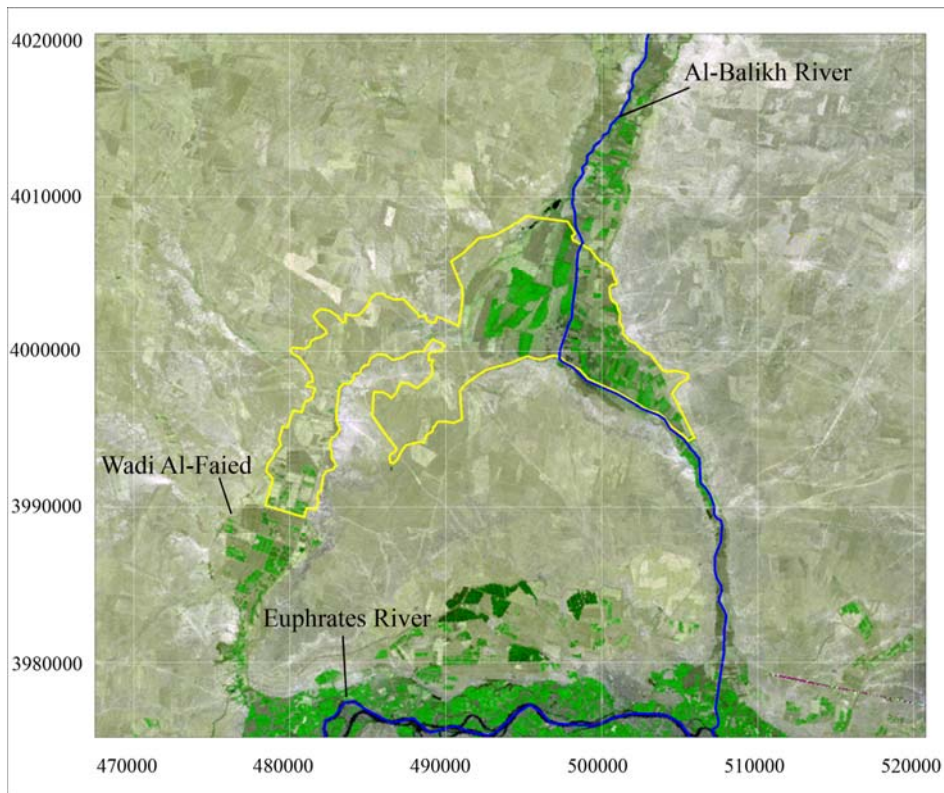


Figure 7.4: Landsat 2, False Color Composite (Red = band 5; Green = band 6; Blue = band 4), August 08, 1975, 09:34 LT.

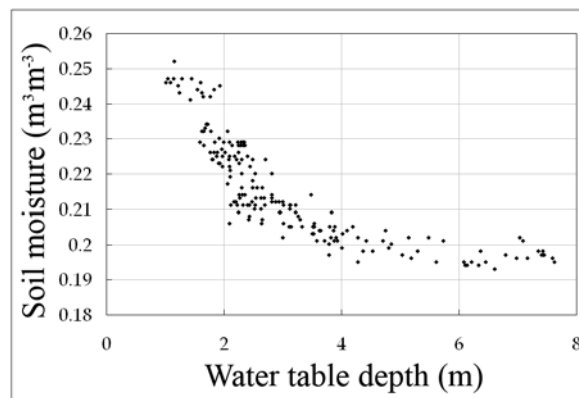


Figure 7.5: The cross-relationship between water table depth map and surface soil moisture map.

7.4.2 Soil temperature maps

By inspecting both day and night maps of land surface temperature extracted from the two MODIS images of January 17, it was found that areas of deeper water table depth were warmer at daytime and cooler in nighttime (Figure 7.6).

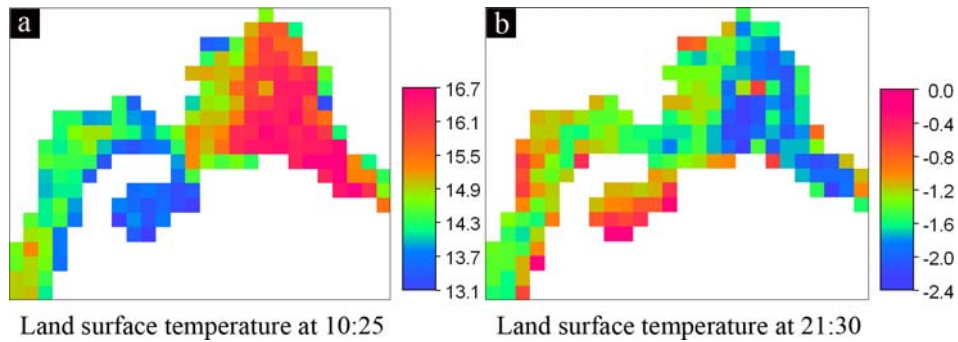


Figure 7.6: Land surface temperature maps ($^{\circ}\text{C}$) of the study area on January 17, 2007. **a)** Daytime temperature, and **b)** nighttime temperature.

Plotting the cross-relationships (Figure 7.7) between water table depth and day and night temperatures at January 17, 2007 showed that, down to 4 m water depth, daytime temperature increased (Figure 7.7a) and nighttime temperature decreased with increasing water table depth (Figure 7.7b).

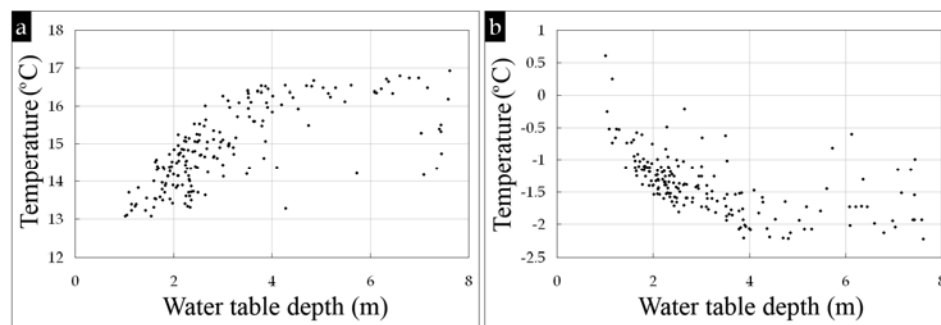


Figure 7.7: Cross-relationships between water table depth and **a)** daytime land surface temperatures and **b)** nighttime land surface temperatures at January 17, 2007.

7.4.3 Surface energy balance maps

The instantaneous maps of surface energy balance at 10:25 LT calculated via SEBS are shown in Figure 7.8. There was a clear trend in the variant energy fluxes to follow the spatial distribution of the water table depth shown in Figure 7.3a. The spatial trend was clearer for both latent and sensible heat fluxes as in Figures 7.8b and 7.8c in which the areas with shallower groundwater showed clearly higher latent heat flux and lower sensible heat flux in comparison to areas with deeper water table depth. The trend was less sharp for the net radiation and ground heat flux (Figures 7.8a and 7.8d). Yet, shallow groundwater areas tended to have higher positive net radiation and ground heat flux. These relationships become clearer in the cross-relationships plotted in Figure 7.8 which shows that latent and sensible heat fluxes had sharper trend to follow water table depth than that of net radiation and ground heat flux. In agreement with the findings and results of the previous chapter (Chapter 6), net radiation, latent and ground heat fluxes, decreased with increasing water table depth, while sensible heat flux increased with increasing water table depth.

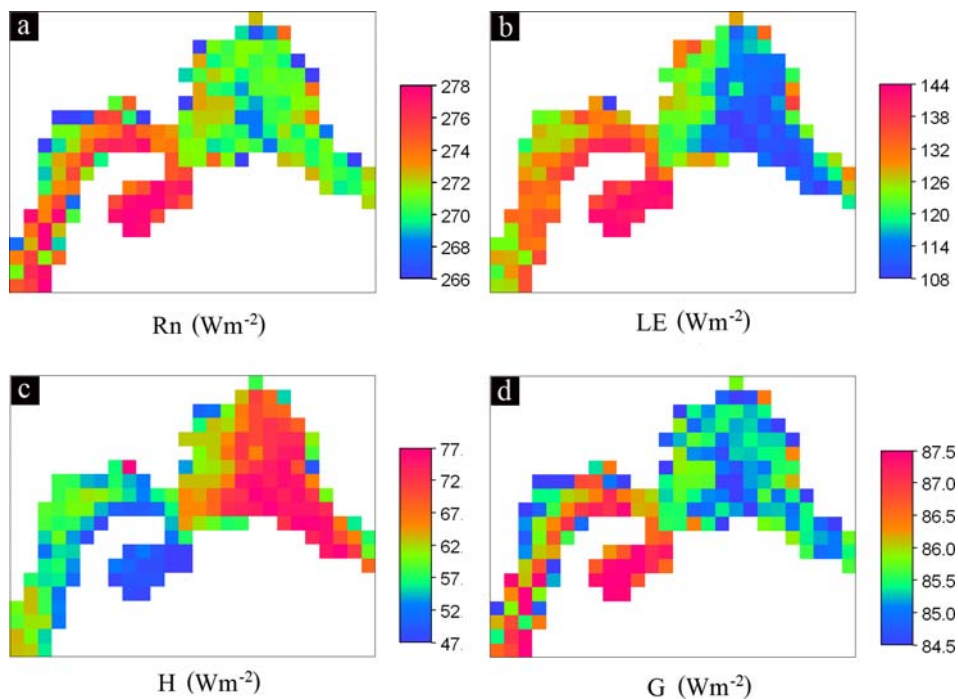


Figure 7.8: The SEBS calculated maps of the instantaneous components of surface energy balance at 10:25 LT, January 17, 2007.

It is noticed that some pixels within the shallower groundwater areas had lower values than the general trend regarding net radiation and ground heat flux (Figures 7.9a and 7.9d). Investigating the reason behind this phenomenon revealed that some spots of these areas suffer soil salinity (Alkhaier, 2003). Where salt crust accumulates at land surface, it increases the albedo (Fujimaki et al., 2003); this in turn magnifies the reflected shortwave radiation (equation (2.2)) and diminishes net radiation. Since ground heat flux is calculated in SEBS as a ratio of net radiation (equation (7.1)), it is diminished also at these pixels (Figure 7.9d).

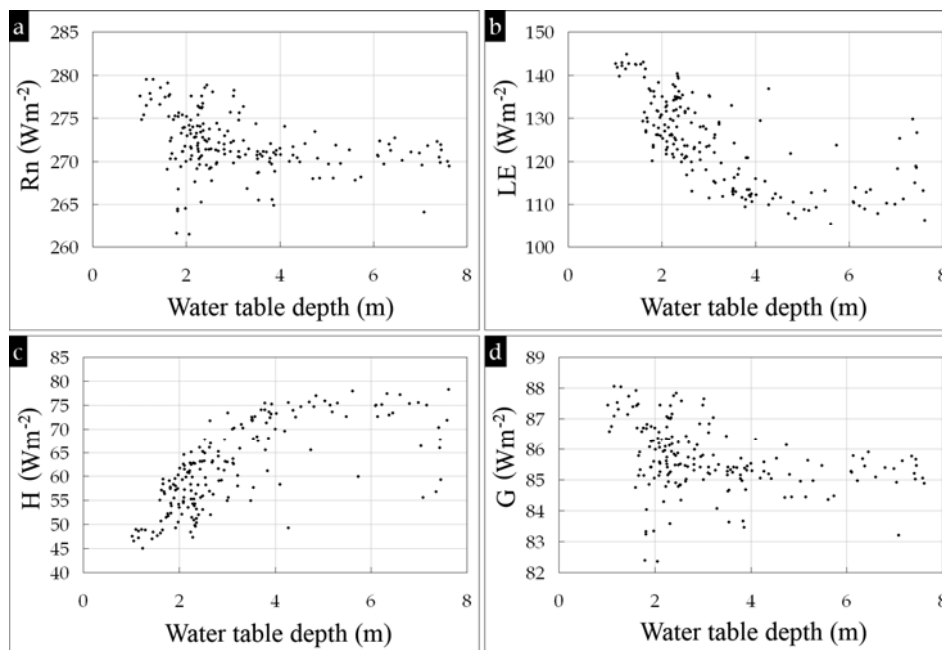


Figure 7.9: The cross-relationships between water table depth and the variant instantaneous components of surface energy balance at 10:25 LT, January 17, 2007.

7.4.4 The maps of evaporative fraction and actual daily evaporation

Figure 7.10 shows the cross-relationships between water table depth and both the evaporative fraction and the actual daily evaporation. Both parameters had their highest values for shallower water table depth. They become smaller with increasing water table depth. Comparing the values of the daily evaporation with the measured pan evaporation (Class A) from the nearby weather station (2.4 mm) for

this day (January 17) certifies that the SEBS estimates of the energy fluxes were reasonable.

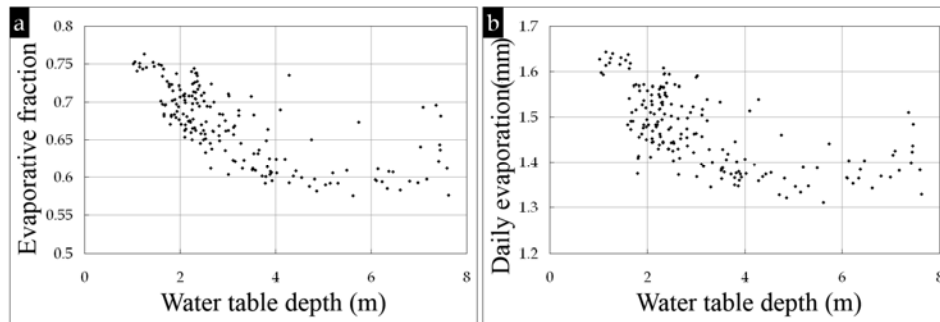


Figure 7.10: The cross-relationships between water table depth and **a)** the evaporative fraction and **b)** the actual daily evaporation.

7.4.5 The soil moisture map estimated from SEBS' actual daily evaporation

Both maps of soil moisture measured in the field and soil moisture estimated from SEBS evaporative fraction were plotted against each other in Figure 7.11, in which a good agreement is clear ($R^2=0.7506$). Yet, the calculated soil moisture was slightly underestimated for lower levels of soil moisture and a little overestimated for higher levels of soil moisture. This phenomenon can be ascribed to the fact that equation (7.9) was originally developed for soil moisture of the complete vadose zone (Bastiaanssen et al., 2000; Scott et al., 2003) whereas the measured soil moisture was only for the upper 5 cm. The agreement between the two soil moisture maps affirms the reasonability of SEBS calculations.

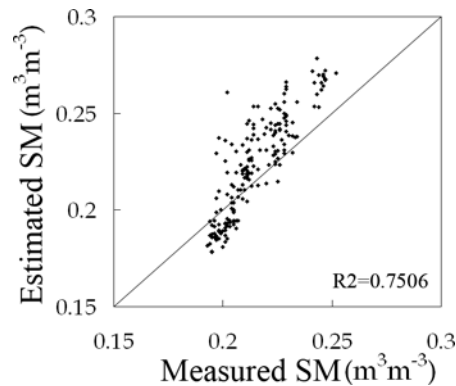


Figure 7.11: Soil moisture of the upper 5 cm measured in field by Stevens' Hydra probe against soil moisture estimated from evaporative fraction using equation (7.9).

7.5 Conclusions and recommendations

It can be concluded that it is possible to map the effect of shallow groundwater on land surface temperature using the freely available satellite data like MODIS. Satellite measurements demonstrated a clear correspondence of surface temperature with water table depth day and night. In parallel, our field measurements demonstrated a clear relationship between surface soil moisture and water table depth. Consequently, the various surface energy balance maps, calculated using SEBS and MODIS data, correlated well with water table depth. Finally it was possible using the SEBS estimate of evaporative fraction to estimate soil moisture distribution in the area reasonably.

It may be appropriate here to address a discussion point which was left open in Chapter 4: It was observed in Figures 4.2 and 4.3 that the maximum temperature was higher for wetter soils which coincide with shallower water table (Figure 4.4). However all the simulation results in Chapter 6 (Figures 6.3b, 6.4b and 6.5b) and the satellite measurements in this chapter (Figure 7.6a) proved with no doubts that areas of deeper water table depth should have higher magnitude of maximum surface temperature at daytime. To solve this puzzling contradiction between the inference from the in situ measurements and that from both the modeling and satellites measurements, we have to keep in mind that the in situ measurements were obtained from loggers deployed a 5 and 10 cm depth below the land surface, while the modeling results represent the temperature of the upper

2.5 cm and the remotely sensed temperatures are of the very top surface (i.e. skin temperature).

Concerning the conditions of the in situ measurements, the following remarks should be considered:

1. Soil thermal conductivity is higher for wetter soil (at places of shallower water table (Figure 4.4).
2. The process of deploying the HOBO Pendant data logger is a destructive process with regards to the soil matrix structure.
3. The soil ability to encompass the data logger is enhanced by increasing its moisture.
4. The big size of the data logger (58 x 33 x 23 mm) makes its temperature measurements affected considerably by the surface area which is in effective contact with soil particles.

Taking into account these four remarks one can perceive that the loggers deployed in shallower groundwater areas were more thermally connected to the soil surface than those deployed in deeper groundwater areas.

To be certain of this interpretation, the correlations between the loggers' measurements and the air temperatures were inspected. It was found that the measurements of the loggers deployed in shallower water table had much higher correlations with air temperature than those deployed in deeper groundwater areas: for loggers deployed at 5 cm, the correlation values ranged from 0.58 for deeper groundwater areas to 0.94 for shallower groundwater areas. And for the 10 cm loggers the correlation values ranged from 0.17 for deeper groundwater areas to 0.70 for shallower groundwater areas. In this way the temperature measurements were still affected by groundwater depth but via indirect way (soil moisture and the related thermal conductivity).

Many factors played a substantial role in the good results of our investigation. In view of the conclusions of the previous chapter (Chapter 6) with regards to the favorable conditions for detecting the effect of shallow groundwater via thermal remote sensing, it is noticed that the two major conditions were met in this day. Whereas the effect of latent heat flux was clear at daytime due to the relatively high potential evaporation under the prevalent dry and sunny conditions, the effect of volumetric heat capacity was clear owing to the high contrast in air temperature between day and night. In this way the circumstances were most expedient for water table depth detection using thermal remote sensing.

The suspension of irrigation activity together with the scantiness of rain incidents for quite some time before the measurement campaign made surface soil moisture and water table depth conditions fairly stable. It can be added here that the short period of our measurement campaign facilitated obtaining reliable data of the two state variables (i.e. soil moisture and water table depth).

Having limited vegetation cover in the study area was advantageous regarding avoiding possible perturbations and complexities imposed by plants on surface temperature measurements. Further investigations of such circumstances, using remote sensing data supported by numerical simulations, are recommended. Actually, the authors are working on this issue.

The limited topographic relief and vegetation cover in the study area helped to avoid possible uncertainty sources (Gibson et al., 2011) in SEBS estimates of energy fluxes. The correspondence of the derived daily evaporation and soil moisture with in field measured values proved that the utilization of SEBS in this area was a success.

The exploitation of MODIS in this study proved to be an excellent choice, since it has many convenient characteristics. The imaging times were appropriate to detect the thermal effect of groundwater at both day and night. Shooting the area four times per day secured abundance in imageries, which in turn improved the chance of finding clear and reliable scenes. Next to the commonly used spectral bands of MODIS for obtaining valuable information about the study area (i.e. vegetation indices, albedo, emissivity, temperature, etc.), It was found that bands 20 and 22, centered at $3.75 \mu m$ and $3.959 \mu m$ respectively, were specifically useful to ascertain that the image is free from perturbation by thin clouds. Concerning sensor accuracy, precision and resolution, MODIS demonstrated satisfactory efficacy. Even at nighttime when land surface temperature ranged within only two degrees Celsius, MODIS could delineate the groundwater effect suitably.

The only feature that prevented MODIS from being perfect for the purpose of our study is the spatial resolution of its thermal bands, i.e. bands 31 and 32 centered at $11.03 \mu m$ and $12.02 \mu m$ respectively. The $1000 m$ pixel of the thermal bands may contain the effect of unrelated surfaces (i.e. vegetated or residential areas, roads, canals, etc.). This was a main reason behind the outliers in the cross-relationship figures. Possible finer resolution in future satellites may enable masking out the undesired effect of such unrelated surfaces, and make the thermal mapping of shallow aquifers more precise.

All cross-relationship figures illustrate that the depth of approximately 4 meters is the critical depth above which groundwater affects surface soil moisture and temperature, and consequently all the surface energy balance components. This critical depth may be a peculiarity for this area and may differ from one region to another according to the conditions of the predominant soils.

The thermal mapping of shallow groundwater demonstrated in this study may be involved in transient three-dimensional groundwater models, especially when these models consider the dynamic interrelationship between the aquifer and the soil moisture above water table. In addition, mapping shallow groundwater effect on surface energy fluxes using remote sensing will be of great help in assessing the interactions among groundwater dynamics, land surface processes and the atmosphere.

Finally, some researches suggested developing a procedure for extricating groundwater influence from that of soil moisture (Heilman and Moore, 1982; Huntley, 1978). Actually, this procedure may not be necessary provided that remote sensing investigations are accompanied with appropriate relevant numerical simulations. In fact, the results of this chapter together with those of Chapter 6 illustrate clearly that the two profiles respond differently to rain incidents in a way that they still differ in surface soil moisture.

8 Conclusions and Recommendations

8.1 Conclusions

The objective of this research was to explore and appreciate the different aspects and basic physical principles involved in the process of shallow groundwater effect on land surface temperature and surface energy balance, and to investigate the potential of remote sensing to delineate this effect.

The main conclusion of this study is that shallow groundwater has a thermal signature on land surface and affects the energy balance at land surface. This effect can be detected via thermal remote sensors under certain conditions. The optimum conditions to detect groundwater effect using thermal remote sensing sensors were addressed. And the ability of a currently operational remote sensor (MODIS) to detect groundwater effect was demonstrated.

Shallow groundwater affects thermal properties of the region below the water table. Moreover, it increases soil moisture of the zone above its water table which results in affecting the soil thermal properties, the magnitude of evaporation, albedo and emissivity. Hence shallow groundwater affects land surface temperature and the surface energy balance in two different ways; direct and indirect. The direct way (the thermodynamic effect) is through its distinctive thermal properties which make groundwater acts as a heat sink in summer and a heat source in winter, and affects heat propagation within soil profile. On the other hand, the indirect way of groundwater effect is through its effect on soil moisture above water table and its related effects (i.e. evaporation, soil thermal properties of vadose zone, land surface emissivity and albedo), and the combined effect is the upshot of the direct and indirect effects.

The field investigations showed a clear relationship between groundwater depth and soil moisture. Besides, a negative correlation was observed between water depth and both maximum and average measured soil temperatures. This observation contradicted with both modeling results and satellite measurements. The puzzling contradiction was solved by the fact that the loggers deployed in shallower groundwater areas were more thermally connected to the soil surface than those deployed in deeper groundwater areas. This is because wet soils have higher thermal conductivity. This was proved by the higher correlations found between the measurements of the loggers deployed in shallower water table and air temperature.

This remark may be of vital importance when planning to conduct future in situ soil temperature measurements. In spite of that it is

difficult and expensive to measure radiant land surface temperature in situ for different locations simultaneously using thermal cameras. However, this would be the only means to obtain reliable surface temperature measurements. Destroying the soil structure to insert extrinsic data logger of wide surface area may not be a wise way of conducting soil temperature measurements if these measurements would be compared to thermal remote sensing measurements.

By numerically separating out the thermodynamic effect, it was concluded that shallow groundwater - regardless of its indirect effect generated via its effect on soil moisture above water table - does indeed affect directly the components of the energy balance system at land surface by its distinctive thermal properties. This thermodynamic effect is primarily obvious on land surface temperature, ground heat flux, sensible heat flux and outgoing long-wave radiation.

In terms of seasonally prospective, the thermodynamic effect on all these components is mostly pronounced in winter and summer. Whereas, in terms of hourly prospective, the difference in land surface temperature and outgoing longwave radiation is higher during nighttime, and the difference in ground and sensible heat fluxes is higher during daytime.

In spite of its small magnitudes, highlighting the different features of the thermodynamic effect is important to make the understanding of the combined effect of groundwater more complete. The importance of the thermodynamic effect comes from its interaction with the indirect effect which originates from soil moisture above water table; this interaction may increase or decrease the upshot of the combined effect.

The combined effect was simulated to explore the features and patterns of shallow groundwater effect. It has been found that areas dominated by shallow groundwater have wetter soil profile due to the upward water and vapor flux; consequently, they respond differently to the prevailing atmospheric forcing.

Generally speaking, shallow groundwater areas reflect less shortwave radiation to the atmosphere due to their lower albedo and therefore, they get higher magnitude of shortwave radiation. When potential evaporation demand is high enough, a large portion of the energy received by these areas is spent on evaporation. This makes the latent heat flux predominant, and leaves less energy to heat the soil.

Consequently, this induces lower magnitudes of both sensible and ground heat fluxes.

The higher soil thermal conductivity in shallow groundwater areas facilitates heat transfer between the top soil and the subsurface which promotes greater provisional heat transfer in both vertical directions. That is to say, soil subsurface is more thermally connected to the atmosphere. Nevertheless, the continuous heat exchange between the surface and the subsurface makes the deep soil temperatures come into equilibrium with surface and climate conditions. As a result, the upshot of ground heat flux in both profiles becomes very close to zero in the long run.

With regards to remote sensors' capability of detecting shallow groundwater effect on land surface temperature, it was found that this effect can be sufficiently clear to be sensed if at least one of two conditions are met: firstly, latent heat flux effect is predominant due to the high potential evaporation, or secondly, soil volumetric heat capacity effect is strong due to the big contrast in air temperature between day and night.

By investigating the relationship between water table depth and remotely measured land surface temperature, it was found that satellite measurements demonstrated a clear correspondence of surface temperature with water table depth day and night. In addition, since it was possible to delineate the effect of shallow groundwater on remotely sensed map of land surface temperature, it was feasible to highlight this effect on surface energy fluxes maps. Consequently, the various surface energy balance maps, calculated using SEBS and MODIS data, correlated well with water table depth. Finally it was possible using the SEBS estimate of evaporative fraction to estimate soil moisture distribution in the area reasonably.

Many factors played a substantial role in the satisfactory results of remote sensing investigation. The two major conditions for optimum thermal detection of shallow groundwater were met, namely: the high potential evaporation and the big contrast in air temperature between day and night. Whereas the effect of latent heat flux was clear at daytime due to the relatively high potential evaporation under the prevalent dry and sunny conditions, the effect of volumetric heat capacity was clear owing to the high contrast in air temperature between day and night. The suspension of irrigation activity together with the scantiness of rain incidents for quite some time before the measurement campaign made surface soil moisture and water table depth conditions fairly stable. It can be added here that the short

period of our measurement campaign facilitated obtaining reliable data of the two state variables (i.e. soil moisture and water table depth). Besides, the predominance of bare soil conditions at the time of the field campaign was advantageous for avoiding possible perturbations and complexities imposed by plant cover on surface temperature measurements. Finally, the limited topographic relief and vegetation cover in the study area helped to avoid possible uncertainty sources (Gibson et al., 2011) in SEBS estimates of energy fluxes. The correspondence of the derived daily evaporation and soil moisture with in field measured values proved that the utilization of SEBS in this area was a success.

It was found that MODIS data was suitable for delineating groundwater effect because it has many convenient characteristics. The imaging times were appropriate to detect the thermal effect of groundwater at both day and night. Shooting the area four times per day secured abundance in imageries, which in turn improved the chance of finding clear and reliable scenes. Next to the commonly used spectral bands of MODIS for obtaining valuable information about the study area (i.e. vegetation indices, albedo, emissivity, temperature, etc.), It was found that bands 20 and 22, centered at $3.75 \mu m$ and $3.959 \mu m$ respectively, were specifically useful to ascertain that the image is free from perturbation by thin clouds. Concerning sensor accuracy, precision and resolution, MODIS demonstrated satisfactory efficacy. Even at nighttime when land surface temperature ranged within only two degrees Celsius, MODIS could delineate the groundwater effect suitably.

The only feature that prevented MODIS from being perfect for the purpose of our study is the spatial resolution of its thermal bands, i.e. bands 31 and 32 centered at $11.03 \mu m$ and $12.02 \mu m$ respectively. The $1000 m$ pixel of the thermal bands may contain the effect of unrelated surfaces (i.e. vegetated or residential areas, roads, canals, etc.). This was a main reason behind the outliers in the cross-relationships figures. Possible finer resolution in future satellites may enable masking out the undesired effect of such unrelated surfaces, and make the thermal mapping of shallow aquifers more precise.

All cross-relationships figures illustrate that the depth of approximately 4 meters is the critical depth above which groundwater affects surface soil moisture and temperature, and consequently all the surface energy balance components. This critical depth may be a peculiarity for this area and may differ from one region to another according to the conditions of the predominant soils.

Finally, some researches suggested developing a procedure for extricating groundwater influence from that of soil moisture. Actually, this procedure may not be necessary provided that remote sensing investigations are accompanied with appropriate relevant numerical simulations. In fact, the results of this study illustrate clearly that the shallow groundwater areas respond differently to rain incidents in a way that they still differ in surface soil moisture behavior.

8.2 Suggestions for further work

The thermal mapping of shallow groundwater demonstrated in this study may be involved in transient three-dimensional groundwater models, especially when these models take into consideration the dynamics interrelationship between the aquifer and the soil moisture above water table. Implementing groundwater models aided by thermal remote sensing measurements of land surface is recommended for further research.

Also it is recommended to conduct further investigations of shallow groundwater effect under vegetated conditions using remote sensing data supported by numerical simulations.

Furthermore, investigating the effect of shallow groundwater on microclimate supported by surface energy fluxes mapping using satellite measurements deserves investigation.

Finally, it is recommended to investigate the joint exploitation of different operational satellites for shallow groundwater studies. And also it is vital to emphasize on enhancing the spatial and temporal resolutions of thermal sensors on board of future satellites. Temperature measurements of Earth surface are proving to be very useful in observing diverse phenomena, and enhancing their quality is important for science.

Appendix A: Some Useful Comments

In the course of this research, two papers (Kollet and Maxwell, 2008) and (Maxwell and Kollet, 2008) were come by. The two papers dealt with issues that have connections to the themes addressed in this research. And it was noticed that there are some remarks regarding the methodology which was followed within these two papers. I think that it is useful to refer to these remarks in order to address them properly in future research.

A.1 Comments on Kollet and Maxwell (2008)

By dint of an integrated and distributed watershed modeling platform the authors examined the influence of groundwater dynamics on the energy and mass balance at the land surface. To simulate water and energy fluxes in the subsurface and at the land surface including saturated flow in the deeper aquifer, they coupled a 3D variably saturated groundwater flow model (ParFlow) to the Common Land Model (CLM). They applied this coupled model, PF.CLM, to the Little Washita watershed, Oklahoma, USA, and forced the model by atmospheric data for the water year 1999. Aiming at a realistic initialization of all state variables, they ran the model repeatedly over one year (model spin-up) for seven times (years).

The originality of accounting for three-dimensional subsurface flow and overland flow to demonstrate the relationship between water table dynamics and surface processes on the watershed scale is an interesting contribution. However, more robust and reliable results would have been reached, if more care had been given to the points presented here. Henceforth, all referencing to figures and equations in this section are in the paper under discussion (Kollet and Maxwell, 2008).

A.1.1 The spin-up process

The spin-up of a Land Surface Model (LSM) is an adjustment process during which the model is approaching its equilibrium. Yet, the equilibrium state of a consistent LSM should be physically realistic, and its behavior within the adjustment period should be physically meaningful and in accord with the real world conditions (Yang et al., 1995). Cosgrove et al. (2003) warned that the model spin-up may severely bias the simulations, and result in questionable LSM output. Applying meteorological forcing of a year that shows anomalies compared to the area climatology is a possible serious problem that can negatively affect the spin-up process. Consequently, the equilibrium state of the model will be different from the average

model state resulting from a long-term data set that characterizes the climatology of the simulated area (Cosgrove et al., 2003).

It is obvious in Kollet and Maxwell (2008) that the repeated application of the atmospheric forcing data of a year that was hotter and wetter than average, severely biased the model results. The yearly average temperature in this year (291 K) was higher than the long term average by about 2 K (Oklahoma Climate Data, <http://climate.mesonet.org/>). Also, the precipitation in this year (956 mm) was higher than the yearly average of the studied watershed (760 mm, (USDA ARS, 2004)) by about 200 mm. Thus, the model domain was wetted and warmed up over and over again until it reached unrealistic initial moisture and temperature state. This bias can be spotted clearly through the comparison in the model output with stream discharge (Figure 5); soil moisture (Figure 6) and latent heat flux (Figure 7). In these three figures, the only match between simulated and measured variables is when the peaks occur which cannot be considered sufficient for a reliable output on its own.

In Figure 5, the comparison of the model output with the measured hydrograph shows that the model generally captures the timing of peak discharges which is insignificant concord because the model overestimates the peak flow rate up to 500 % or more at some points.

Similarly, Figure 6 demonstrates that the measured soil moisture does not agree with the simulated values. It is assumed that this disagreement (over and above the spin-up) is due to the fact that the adjusted saturated hydraulic conductivity value for the homogeneous subsurface was five times larger than the arithmetic mean obtained from the 200 boreholes information (Maxwell et al. 2007). This would increase the deep percolation rate and enhance the dry out of the model top layer. Thus, the model subsurface absorbs the excess precipitation during the spin-up and diverts it to the stream flow (Figure 5). Nevertheless, the model failed to absorb the excess water in the period from mid-June until mid-July 1999, due to the preceding intense spring rain.

Finally, Figure 7 shows large and unsystematic overestimation (up to 350 % or more) of the simulated latent heat flux in comparison to the values obtained from the Ameriflux tower. It is worth mentioning here that Twine et al. (2000) assumed that the eddy-covariance systems may under-measure latent and sensible heat fluxes systematically and by 10 to 30%.

It is proposed, for the model spin-up, using atmospheric data of a year that is free of an abrupt variation between the beginning and end of the year and represents rationally the watershed climatology. The data of this year can be obtained by averaging a long-term data set of the watershed. Moreover, the spin-up should bring the model to its equilibrium state some years before the year being considered. From that time on, the actual atmospheric data should be applied. By that it may be ensured that the simulated data can match the measured data if the model was coherently built.

A.1.2 The used integrated and distributed watershed modeling platform (PF.CLM)

In Kollet and Maxwell (2008), the authors mentioned that after each time step, the coupled model calculates the error in the mass and energy balance, which implies that the model should basically be mass and energy conservative. However, an instant glance at Figure 9 reveals that the energy balance (equation 2.1) is not preserved in the model output. That is, the net radiation is not equal to the sum of the three heat fluxes (i.e. latent, sensible and ground heat fluxes). The easiest to notice is the unbalanced energy state of the grassland: While the net radiation, latent and sensible heat fluxes preserve constant values along the range of water table depth, the ground heat flux changes from about 15 Wm^{-2} for deep water table to about 18.5 Wm^{-2} for very shallow water table.

Also it would be more helpful to investigate the reason behind the huge unrealistic values of ground heat flux in Figure 9d. Naturally, the yearly average value of ground heat flux tends to be small and ranges in the vicinity of ± 0 , according to the specific atmospheric forcing of a simulated year.

A.1.3 Model validation against ground truth data

Within the course of the comparison with field data in this paper, it is noticed the absence of the first two and half months (from September to mid-November 1998) in soil moisture comparison (Figure 6). Similarly, measured data for the last four months (May-August 1999) of the latent heat flux from the Ameriflux tower were not shown in Figure 7.

Furthermore, the key parameter, i.e. groundwater depth, which should be compared to the simulation output, was reported to be unavailable. The authors could make use of the historical database

which contains data for 34 drill holes, for which 21 were used to monitor groundwater levels within the Little Washita River Experimental Watershed (USDA ARS, 2004). Another very helpful source of data that could be used for model validation is the reported-available remote sensing data of the watershed. In that course, the comparison to remotely sensed surface temperature would be very useful.

Finally, it is believed that the spatial statistical study of the connection between groundwater dynamics and the land energy balance could have been more applicable if it had been conducted after the model had been ensured to simulate the real state of the watershed to an adequate extent. This could be reached through a more careful application of the spin-up process, testing the coupled model and ensuring its energy conservation, and validating its output more coherently with ground truth data.

A.2 Comments on Maxwell and Kollet (2008)

Using a variably saturated groundwater flow model (ParFlow) with integrated overland flow and land-surface model processes (CLM), Maxwell and Kollet (2008) examined the interaction between water and energy flows in a changing climate for the southern Great Plains, USA.

They compare three different future scenarios with a simulation of present-day climate. The simulation of the current climate scenario (control run, CNTRL) was based on water-year 1999 and documented in Kollet and Maxwell (2008). The three future climate scenario simulations were generated by modifying the water-year 1999 time series in relation to temperature and precipitation according to future global climate model predictions (Solomon et al., 2007). Each of the three scenarios was initiated from the CNTRL state and forced repetitively (model spin-up) with the modified data set until the model approached its equilibrium state.

The supposed current climate scenario (CNTRL), which is the foundation of the three future scenario simulations, does not concord with the real world conditions. The model output was severely biased from the measurements of the hydrograph, the soil moisture and the latent heat flux subject of the study as illustrated in section (8.1.1).

This deviation was due to the inappropriate application of the spin-up process: the applied year was a deviation from the climatology of the

Some Useful Comments

simulated area, (i.e. excess precipitation of 200 mm and higher temperature by 2 K).

Furthermore, the coupled model (PF-CLM) which was used both in Kollet and Maxwell (2008) and Maxwell and Kollet (2008), is not energy conservative, and produces unrealistically high values for ground heat flux. More significantly, the key parameter (i.e. groundwater depth) which authenticates the simulation validity was reported to be unavailable.

Finally, Kollet and Maxwell (2008), specifically in page 8, states that due to discrepancies between the simulated and the measured data, the model was considered inadequate for prediction purposes unless it is calibrated comprehensively. Inconsistently, Maxwell and Kollet (2008) used the same model for future simulations that cannot be reliable for such a purpose.

In conclusion, it should be emphasize that the future vision of climate change impact on hydrologic cycle should be based on realistic foundation and reliable simulations.

Bibliography

- Alkhaier, F. (2003), Soil salinity detection using satellite remote sensing, MSc. thesis, *International Institute for Geo-Information Science and Earth Observation*, Enschede, the Netherlands.
- Alkhaier, F., R. J. Schotting, and Z. Su (2009), A qualitative description of shallow groundwater effect on surface temperature of bare soil, *Hydrology and Earth System Sciences*, 13, 1749–1756.
- Alkhaier, F., and Z. Su (2009), The effect of shallow groundwater on soil temperature and soil heat flux near land surface, *Geophysical Research Abstracts*, 11, EGU2009-1008-2.
- Alkhaier, F., G. N. Flerchinger, and Z. Su (2011), The thermodynamic effect of shallow groundwater on temperature and energy balance at bare land surface, In: “*Heat Transfer and Thermodynamic Effects*”, ed. By A. Ahsan: InTech, 394 p. ISBN: 978-953-307-585-3, p.p. 19-34.
- Alkhaier, F., G. N. Flerchinger, and Z. Su (2011), Shallow groundwater effect on land surface temperature and surface energy balance under bare soil conditions: modeling and description, *Hydrology and Earth System Sciences Discussions*, 8, 8639-8670, doi:10.5194/hessd-8-8639-2011.
- Alkhaier, F., Z. Su, and G. N. Flerchinger (2011), Reconnoitering the effect of shallow groundwater on land surface temperature and surface energy balance using MODIS and SEBS, *Hydrology and Earth System Sciences Discussions*, 8, 8671-8700, doi:10.5194/hessd-8-8671-2011.
- Anderson, M. P. (2005), Heat as a ground water tracer, *Ground Water*, 43(6), 951-968.
- Andrews, C. B., and M. P. Anderson (1979), Thermal alteration of groundwater caused by seepage from a cooling lake, *Water Resources Research*, 15(3), 595–602,.
- Badola, A. (2009), Validation of Surface Energy Balance System (SEBS) over forest land cover and sensitivity analysis of the model, MSc thesis, *International Institute for Geo-information Science and Earth Observation*, Enschede, The Netherlands.
- Bastiaanssen, W. G. M. (1995), Regionalization of surface flux densities and moisture indicators in composite terrain – A remote sensing approach under clear skies in Mediterranean climates, Ph.D. Thesis, 273 pp., *Wageningen Agricultural University*, the Netherlands.
- Bastiaanssen, W. G. M., D. J., Molden, and I. W., Makin (2000), Remote sensing for irrigated agriculture: examples from

- research and possible applications, *Agricultural Water Management*, 46, 137–155.
- Batelaan, O., F. De Smedt, P. de Becker, and W. Huybrechts (1998), Characterization of a regional ground water discharge area by combined analysis of hydrochemistry, remote sensing and groundwater modeling, In: *Shallow Groundwater Systems*, Ed. P. Dillon and I. Simmers, pp. 75–86. Rotterdam, the Netherlands: A. A. Balkema
- Becker, M. W. (2006), Potential for satellite remote sensing of ground water. *Ground Water*, 44(2), 306–318.
- Becker, M. W., T. Georgian, H. Ambrose, J. Siniscalchi, and K. Fredrick (2004), Estimating flow and flux of groundwater discharge using water temperature and velocity, *Journal of Hydrology*, 296(1–4), 221–233.
- Bense, V. F., and H. Kooi (2004), Temporal and spatial variations of shallow subsurface temperature as a record of lateral variations in groundwater flow, *Journal of Geophysical Research*, 109, B04103, doi:10.1029/2003JB002782.
- Birman, H. (1969), Geothermal exploration for groundwater, *Geological Society of America Bulletin*, 80(4), 617–630.
- Bobba, A. G., R. P. Bukata, and J. H. Jerome (1992), Digitally processed satellite data as a tool in detecting potential groundwater flow systems, *Journal of Hydrology*, 131(1–4), 25–62.
- Bosilovich, M., S. Hook, R. Knuteson, A. Pinheiro, C. Prigent, W. Rossow, and P. Viterbo (2008), International workshop on the retrieval and use of land surface temperature: bridging the gaps, *Summary Report, NOAA's National Climatic Data Center (NCDC)*, Asheville, 7–9 April 2008.
- Bravo, H. R., J. Feng, and R. J. Hunt, Using groundwater temperature data to constrain parameter estimation in a groundwater flow model of a wetland system. *Water Resources Research* 38, no. 8: 10.1029/2000WR000172, 2002.
- Bredehoeft, J. D., and I. S. Papadopulos (1965), Rates of vertical ground-water movement estimated from the Earth's thermal profile, *Water Resources Research*, 1(2), 325–328.
- Brooks, R. H. and A. T. Corey (1966), Properties of porous media affecting fluid flow, *Journal of the Irrigation and Drainage Division, ASCE*. 92(IR2), 61–88.
- Brown, R. B. (2003), Soil Texture, University of Florida, *Institute of Food and Agricultural Sciences*, fact sheet SL-29.
- Brunner, P., H.-J. Hendricks Franssen, L. Kgotlhang, P. Bauer-Gottwein, and W. Kinzelbach (2007), How can remote sensing contribute in groundwater modeling? *Hydrogeology journal*, 15(1), 5–18, doi:10.1007/s10040-006-0127-z.

- Brutsaert, W., (1999), Aspects of bulk atmospheric boundary layer similarity under free-convective conditions, *Reviews of Geophysics*, 37, 439–451.
- Burow, K. R., J. Constantz, and R. Fujii (2005), Using heat as a tracer to estimate dissolved organic carbon flux beneath a restored wetland, *Ground Water*, 43(4), 545–556,.
- Campbell, G. S. (1974), Simple method for determining unsaturated conductivity from moisture retention data, *Soil Science*, 117(6), 311–314.
- Campbell, G. S. (1977), *An Introduction to Environmental Biophysics*. Springer-Verlag, New York.
- Campbell, G. S. (1985), *Soil Physics with BASIC: Transport models for soil-plant systems*, Elsevier, Amsterdam.
- Cartwright, K. (1968), Thermal prospecting for groundwater, *Water Resources Research*, 4(2), 395–401.
- Cartwright, K. (1970), Groundwater discharge in the Illinois basin as suggested by temperature anomalies, *Water Resources Research* 6(3), 912–918.
- Cartwright, K. (1971), Redistribution of geothermal heat by a shallow aquifer, *Geological Society of America Bulletin*, 82, 3197–3200.
- Cartwright, K. (1974), Tracing shallow groundwater systems by soil temperatures, *Water Resources Research*, 10(4), 847–855.
- Chase, M. E. (1969), Airborne remote sensing for groundwater studies in prairie environment, *Canadian Journal for Earth Science*, 6, 737–741.
- Chen, X., and Q. Hu (2004), Groundwater influences on soil moisture and surface evaporation, *Journal of Hydrology*, 297, 285–300.
- Clapp, R. B., and G. M. Hornberger (1978), Empirical equations for some soil hydraulic properties, *Water Resources Research*, 14, 601–604.
- Conant, B. J. (2004), Delineating and quantifying ground water discharge zones using streambed temperature, *Ground Water*, 42(2), 243–257.
- Constantz, J. (1998), Interaction between stream temperature, stream flow and groundwater exchanges in alpine streams, *Water Resources Research*, 34(7), 1609–1616.
- Constantz, J., and D. A. Stonestrom (2003), Heat As A Tracer Of Water Movement Near Streams. In: *Heat as a Tool for Studying the Movement of Ground Water Near Streams*, Ed. D. A. Stonestrom and J. Constantz, 21–27, USGS Circular 1260, Reston, Virginia: USGS.
- Cosgrove, B. A., D. Lohmann, K. E. Mitchell, P. R. Houser, E. F. Wood, J. C. Schaake, A. Robock, J. Sheffield, Q. Duan, L. Luo, R. W. Higgins, R. T. Pinker, and J. D. Tarpley (2003), Land

- surface model spin-up behavior in the North American Land Data Assimilation System (NLDAS), *Journal of Geophysical Research*, 108(D22), 8845, doi:10.1029/2002JD003316.
- Darcy, H. P. G. (1856), *Les fontaines publiques de la Ville de Dijon*. Paris, France: *Victon Dalmont*.
- de Vries, A. D. (1963), Thermal properties of soils, In: *Physics of plant environment*, pp. 210–235, North Holland Publication Company, Amsterdam, the Netherlands.
- Dingman, S. L. (2002), *Physical Hydrology*, Prentice-Hall Inc., Upper Saddle River, New Jersey.
- Dregne, H. E., Z. Xiong, and S. Xiong (1996), Soil salinity in China, *Desertification Control Bull.*, 28, 28–33.
- Evans, E. C., M. T. Greenwood, and G. E. Petts (1995), Thermal profiles within river beds, *Hydrological Processes* 9(1), 19–25.
- Falconer, A., L. Myers, and M. Deutsch (1981), Observations on Lake Ontario Basin hydrology from optical enhancements of Landsat imagery, in: Deutsch, M., D. R. Weisnet, and A. Rango (Eds), *Satellite Hydrology*, American Water Resources Association, Minneapolis, Minnesota, 427–436.
- Fan, Y., G. Miguez-Macho, C. P. Weaver, R. Walko, and A. Robock (2007), Incorporating water table dynamics in climate modeling: 1. Water table observations and equilibrium water table simulations, *Journal of Geophysical Research*, 112, D10125, doi:10.1029/2006JD008111.
- Ferguson, G., A. D. Woodbury, and G. L. D. Matile (2003), Estimating deep recharge rates beneath an interpolate moraine using temperature logs, *Ground Water*, 41(5), 640–646.
- Ferguson, G., and A.D. Woodbury (2005), The effects of climatic variability on estimates of recharge from temperature profiles, *Ground Water*, 43(6), 837–842.
- Flerchinger, G. N. (2000). The simultaneous heat and water (SHAW) model, Technical Report, pp. 37, Northwest Watershed Research Centre, USDA Agricultural Research Service, Boise, Idaho.
- Flerchinger, G. N. and K. E. Saxton (1989), Simultaneous heat and water model of a freezing snow-residue-soil system: I. Theory and development, *Transactions of ASAE*, 32(2), 565–571.
- Flerchinger, G. N., and K. R. Cooley (2000), A ten-year water balance of a mountainous semi-arid watershed, *Journal of Hydrology*, 237, 86–99.
- Flerchinger, G. N., and S. P. Hardegree (2004), Modelling near-surface soil temperature and moisture for germination response predictions of post-wildfire seedbeds, *Journal of Arid Environments*, 59, 369–385, doi:10.1016/j.jaridenv.2004.01.016.

- Flerchinger, G. N., T. J. Sauer, and R. A. Aiken (2003), Effects of crop residue cover and architecture on heat and water transfer at the soil surface, *Geoderma*, 116, 217–233, doi:10.1016/S0016-7061(03)00102-2.
- Flerchinger, G. N., W. Xiao, T. J. Sauer, and Q Yu (2009), Simulation of within-canopy radiation exchange, *NJAS - Wageningen Journal of Life Sciences*, 57, 5–15.
- Freeze, R. A. and J. A. Cherry (1979), *Groundwater*, Prentice-Hall, Inc. Englewood Cliffs, NJ., pp. 604.
- Freeze, R. A. (1985), Historical correspondence between C.V. Theis and C.I. Lubin, *Eos, Transactions American Geophysical Union*, 66(20), 442-442.
- Fryar, A. E., E. J. Wallin, and D. L. Brown (2000), Spatial and temporal variability in seepage between a contaminated aquifer and tributaries to the Ohio River, *Ground Water Monitoring and Remediation*, 20(3), 129–146.
- Fujimaki, H., S. Shiozawa and M. Inoue (2003), Effect of salty crust on soil albedo, *Agricultural and Forest Meteorology*, 118(1-2), 125-135. doi:10.1016/S0168-1923(03)00110-2
- Furuya, G., A. Suemine, K. Sassa, T. Komatsubara, N. Watanabe, and H. Marui (2006), Relationship between groundwater flow estimated by soil temperature and slope failures caused by heavy rainfall, Shikoku Island, *southwestern Japan, Engineering Geology*, 85, 332–346, doi:10.1016/j.enggeo.2006.03.002.
- Gibson L. A., Z. Münch, and J. Engelbrecht (2011), Particular uncertainties encountered in using a pre-packaged SEBS model to derive evapotranspiration in a heterogeneous study area in South Africa. *Hydrology Earth System Sciences*, 15, 295-310.
- Grismer, M. E., M. N. Orang, V. Clausnitzer, and K. Kinney (1994), Effects of air compression and counterflow on infiltration into soils, *Journal of Irrigation and Drainage Engineering*, 120(4), 775–795, doi:10.1061/(ASCE)0733-9437(1994)120:4(775).
- Groenevelt, P. H. (2003), The place of Darcy's law in the framework of non-equilibrium thermodynamics, In: Henry P. G. Darcy and Other Pioneers in Hydraulics, Ed. G. O. Brown, J. D. Garbrecht, and W. H. Hager, pp. 310. Reston, Virginia: *American Society of Civil Engineers*.
- Gulden, L. E., E. Rosero, Z. Yang, M. Rodell, C. S. Jackson, G. Niu, P. J. -F. Yeh, and J. Famiglietti (2007), Improving land-surface model hydrology: Is an explicit aquifer model better than a deeper soil profile?, *Geophysical Research Letters*, 34, L09402, doi:10.1029/2007GL029804.

- Heilman, J. L., and D. G. Moore (1982), Evaluating depth to shallow groundwater using heat capacity mapping mission (HCMM) data, *Photogrammetric Engineering and Remote Sensing*, 48(12), 1903–1906.
- Herman, A., V. B. Kumar, P. A. Arkin, and J. V. Kousky (1997), Objectively determined 10-day African rainfall estimates created for famine early warning systems, *International Journal of Remote Sensing*, 18(10), 2147-2159.
- Horton, R., and P. J. Wierenga (1983), Estimating the soil heat flux from observations of soil temperature near the surface. Soil Science Society of America, Vol. 47, pp. 14-20.
- Huang, M., and J. Gallichand (2006), Use of the SHAW model to assess soil water recovery after apple trees in the gully region of the Loess Plateau, China, *Agricultural Water Management*, 85, 67–76, doi:10.1016/j.agwat.2006.03.009.
- Hunt, R. J., D. P. Krabbenhoft, and M. P. Anderson (1996), Groundwater inflow measurements in wetland systems, *Water Resources Research*, 32(3), 495–508.
- Huntley, D. (1978), On the detection of shallow aquifers using thermal infrared imagery, *Water Resources Research*, 14(6), 1075– 1083.
- Idso, S. B., R. D. Jackson, R. J. Reginato, B. A. Kimball, and F. S. Nakayama (1975), The dependence of bare soil albedo on soil water content, *Journal of Applied Meteorology*, 14, 109-113.
- Jia, L., G. Xi, , S. Liu, C. Huang, Y. Yan, and G. Liu (2009), Regional estimation of daily to annual regional evapotranspiration with MODIS data in the Yellow River Delta wetland, *Hydrology and Earth System Sciences*, 13, 1775–1787, doi:10.5194/hess-13-1775- 2009.
- Jia, L., Z. Su, B. van den Hurk, M. Menenti, H. A. R. Moene, J. J. Basalga Yrisarry, M. Ibanez, and A. Cuesta (2003), Estimation of sensible heat flux using the Surface Energy Balance System (SEBS) and ATSR measurements, *Physics and Chemistry of the Earth*, 28, 77– 88.
- Jiang, X., G.-Y. Niu, and Z.-L. Yang (2009), Impacts of vegetation and groundwater dynamics on warm season precipitation over the Central United States, *Journal of Geophysical Research*, 114, D06109, doi:10.1029/2008JD010756.
- Kappelmeyer, O. (1957), The use of near surface temperature measurements for discovering anomalies due to causes at depths, *Geophysical Prospective*, 5(3), 239–258.
- Kilty, K., and D. S. Chapman (1980), Convective heat transfer in selected geologic situations, *Ground Water*, 18, (4), 386–394.

- Klijn, F., and J. P. M. Witte (1999), Eco-hydrology: Groundwater flow and site factors in plant ecology, *Hydrogeology Journal*, 7(1), 65–77.
- Kollet, S. J., and R. M. Maxwell (2008), Capturing the influence of groundwater dynamics on land surface processes using an integrated, distributed watershed model, *Water Resources Research*, 44, W02402, doi:10.1029/2007WR006004.
- Krcmar, B., and J. Masin (1970), Prospecting by the geotherm method, *Geophysical Prospecting*, 18, 255–260, doi:10.1111/j.1365-2478.1970.tb02106.x
- Lee, D. R., (1985), Method for locating sediment anomalies in Lakebeds that can be caused by groundwater flow, *Journal of Hydrology*, 79, 187-193.
- Liang X., and Z. Xie (2003), Important factors in land-atmosphere interactions: surface runoff generations and interactions between surface and groundwater, *Global and Planetary Change*, 38, 101-114.
- Lo, M-H., P. J.-F. Yeh, and J. S. Famiglietti (2008), Constraining water table depth simulations in a land surface model using estimated baseflow, *Advances in Water Resources*, 31(12), 1552-1564, ISSN 0309-1708, doi:10.1016/j.advwatres.2008.06.007.
- Ma, W., Y. Ma, and Z. Su (2011), Feasibility of retrieving land surface heat fluxes from ASTER data using SEBS: a case study from the Namco area of the Tibetan plateau, *Arctic, Antarctic, and Alpine Research*, 43(2), 239-245.
- Mabee, S. B. and K. C. Hardcastle (1997), Analyzing outcrop scale fracture features to supplement investigations of bedrock aquifers, *Hydrogeology Journal*, 5(4), 21-36.
- Macfarlane, P. A., A. Forster, D. F. Merriam, J. Schrotter, and J. M. Healey (2002), Monitoring artificially stimulated fluid movement in the Cretaceous Dakota aquifer, western Kansas. *Hydrogeology Journal*, 10(6), 662–673.
- Maxwell, R. M., and N. L. Miller (2005), Development of a coupled land surface and groundwater model, *Journal of Hydrometeorology*, 6, 233–247.
- Maxwell, R. M., and S. J. Kollet (2008), Interdependence of groundwater dynamics and land-energy feedbacks under climate change, *Nature Geoscience*, 1, 665-669, doi:10.1038/ngeo315.
- Maxwell, R. M., F. K. Chow, and S. J. Kollet (2007), The groundwater-land-surface-atmosphere connection: Soil moisture effects on the atmospheric boundary layer in fully-coupled simulations, *Advances in Water Resources*, 30(12), doi:10.1016/j.advwatres.2007.05.018.

- McCabe, M. F., and E. F. Wood (2006), Scale influences on the remote estimation of evapotranspiration using multiple satellite sensors, *Remote Sensing of Environment*, 105, 271–285.
- McCabe, M. F., E. F. Wood, R. Wojcik, M. Pan, J. Sheffield, H. Gao, and H. Su (2008), Hydrological consistency using multi-sensors remote sensing data for water and energy cycle studies, *Remote Sensing of Environment*, 112, 430–444.
- Meijerink, A. M. J., D. Bannert, O. Batelaan, M. W. Lubczynski, and T. Pointet (2007), Remote sensing applications to groundwater, Paris, United Nations Educational Scientific and Cultural Organization (UNESCO), 2007. IHP-VI Series on Groundwater 16, pp. 304.
- Middleton, N., (editor) and D. Thomas (editor) (1997), World Atlas of Desertification, Second Edition, Wiley, New York, publisher Arnold United Nations Environment Programme (UNEP).
- Mink, J. F. (1964), Groundwater temperatures in a tropical island environment, *Journal of Geophysical Research*, 69(24), 5225–5230.
- Mohamed, Y. A., W. G. M. Bastiaanssen, and H. H. G. Savenije (2004), Spatial variability of evaporation and moisture storage in the swamps of the upper Nile studied by remote sensing techniques, *Journal of Hydrology*, 289, 145–164.
- Moore, R. B., G. E. Schwartz, S. F. Clark Jr., G. J. Walsh, and J. R. Degnan (2002), Factors related to well yield in the fractured bedrock aquifer of New Hampshire, USGS Professional Paper, U.S. Geological Survey, Reston, Virginia.
- Mulwa, J. K., S. J. Gaciri, J. O. Barongo, N. Opiya-Akech and G. K. Kijanji (2005), Geological and structural influence on groundwater distribution and flow in Ngong area, Kenya, *African Journal of Science and Technology*, Science and Engineering Series, 6(1), 105–115.
- Myers, V. I., and D. G. Moore (1972), Remote sensing for defining aquifers in glacial drift, *Proceedings of Eighth International Symposium on Remote Sensing of Environment*, 1, 715–728, University of Michigan, October 1972.
- Nichols, W. D. (1994), Groundwater discharge by phreatophyte shrubs in the Great Basin as related to depth to groundwater, *Water Resources Research*, 30(12), 3265–3274.
- Niu, G.-Y., Z.-L. Yang, R. E. Dickinson, L. E. Gulden, and H. Su (2007), Development of a simple groundwater model for use in climate models and evaluation with Gravity Recovery and Climate Experiment data, *Journal of Geophysical Research*, 112, D07103, doi:10.1029/2006JD007522.

- Northey, J. E., E. W. Christen, J. E. Ayars, and J. Jankowski (2006), Occurrence and measurement of salinity stratification in shallow groundwater in the Murrumbidgee Irrigation Area, south-eastern Australia, *Agricultural Water Management*, 81, 23-40.
- Olmsted, F. H., A. H. Welch, and S. E. Ingebritsen (1986), Shallow subsurface temperature surveys in the basin and range province, U.S.A. I. Review and evaluation, *Geothermics*, 15(3), 251 -265.
- Painter, S. L., A. D. Woodbury, and Y. Jiang (2007), Transmissivity estimation for highly heterogeneous aquifers: Comparison of three methods applied to the Edwards aquifer, Texas, USA. *Hydrogeology Journal*, 15(2), 315-331.
- Pan, M., E. F. Wood, R. Wojcik, and M. F. McCabe (2008), Estimation of regional terrestrial water cycle using multi-sensor remote sensing observations and data assimilation, *Remote Sensing of Environment*, 112, 1282-1294,.
- Parsons, M. L. (1970), Groundwater thermal regime in a glacial complex, *Water Resources Research*, 6(6), 1701-1720.
- Quiel, F. (1975), Thermal/IR in geology, *Photogrammetric Engineering and Remote Sensing*, 41(3), 341-346.
- Rahman, A. (2008), A GIS based DRASTIC model for assessing groundwater vulnerability in shallow aquifer in Aligarh, India, *Applied Geography*, 28, 32-53.
- Rodell, M. and J. S., Famiglietti (2002), The potential for satellite based monitoring groundwater storage changes using GRACE; the High Plains aquifer, central US, *Journal of Hydrology*, 263(1-4), 245-56.
- Rodell, M., J. Chen, H. Kato, J. S. Famiglietti, J. Nigro, and C. R. Wilson (2007), Estimating groundwater storage changes in the Mississippi River basin (USA) using GRACE, *Hydrogeology Journal*, 15(1), 159-166.
- Salvucci, G. D., and D. Entekhabi (1995), Pondered infiltration into soils bounded by a water table, *Water Resources Research*, 31(11), 2751-2759.
- Santanello, J. A., and M. A. Friedl (2003), Diurnal covariation in soil heat flux and net radiation, *Journal of Applied Meteorology*, 42, 851-862.
- Schervish, M. J. (1996), P-values: what they are and what they are not, *The American Statistician*, 50(3), 203-206, doi:10.2307/2684655.
- Scott, C. A., W. G. M. Bastiaanssen and M. D. Ahmad (2003), Mapping spatio-temporal distributions of soil moisture throughout irrigated watersheds using optical and high

- resolution imagery, *ASCE Irrigation and Drainage Engineering*, 129(5), 326–335.
- Seo, K.-W., C. R. Wilson, J. S. Famiglietti, J. L. Chen, and M. Rodell (2006), Terrestrial water mass load changes from Gravity Recovery and Climate Experiment (GRACE), *Water Resources Research*, 42, W05417, doi:10.1029/2005WR004255.
- Shaban, A., M. Khawlie, and C. Abdalla (2006), Use of GIS and remote sensing to determine recharge potential zones; the case of occidental Lebanon, *Hydrogeology Journal*, 14(4), 433–443.
- Silliman, S. E., J. Ramirez, and R. L. McCabe (1995), Quantifying down flow through creek sediments using temperature time series: One-dimensional solution incorporating measured surface temperature, *Journal of Hydrology*, 167(1–4), 99–119.
- Silliman, S. E., and D. F. Booth (1993), Analysis of time-series measurements of sediment temperature for identification of gaining vs. losing portions of Juday Creek, Indiana, *Journal of Hydrology*, 146, 131–148.
- Solomon, S., D. Qin, M. Manning, Z. Chen, M. Marquis, K. B. Averyt, M. Tignor, and H. L. Miller (eds.) (2007), *Climate Change: The Physical Science Basis. Contribution of Working Group I to the Fourth Assessment Report of the Intergovernmental Panel on Climate Change*, Cambridge University Press, Cambridge, United Kingdom and New York, NY, USA.
- Stallman, R. W. (1965), Steady one-dimensional fluid flow in a semi-infinite porous medium with sinusoidal surface temperature, *Journal of Geophysical Research*, 70(12), 2821–2827.
- Stonestrom, D. A., and J. Constantz, ed. (2003), *Heat as a tool for studying the movement of ground water near streams*, USGS Circular 1260. USGS.
- Su, G. W., J. Jasperse, D. Seymour, and J. Constantz (2004), Estimation of hydraulic conductivity in an alluvial system using temperatures, *Ground Water*, 42(6), 890–901.
- Su, H., M. F. McCabe, and E. F. Wood (2005), Modeling evapotranspiration during SMACEX: Comparing two approaches for local and regional-scale prediction, *Journal of Hydrometeorology – Special Section*, 6, 910–922.
- Su, Z. (2001), A Surface Energy Balance System (SEBS) for estimation of turbulent heat fluxes from point to continental scale, Publications of the National Remote Sensing Board (BCRS), USP-2.
- Su, Z. (2002), The Surface Energy Balance System (SEBS) for estimation of turbulent heat fluxes, *Hydrology and Earth System Sciences*, 6, 85–100, doi:10.5194/hess-6-85-2002.

- Su, Z. (2005), Estimation of the surface energy balance, In: *Encyclopedia of hydrological sciences: 5 Volumes.* / Ed. by M. G. Anderson and J. J. McDonnell, Chichester etc., Wiley and Sons, 2005, 3145 p. ISBN: 0-471-49103-9. Vol. 2, pp. 731-752.
- Suzuki, S. (1960), Percolation measurements based on heat flow through soil with special reference to paddy fields, *Journal of Geophysical Research*, 65, (9), 2883–2885.
- Swenson, S., J. Wahr, and P. C. D. Milly (2003), Estimated accuracies of regional water storage variations inferred from the Gravity Recovery and Climate Experiment (GRACE), *Water Resources Research*, 39(8), 1223, doi:10.1029/2002WR001808.
- Takeuchi, A. (1980), Method of investigating groundwater-vein-streams by measuring one-meter-depth in landslide areas (I), *Journal of Japanese Association of Groundwater Hydrology*, 22(2), 11–39.
- Takeuchi, A. (1981), Method of investigating groundwater-vein-streams by measuring one-meter-depth in landslide areas (II), *Journal of Japanese Association of Groundwater Hydrology*, 23(1), 1–27.
- Takeuchi, A. (1996), Investigation methods of flowing groundwater by temperature measurements, *Kokon Shoin*, 367–468, (in Japanese).
- Taniguchi, M., J. Shimada, T. Tanaka, I. Kayane, Y. Sakura, Y. Shimano, S. Dapaah-Siakwan, and S. Kawashima (1999), Disturbances of temperature-depth profiles due to surface climate change and subsurface water flow: 1. An effect of linear increase in surface temperature caused by global warming and urbanization in the Tokyo metropolitan area, Japan, *Water Resources Research*, 35(5), 1507–1517.
- Theis, C. V. (1935), The relation between lowering of the piezometric surface and rate and duration of discharge of a well, using groundwater storage, *Transactions of the American Geophysical Union*, 16, 519–524.
- Townley, L. R., and M. G. Trefry (2000), Surface water-groundwater interaction near shallow circular lakes: Flow geometry in three dimensions, *Water Resources Research*, 36, (4), 935–949.
- Travaglia, C. (1996), Groundwater exploration by Satellite Remote Sensing in the Syrian Arab Republic FAO - Environment and Natural Resources Service (SDRN) Vol/Iss No. 76, Water Reports, No. 25.
- Twine, T. E., W. P. Kustas, J. M. Norman, D. R. Cook, P. R. Houser, T. P. Meyers, J. H. Prueger, P. J. Starks, and M. L. Wesley (2000), Correcting eddy-covariance flux underestimates over

- a grassland, *Agricultural and Forest Meteorology*, 103(3), 279–300.
- Umali, D. L. (1993), Irrigation-induced salinity: A growing problem for development and the environment, Technical Paper, 215, World Bank, Washington, DC.
- USDA ARS (2004), Conservation Effects Assessment Project – The Agricultural Research Service Watershed Assessment Study, Project Plan. Washington, DC. <http://ars.usda.gov/Research>.
- van den Bouwhuysen, J. N. A. (1934), The thermocouple proves useful on a geophysical survey, *Engineering and Mining Journal*, 135, 342-344.
- van der Kwast, J., W. Timmermans, A. Gieske, Z. Su, A. Olioso, L. Jia, J. Elbers, D. Karssenbergh and S. de Jong (2009), Evaluation of the Surface Energy Balance System (SEBS) applied to ASTER imagery with flux measurements at the SPARC 2004 site (Barrax, Spain), *Hydrology Earth System Sciences*, 13, 1337–1347, doi:10.5194/hess-13-1337-2009.
- Wade, S.C., and M. Reiter (1994), Hydrothermal estimation of vertical ground-water flow, Canutillo, Texas, *Ground Water*, 32, (5), 735–742.
- Wichelns, D. (1999), An economic model of waterlogging and salinization in arid regions, *Ecological Economics*, 30, 475–491.
- Wierenga, P. J. and Wit, C. T. De (1970), Simulation of heat transfer in soils, *Soil Science Society of America*, 34, 845-848.
- Woodbury, A.D., and L. Smith (1988), Simultaneous inversion of hydrogeologic and thermal data, 2. Incorporation of thermal data, *Water Resources Research*, 23(8), 356–372.
- World Bank (1992), Development and the Environment, World Development Report, 1992, World Bank, Washington, DC.
- Xiong, S., Z. Xiong, and P. Wang (1996), Soil salinity in the irrigated area of the Yellow River in Ningxia, China, *Arid Soil Research and Rehabilitation*, 10, 95–101.
- Yang, Z.-L., R. E. Dickinson, A. Henderson-Sellers, and A. J. Pitman (1995), Preliminary study of spin-up processes in land surface models with the first stage data of Project for Intercomparison of Land Surface Parameterization Schemes Phase 1(a), *Journal of Geophysical Research*, 100(D8), 16,553 – 16,578.
- Yeh, P. J-F., and Eltahir, E. A. B., (2005), Representation of Water Table Dynamics in a Land Surface Scheme, Part I: Model Development, *Journal of Climate*, 18, 1861–1880, doi:10.1175/JCLI3330.1
- York, J. P., M. Person, W. J. Gutowski, and T. C. Winter (2002), Putting aquifers into atmospheric simulation models: an

- example from the Mill Creek watershed, northeastern Kansas, *Advances in Water Resources*, 25, 221–238.
- Yuhara, K. (1998), Isothermal layer, *Groundwater handbook*, revised version, Editorial committee of *Groundwater handbook* (ed.), Kensetsu Sangyo Chosakai, (in Japanese).
- Zwart, S. J., and W. G. M. Bastiaanssen (2006), SEBAL for the description of spatial variability of water productivity in various wheat systems, *Agricultural Water Management*, 89, 287–296.
- Bense, V. F., M. A. Person, K. Chaudhary, Y. You, N. Cremer, and S. Simon (2008), Thermal anomalies indicate preferential flow along faults in unconsolidated sedimentary aquifers, *Geophysical Research Letters*, 35, L24406, doi:10.1029/2008GL036017.
- Bianchin, M., L. Smith, and R. Beckie (2010), Quantifying hyporheic exchange in a tidal river using temperature time series, *Water Resources Research*, 46, W07507, doi:10.1029/2009WR008365.
- Cardenas, M. B. (2010), Thermal skin effect of pipes in streambeds and its implications on groundwater flux estimation using diurnal temperature signals, *Water Resources Research*, 46, W03536, doi:10.1029/2009WR008528.
- Chen, J. L., C. R. Wilson, B. D. Tapley, L. Longuevergne, Z. L. Yang, and B. R. Scanlon (2010), Recent La Plata basin drought conditions observed by satellite gravimetry, *Journal of Geophysical Research*, 115, D22108, doi:10.1029/2010JD014689.
- Constantz, J. (2008), Heat as a tracer to determine streambed water exchanges, *Water Resources Research*, 44, W00D10, doi:10.1029/2008WR006996.
- Gerecht, K. E., M. B. Cardenas, A. J. Guswa, A. H. Sawyer, J. D. Nowinski, and T. E. Swanson (2011), Dynamics of hyporheic flow and heat transport across a bed-to-bank continuum in a large regulated river, *Water Resources Research*, 47, W03524, doi:10.1029/2010WR009794.
- Hatch, C. E., A. T. Fisher, J. S. Revenaugh, J. Constantz, and C. Ruehl (2006), Quantifying surface water–groundwater interactions using time series analysis of streambed thermal records: Method development, *Water Resources Research*, 42, W10410, doi:10.1029/2005WR004787.
- Hatch, C. E., A. T. Fisher, C. Ruehl, and G. Stemler (2010), Spatial and temporal variations in streambed hydraulic conductivity quantified with time-series thermal methods, *Journal of Hydrology*, 389, 276–288.
- Lautz, L. K. (2010), Impacts of nonideal field conditions on vertical water velocity estimates from streambed temperature time

- series, *Water Resources Research*, 46, W01509, doi:10.1029/2009WR007917.
- Lowry, C. S., J. F. Walker, R. J. Hunt, and M. P. Anderson (2007), Identifying spatial variability of groundwater discharge in a wetland stream using a distributed temperature sensor, *Water Resources Research*, 43, W10408, doi:10.1029/2007WR006145.
- M. Shanafield, G. Pohl, and R. Susfalk (2010), Use of heat-based vertical fluxes to approximate total flux in simple channels, *Water Resources Research*, 46, W03508, doi:10.1029/2009WR007956.
- Manning, A. H., and D. K. Solomon (2005), An integrated environmental tracer approach to characterizing groundwater circulation in a mountain block, *Water Resources Research*, 41, W12412, doi:10.1029/2005WR004178.
- Matheswaran, K., M. Blemmer, J. Mortensen, D. Rosbjerg and E. Boegh, (2011), Investigating the effect of surface water-groundwater interactions on stream temperature using Distributed Temperature Sensing and an instream temperature modeling, in: *Conceptual and Modelling Studies of Integrated Groundwater, Surface Water, and Ecological Systems*, Proceedings of Symposium H01 held during IUGG2011 in Melbourne, Australia, July 2011) (IAHS Publ. 345, 2011). 23-29
- Saar, M. O. (2011), Review: Geothermal heat as a tracer of large-scale groundwater flow and as a means to determine permeability fields, *Hydrogeology Journal*, 19(1), 31-52
- Schuetz, T., and M. Weiler (2011), Quantification of localized groundwater inflow into streams using ground-based infrared thermography, *Geophysical Research Letters*, 38, L03401, doi:10.1029/2010GL046198.
- Selker, J., N. van de Giesen, M. Westhoff, W. Luxemburg, and M. B. Parlange (2006), Fiber optics opens window on stream dynamics, *Geophysical Research Letters*, 33, L24401, doi:10.1029/2006GL027979.
- Steele-Dunne, S. C., M. M. Rutten, D. M. Krzeminska, M. Hausner, S. W. Tyler, J. Selker, T. A. Bogaard, and N. C. van de Giesen (2010), Feasibility of soil moisture estimation using passive distributed temperature sensing, *Water Resources Research*, 46, W03534, doi:10.1029/2009WR008272
- Tyler, S. W., J. S. Selker, M. B. Hausner, C. E. Hatch, T. Torgersen, C. E. Thodal, and S. G. Schladow (2009), Environmental temperature sensing using Raman spectra DTS fiber-optic methods, *Water Resources Research*, 45, W00D23, doi:10.1029/2008WR007052.

- Westhoff, M. C., T. A. Bogaard, and H. H. G. Savenije (2011), Quantifying spatial and temporal discharge dynamics of an event in a first order stream, using distributed temperature sensing, *Hydrology and Earth System Sciences*, 15(6), 1945–1957.
- Westhoff, M. C., M. N. Gooseff, T. A. Bogaard, and H. H. G. Savenije (2011), Quantifying hyporheic exchange at high spatial resolution using natural temperature variations along a first-order stream, *Water Resources Research*, 47, W10508, doi:10.1029/2010WR009767.
- Yuan, X., Z. Xie, J. Zheng, X. Tian, and Z. Yang (2008), Effects of water table dynamics on regional climate: A case study over east Asian monsoon area, *Journal of Geophysical Research*, 113, D21112, doi:10.1029/2008JD010180.

Bibliography

Summary

Shallow groundwater usually characterizes low lands within watersheds. Besides, many newly reclaimed irrigation lands suffer shallow water table conditions. Groundwater flow models and the management of irrigation systems can be greatly supported by satellite thermal recurrent measurements, provided that these measurements were capable of detecting the depth and the areal extent of shallow groundwater. Such measurements have additional advantage in monitoring the shallow groundwater effect on surface energy balance, and in bringing that effect within land surface and climate models on more solid basis.

The objective of this Research is to explore and appreciate the different aspects and basic physical principles involved in the process of shallow groundwater effect on land surface temperature and surface energy balance, and to investigate the potential of remote sensing to delineate this effect. To reach the goal of this study, three paths were followed: in situ measurements, numerical simulations and remote sensing data manipulations.

The in situ measurements were conducted within Al-Balikh river basin in northern Syria. The study area represents a flat region of agricultural fields that suffers shallow water tables conditions. The field measurements included surface soil moisture and temperature measurements, water table depth readings, soil composition analysis, geologic maps and weather data collection. Variant numerical experiments were conducted to explore the processes that play a role in groundwater effect on land surface temperature and surface energy balance. The last path in this study involved using MODIS data and SEBS algorithm to inspect the spatial and temporal patterns of shallow groundwater effect on land surface temperature and surface energy balance in the study area.

Shallow groundwater affects thermal properties of the region below its water table. Moreover, it alters soil moisture of the zone above its water table which results in affecting its thermal properties, the magnitude of evaporation, albedo and emissivity. Hence shallow groundwater affects land surface temperature and the surface energy balance in two different ways; direct and indirect: The direct way (thermodynamic effect) takes place through groundwater distinctive thermal properties and affects heat propagation within soil profile. The indirect way is through its effect on soil moisture above water table and its related effects (i.e. evaporation, soil thermal properties of vadose zone, land surface emissivity and albedo).

With the aid of numerical modeling the thermodynamic effect was separated out numerically from the indirect effect. It was shown that the presence of groundwater, through its distinctive thermal properties within the yearly depth of heat penetration, affects directly land surface temperature and the entire surface energy balance system thereby. In spite of its small magnitudes, highlighting the different features of the thermodynamic effect is useful to complete the understanding of groundwater effect. The interaction of the thermodynamic effect with the indirect effect may increase or decrease the upshot of the combined effect.

To know when and how groundwater effect takes place or whether it is possible to utilize currently operational satellites in its detection, the combined effect of shallow groundwater was simulated. In this simulation, the majority of the aspects through which shallow groundwater affects land surface temperature and the various components of surface energy balance were taken into consideration.

The results show that shallow groundwater areas reflect less shortwave radiation due to their lower albedo and therefore, they get higher magnitude of shortwave radiation. When potential evaporation demand is high enough, a large portion of the energy received by these areas is spent on evaporation. This makes the latent heat flux predominant, and leaves less energy to heat the soil. Consequently, this induces lower magnitudes of both sensible and ground heat fluxes. The higher soil thermal conductivity in shallow groundwater areas facilitates heat transfer between the top soil and the subsurface which promotes greater provisional heat transfer in both vertical directions. i.e., soil subsurface is more thermally connected to the atmosphere. Nevertheless, the continuous heat exchange between the surface and the subsurface makes the deep soil temperatures come into equilibrium with surface and climate conditions. As a result, the upshot of ground heat flux in both profiles is very close to zero in the long run.

With regards to remote sensors' capability of detecting shallow groundwater effect on land surface temperature, it was found that this effect can be sufficiently clear to be sensed if at least one of two conditions are met: firstly, latent heat flux effect is predominant due to the high potential evaporation, or secondly, soil volumetric heat capacity effect is strong due to the big contrast in air temperature between day and night.

The remote sensing data investigations showed that it is possible to map the effect of shallow groundwater on land surface temperature

using the freely available satellite data like MODIS. Satellite measurements demonstrated a clear correspondence of surface temperature with water table depth day and night. Consequently, the various surface energy balance maps, calculated using SEBS and MODIS data, correlated well with water table depth.

Many factors played a role in the good results of remote sensing investigation. Firstly, the two major conditions were met in this day of investigation, i.e. high potential evaporation and high contrast in air temperature. Secondly, the surface soil moisture and water table depth conditions were fairly stable. Thirdly, the limited topographic relief and vegetation cover in the study area helped to avoid possible uncertainty sources in surface temperature measurements and SEBS estimates of energy fluxes. Finally, due to its imaging times and visiting frequency, bands diversity, sensor accuracy, precision and resolution, MODIS proved to be useful in this study. Yet, its spatial resolution was disadvantageous.

Possible finer resolution in future satellites may enable masking out the undesired effect of unrelated surfaces, and make the thermal mapping of shallow aquifers more precise. Advanced investigations of groundwater effect under vegetated and dynamic conditions are recommended for further research using remote sensing data and dynamic 3-D numerical simulations.

Summary

Samenvatting

Oppervlakkig grondwater is van groot belang voor laaggelegen gebieden binnen watersheds. Vooral voor nieuw ontgonnen irrigatie is dit belangrijk omdat hier het grondwater erg dicht op de oppervlakte zit. Grondwater modellen en het management modellen voor irrigatie systemen kunnen geholpen worden door satelliet thermische metingen, indien deze metingen geschikt zijn om de diepte en de spatiale schaal te kunnen meten. Dit soort metingen heeft als extra voordeel dat zij het onderzoek over het effect oppervlakkige grondwater niveaus op land oppervlakte energie en klimaat modellen op een solidere manier mogelijk maken dan op dit moment word gedaan.

Het doel van dit onderzoek is het onderzoeken van de verschillende aspecten en basisch principes van oppervlakkig grondwater die een rol spelen op het land temperatuur en de oppervlakte energie balans. Hierbij word ook de potentiaal van aard observatie bekeken om dit effect te kunnen karakteriseren. Om dit doel te bereiken zijn er drie methodes gevolgd: grond metingen, numerieke simulaties and aard observatie data manipulaties.

De grond metingen zijn uitgevoerd in de Al-Balikh rivier bassin in Noord Syrië. De studie omgeving betreft een zeer vlak gebied met voornamelijk landbouw grond welke beïnvloed worden door oppervlakkig grondwater tables condities. De experimenten bevatten metingen van bodem vocht en bodem temperatuur, grondwater diepte, bodem compositie en geologische kaarten en weer data. Verschillende numerieke experimenten zijn uitgevoerd om de processen die een rol spelen in het grondwater effect op de oppervlakte temperatuur en energie balans te onderzoeken. De laatste methode bevatte het gebruik van MODIS data en de SEBS algoritme om de spatiale en temporale patronen van oppervlakkig grondwater en land oppervlakte temperatuur te onderzoeken.

Oppervlakkig grondwater beïnvloedt de thermische eigenschappen van de omgeving. Bovendien zorgt het grondwater er ook voor dat het bodemvocht boven het grondwater niveau ook word beïnvloed, welke effect ook heeft op de thermische eigenschappen en de hoeveelheid water welke verdampt. De invloed van oppervlakkig grondwater op het land oppervlakte temperatuur en energie balans is dus tweezijdig: direct and indirect. De directe invloed (thermodynamisch effect) vind plaats door specifieke thermale eigenschappen van het grondwater en heeft effect op de hitte stuwing binnen de bodem profiel. De indirecte invloed is door het effect van

de bodem vocht en gerelateerde processen als verdamping, bodem thermische eigenschappen in de vadose zone, land emissiviteit en de albedo.

Met de hulp numerieke modellen was de directe invloed van thermodynamisch effect gescheiden van de indirecte invloed. Er is aangetoond dat de aanwezigheid van grondwater door haar karakteristieke thermische eigenschappen binnen de jaarlijkse diepte van hitte penetratie, direct effect heeft op land oppervlakte temperatuur en de totale energie balans. Ondanks een de kleine amplitude is het zeer bruikbaar om de verschillende effecten van het thermodynamische effect te karakteriseren voor een complete kennis van het grondwater effect. De interactie van het thermodynamisch effect met het indirecte effect kan voor een verlaging/verhoging van het gecombineerde effect zorgen.

Om te weten wanneer en hoe het grondwater effect plaats vind en of het mogelijk is om operationele satelliet data te gebruiken voor detectie werd het gecombineerde effect van oppervlakkige grond water gesimuleerd. In deze simulatie werden de meeste van het grondwater effecten op het land temperatuur en de overige componenten van energie balans meegenomen.

De resultaten laten zien dat het oppervlakkige grondwater gebieden de kortgolvlige straling minder reflecteren door een lagere albedo en daardoor een meer straling absorberen. Wanneer de potentiële verdamping hoog genoeg is, zal een groot gedeelte van de ontvangen energie omgezet worden in verdamping. Dit zorgt dat de latente warmte dominant en zorgt voor minder energie toevoer naar de grond. Als een consequentie zorgt dit voor lagere sensibele en grond warmte fluxen. De hogere bodem thermische geleiding in oppervlakkig grondwater gebieden maakt het makkelijk voor warmte te verplaatsen tussen de top en subsurface laag. Ondanks dit zorgt de continue warmte uitwisseling tussen de oppervlakte en de subsurface ervoor dat de diepere bodem temperaturen in evenwicht zijn met de oppervlakte en de klimatologische condities. Hierdoor word de grond warmte flux gemeten over een langere periode zeer klein.

Hierna werd de gevoeligheid van de aardobservatie sensoren om het oppervlakkige grondwater effect op land temperatuur te detecteren onderzocht. Er is aangetoond dat dit effect voldoende duidelijk is als in ieder geval aan twee condities word voldaan: ten eerste de latente warmte flux is prominent door hoge potentiële verdamping en ten

tweede de bodem volumetrische warmte capaciteit is zeer sterk door het hoge contract in lucht temperatuur tussen nacht en dag

Het onderzoek met aardobservatie data toonde aan dat het mogelijk is om de effecten van oppervlakkig grondwater op het land oppervlakte temperatuur in kaart te brengen met vrij-toegankelijke satelliet data zoals MODIS. Satelliet metingen lieten een duidelijke overeenkomst zien tussen de oppervlakte temperatuur met grondwater niveau gedurende dag en nacht. Dit had als effect dat de verschillende energie balans kaarten berekend met SEBS en MODIS data zeer goed correleerden met de grond water diepte.

Veel factoren spelen in een rol in het krijgen van goede resultaten met aardobservatie metingen. Ten eerste, er werd voldaan aan de twee grote condities beschreven in dit onderzoek (namelijk hoge potentiële verdamping and een hoog contract in lucht temperatuur. Ten tweede, het bodemvocht en grondwater niveau waren redelijk stabiel. Ten derde, de bescheiden hoogte verschillen in lage vegetatie factie in het gebied zorgden ervoor zorgden voor een lage onzekerheid in de temperatuur metingen en de verdamping berekeningen door SEBS. Als laatste, waren de specificaties van de MODIS sensor (overvlieg tijden, hoge frequentie van metingen, de bands spectrale verscheidenheid, de hoge accuratesse en precisie) zeer nuttig voor deze studie, ondanks dat haar spatiale resolutie verre van optimaal was.

Hogere resoluties in toekomstige satellieten kunnen het maskeren van ongewilde effecten van ongerelateerde oppervlakte mogelijk maken, en daardoor het in kaart brengen van de thermische eigenschappen van oppervlakkige bodemreservoirs verbeteren. Geavanceerde onderzoeken naar het grondwater effect onder begroeide en dynamische condities zijn aanbevolen voor verder onderzoek met aard observatie data en dynamische 3D numerieke simulaties.

ITC Dissertation List

http://www.itc.nl/Pub/research_programme/Graduate-programme/Graduate-programme-PhD_Graduates.html